Molecular Structure at a Distance – Quantitative Interpretation of Pulsed Electron– Electron Double Resonance Data

Dissertation

zur Erlangung des Doktorgrades der Naturwissenschaften

vorgelegt dem Fachbereich 14

der Johann Wolfgang Goethe-Universität

in Frankfurt am Main

von

Bela Bode

aus Frankfurt am Main

Frankfurt am Main 2008

D30

Vom Fachbereich Biochemie, Chemie und Pharmazie der Johann Wolfgang Goethe-Univerität als Dissertation angenommen

Dekan: Prof. Dr. Harald Schwalbe

Gutachter: Dr. Olav Schiemann
                   Prof. Dr. Thomas F. Prisner
                   Prof. Dr. Clemens Glaubitz
                   Prof. Dr. Gunnar Jeschke

Datum der Disputation: 05.09.2008

Now my charms are all o'erthrown,
And what strength I have's mine own,
Which is most faint: now, 'tis true,
I must be here confined by you,
Or sent to Naples. Let me not,
Since I have my dukedom got
And pardon'd the deceiver, dwell
On this bare island by your spell;
But release me from my bands
With the help of your good hands:
Gentle breath of yours my sails
Must fill, or else my project fails,
Which was to please. No I want
Spirits to enforce, art to enchant,
And my ending is despair,
Unless I be relieved by prayer,
Which pierces so that it assaults
Mercy itself and frees all faults.
As you from crimes would pardon'd be,
Let your indulgence set me free.

Prospero's epilogue of The Tempest
By *William Shakespeare*

This thesis was prepared under the supervision of Dr. Olav Schiemann between April 2004 and March 2008 at the Institute for Physical and Theoretical Chemistry of the Johann Wolfgang Goethe University Frankfurt am Main.

Abstract

Pulsed electron-electron double resonance (PELDOR) is a well established method concerning nanometer distance measurements involving two nitroxide spin-labels. In this thesis the applicability of this method to count the number of spins is tested. Furthermore, this work explored the limits, up to which PELDOR data obtained on copper(II)-nitroxide complexes can be quantitatively interpreted.

Spin counting provides access to oligomerization studies – monitoring the assembly of homo- or hetero-oligomers from singly labeled compounds. The experimental calibration was performed using model systems, which contain one to four nitroxide radicals. The results show that monomers, dimers, trimers, and tetramers can be distinguished within an error of 5% in the number of spins. Moreover, a detailed analysis of the distance distributions in model complexes revealed that more than one distance can be extracted from complexes bearing several spins, as for example three different distances were resolved in a model tetramer – the other three possible distances being symmetry related. Furthermore, systems exhibiting mixtures of oligomeric states complicate the analysis of the data, because the average number of spin centers contributes nonlinearly to the signal and different relaxation behavior of the oligomers has to be treated explicitly. Experiments solving these problems are proposed in the thesis.

Thus, for the first time spin counting has been experimentally calibrated using fully characterized test systems bearing up to four spins. Moreover, the behavior of mixtures was quantitatively interpreted. In addition, it has been shown that several spin-spin distances within a molecule can be extracted from a single dataset.

In the second part of the thesis PELDOR experiments on a spin-labeled copper(II)-porphyrin have been quantitatively analyzed. Metal-nitroxide distance measurements are a valuable tool for the triangulation of paramagnetic metal ions. Therefore, X-band PELDOR experiments at different frequencies have been performed. The data exhibits only weak orientation selection, but a fast damping of the oscillation. The experimental data has been interpreted based upon quantitative simulations. The influence of orientation selection, conformational flexibility, spin-density distribution, exchange interaction J, as well as anisotropy and strains of the **g**-tensor has been examined. An estimate of the spin-density delocalization has been obtained by density functional theory calculations. The dipolar

interaction tensor was calculated from the point-charge model, the extension of the point-dipole approximation to several spin bearing centers.

Even assuming asymmetric spin distributions induced by an ensemble of asymmetrically distorted porphyrins the effect of delocalization on the PELDOR time trace is weak. The observed damping of dipolar oscillations has been only reproduced by simulations, if a small distribution in J was assumed. It has been shown that the experimental damping of dipolar modulations is not solely due to conformational heterogeneity.

In conclusion the quantitative interpretation of PELDOR data is extended to copper-nitroxide- and multi-spin-systems. The influence of the mean distance, of the number of coupled spins, of the conformational flexibility, of spin-density distribution and of the electronic structure of the spin centers has been analyzed using model systems. The insights on model compounds mimicking spin-labeled biomacromolecules – in oligomeric or metal bound states – calibrate the method with respect to the information that can be deduced from the experimental data. The resulting in-depth understanding allows correlating experimental results (from for example biological systems) with models of structure and dynamics. It also opens new fields for PELDOR as for example triangulation of metal centers and oligomerization studies. In general, this thesis has demonstrated that modern pulsed electron paramagnetic resonance techniques in combination with quantitative data analysis can contribute to a detailed insight into molecular structure and dynamics.

Table of Contents

1. Introduction

1.1. Preamble

One of the key concepts in natural sciences is the structure-function paradigm, postulating that all biomolecular and material properties as well as their functions are encoded in the structure. One approach to unravel molecular functions is to study molecular structure, and structural dynamics. X-ray diffraction is one powerful method to distentangle the structure of large biomacromolecules and complexes.[1] Structures gained in this way result from species in a non-native crystalline state, and can only be obtained for systems that crystallize as opposed to e.g. polymers and fibroid samples. Furthermore, structural dynamics lead to a loss of resolution in X-ray studies. Nuclear magnetic resonance (NMR), on the other hand, can yield deep insights on the structure and dynamics of molecules in solution.[2] High resolution NMR methods are, however, limited to macromolecules up to ~50 kDa, whereas high resolution solid-state NMR methods for structure determination of large complexes are still under development.[3, 4] For the study of structure, folding, dynamics, and conformational changes in large biomolecules, membrane bound or paramagnetic systems, additional biophysical methods are applied, like fluorescence[5] and electron paramagnetic resonance (EPR)[6, 7] spectroscopy. Fluorescence resonance energy transfer (FRET) and several EPR techniques have proven to be highly sensitive and accurate in measuring long range distances and their changes upon effectors or altered conditions. Mapping several long-range distance constraints over the macromolecule or complex may enhance the understanding of the folding of tertiary structure elements, the assembly of quaternary complexes, and changes upon ligand binding. This approach is extremely valuable in combination with molecular dynamics (MD) simulations.[8] Generally FRET can be applied in liquid solution at room temperature with a sensitivity reaching the single molecule level resolving molecular dynamics in real time. EPR methods, on the other hand, allow extraction of distances without deconvolution of quenching mechanisms and assumptions of orientation factors. Labels commonly used in EPR are smaller and more rigid than chomophores allowing easier correlation of the measured distance with the structure of the studied molecule, even though EPR methods are less sensitive and mostly applied in frozen solution. Thus, EPR studies of dynamics by long-range distance measurements rely on capturing snapshots of molecular motion using for example freeze-quench techniques.

In contrast to early approaches using continuous wave (cw) EPR in combination with site-directed spin-labeling (SDSL),[9, 10] the technological improvement of EPR-spectrometers working at high field/high frequency,[11, 12] as well as the development of sophisticated pulse sequences,[13, 14] have tremendously improved the quality and reliability of the data. EPR distance measurements have evolved to a growing field in biomolecular[15] and material[16, 17] sciences. The number of publications dealing with pulse EPR distance measurements has rapidly increased in the past years. Especially the use of pulsed electron-electron double resonance (PELDOR),[18] often also called double electron-electron resonance (DEER)[19] has increased drastically since its invention in 1981, as can be visualized by scanning the keywords, "pulse EPR distance measurements" and "PELDOR or DEER" in literature databases (Figure 1.1.1).
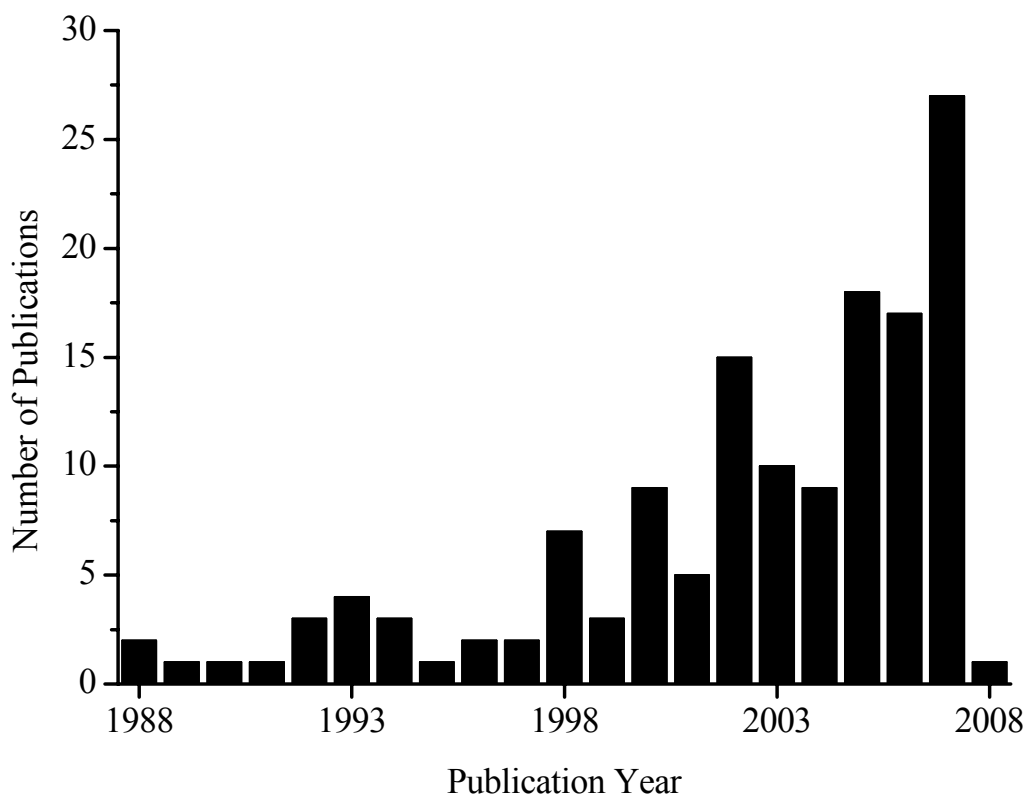
Figure 1.1.1. Pulse EPR distance measurements in the literature of the past twenty years. The literature search was performed on January 4th, 2008.

The combination of PELDOR and SDSL permits gathering long-range constraints for structure determination. The theory of 4-pulse PELDOR is well established for the most common case, i.e. biradicals labeled with two identical, flexible nitroxide spin-probes which are uncorrelated in their relative orientations. However, the approximations made in this

theory, as for example the neglect of angular correlations, are not always well suited. But, a quantitative understanding of the data obtained by pulse EPR distance measurements is crucial for the conclusions derived.

1.1.1. Motivation and Aim

The aim of this work is to gain insight into the PELDOR time domain signal dependencies on the spin Hamiltonian parameters and molecular structure of the studied system. The time trace does not only encode the distance, but also the number of coupled spin centers,[20] their relative orientation,[21] the conformational flexibility,[22] and the electronic structure of the spin centers themselves.[23] All of the above parameters have already been treated in theory and applied for data analysis, but quantitative, systematic studies of these parameters on well defined systems are still lacking in literature. Herein, fully characterized model complexes are employed to perform such studies. Thus, the number of spin centers and distances are defined by synthesis design, limits of conformational flexibility and relative orientations can be set by the rigidity of the complex, and the electronic structure is known from literature or can be calculated using quantum chemistry. This allows benchmarking the method towards applications on more complex systems. One major goal is the study of the time domain signal in dependence of the number of spins in oligomers of nitroxides for pure states and for mixtures of oligomers. This dependency is the basis of spin counting, permitting to monitor the assembly of singly-labeled monomers into oligomers. Another major point of this study is the quantitative interpretation of the experimental data, when a nitroxide is coupled to metal center, such as a copper(II)-porphyrin, leading to different orientation selection and electronic structure of the second spin center. This will allow triangulating metal ions by measuring several distances and determining relative orientations of the spin-labels with respect to the metal center.

1.1.2. Outline

This chapter gives an introduction and motivation of the thesis. A list of publications and conference contributions associated with the results of this work is presented.

Chapter 1.2 summarizes the theory of PELDOR distance measurements. A brief review of the spin Hamiltonian is followed by a more detailed overview of the PELDOR theory for explicit treatment of relative orientations. Furthermore, the limit of uncorrelated mutual

orientations is discussed preceding the extension to multi-spin systems. Different methods for data analysis are also introduced. The chapter closes with a short summary of other methods for pulsed EPR distance measurements.

In chapter 1.3 the applications of PELDOR on models systems, materials, peptides and proteins, nucleic acids, and metal centers are presented.

Chapter 2.1 contains the experimental results obtained on nitroxide poly-radicals including modulation depths in pure oligomeric states and in mixtures thereof. The influence of pulse excitation bandwidths, angular correlation, and dipolar relaxation are discussed. This part has already been published in *The Journal of the American Chemical Society*.

In chapter 2.2 PELDOR measurements on a nitroxide spin-labeled copper(II)-porphyrin are presented and the influence of orientation selection, conformational flexibility, exchange interaction, and spin-density delocalization is quantitatively described by simulations. This chapter has been accepted for publication in *The Journal of Physical Chemistry A*.

The conclusions derived from this work and the wide fields of opportunities for future systematic studies are described in chapter 3.

Chapter 4 comprises the German summary.

The Appendix gives a list of abbreviations, constants and variables, and the experimental section.

The thesis ends by giving the bibliography, the list of figures, the list of tables, an acknowledgement, and the author's *curriculum vitae*.

1.1.3. Publications and Conference Contributions

The major part of the results obtained in this thesis have been published and presented at conferences as oral or poster presentations or in seminars. Only the posters presented by the author are given in the list below.

Publications

Bela E. Bode, Dominik Margraf, Jörn Plackmeyer, Gerd Dürner, Thomas F. Prisner, Olav Schiemann "Counting the Monomers in Nanometer-Sized Oligomers by Pulsed Electron–Electron Double Resonance" *J. Am. Chem. Soc.* **2007**, *129*, 6736-6745.

Olav Schiemann, Nelly Piton, Jörn Plackmeyer, Bela E. Bode, Thomas F. Prisner, Joachim W. Engels "Spin-labeling of oligonucleotides with the nitroxide TPA and use of PELDOR, a pulse EPR method, to measure intramolecular distances" *Nat. Protoc.* **2007**, *2*, 904 -922.

Dominik Margraf, Bela E. Bode, Andriy Marko, Olav Schiemann, Thomas F. Prisner "Conformational Flexibility of Nitroxide Biradicals Determined from X-Band PELDOR Experiments" *Mol. Phys.* **2007**, *105*, 2153-2160.

Bela E. Bode, Jörn Plackmeyer, Thomas F. Prisner, Olav Schiemann, "PELDOR Measurements on a Nitroxide Labeled Cu(II) Porphyrin: Orientation Selection, Spin-Density Distribution and Conformational Flexibility" *J. Phys. Chem. A*. accepted.

Oral Presentations

"PELDOR Distance Measurements Between Metals and Nitroxides"
DFG-Rundgespräch "Magnetische Spektroskopie der Struktur und Dynamik nano- und mesoskopischer Systeme", Hirschegg, 2005 *(invited talk)*.

"PELDOR – Metal-Nitroxide Distances"
Group Seminar Dr. Schiemann, TU Munich, 2005.

"PELDOR – Metal-Nitroxide Distances and Spin Counting"
Group Seminar Prof. Dinse, TU Darmstadt, 2005.

"PELDOR – Metal-Nitroxide Distances"
Retreat of the DFG Sonderforschungsbereich 579 RNA-Ligand Interactions, Weilburg, 2005.

"PELDOR – Extension to Metal-Nitroxide Distances"
Seminar of the Institute for Physical and Theoretical Chemistry, J. W. Goethe University*, Hirschegg, 2006.

"PELDOR – Metal-Nitroxide Distances an Update"
Seminar of the DFG Sonderforschungsbereich 579 "RNA-Ligand Interactions", Frankfurt a. M., 2006.

"PELDOR – Metal-Nitroxide Distances and Spin Counting"
28th GDCh Magnetic Resonance Meeting, Tübingen University, 2006.

"Counting the Monomers in Nanometer-Sized Oligomers by PELDOR"
MRC Young Investigators Award Lecture, EUROMAR, Tarragona, 2007.

"Counting the Monomers in Nanometer-Sized Oligomers by PELDOR"
Ernst Award Lecture, 29th GDCh Magnetic Resonance Meeting, Göttingen University, 2007.

"Structure at a Distance – Quantitative Interpretation of PELDOR Time Domain Data"
Seminar of the Institute for Physical and Theoretical Chemistry, J. W. Goethe-University, Frankfurt a. M., 2007.

Poster Presentations
"Model Systems for Pulse EPR Distance Measurements between Metal Centers and Nitroxides"
Jörn Plackmeyer, Bela E. Bode, Thomas F. Prisner, Olav Schiemann, *104th General Assembly of the Bunsen Society for Physical Chemistry*, Frankfurt a. M, 2005.

"Model Systems for Pulse EPR Distance Measurements Applied to Spin-Labeled Metal Complexes"
Bela E. Bode, Jörn Plackmeyer, Thomas F. Prisner, Olav Schiemann, *3rd European EPR Summer School and COST Training School*, Wiesbaden 2005.

"Pulse EPR Distance Measurements between Metal Centers and Nitroxides"
Bela E. Bode, Jörn Plackmeyer, Thomas F. Prisner, Olav Schiemann, *27th GDCh Magnetic Resonance Meeting*, Max-Planck Institute for Polymer Research Mainz, 2005.

"Pulse EPR Distance Measurements of Metal-Nitroxide Complexes"
Bela E. Bode, Jörn Plackmeyer, Thomas F. Prisner, Olav Schiemann, *Minerva-Gentner Symposium*, Eilat, Israel, 2005.

"PELDOR Constraints for NMR Multi-Domain Structure Determination of Pleckstrin"

<u>Bela E. Bode</u>, Gunter Stier, Bernd Simon, Michael Sattler, Olav Schiemann, *22nd International Conference on Magnetic Resonance in Biological Systems*, Göttingen University, 2006.

„PELDOR – Metal-Nitroxide Distances and Spin Counting"

<u>Bela E. Bode</u>, Jörn Plackmeyer, Dominik Margraf, Thomas F. Prisner, Olav Schiemann, *6th European Federation of EPR Groups Meeting*, Madrid, Spain, 2006.

„PELDOR – Metal-Nitroxide Distances and Spin Counting"

<u>Bela E. Bode</u>, Jörn Plackmeyer, Dominik Margraf, Thomas F. Prisner, Olav Schiemann, *28th GDCh Magnetic Resonance Meeting*, Tübingen University, 2006.

"PELDOR Constraints for NMR Multi-Domain Structure Determination of Pleckstrin"[1]

<u>Bela E. Bode</u>, Gunter Stier, Bernd Simon, Michael Sattler, Olav Schiemann, *29th GDCh Magnetic Resonance Meeting*, Göttingen University, 2007.

Awards

MRC Young Investigators Award, EUROMAR, Tarragona, 2007 for the contribution:

"Counting the Monomers in Nanometer-Sized Oligomers by PELDOR"

Ernst Award, 29th GDCh Magnetic Resonance Meeting, Göttingen University, 2007 for the publication:

Bela E. Bode, Dominik Margraf, Jörn Plackmeyer, Gerd Dürner, Thomas F. Prisner, Olav Schiemann "Counting the Monomers in Nanometer-Sized Oligomers by Pulsed Electron–Electron Double Resonance" *J. Am. Chem. Soc.* **2007**, *129*, 6736-6745.

---

[1] Title and authors differ from the Book of Abstracts.

1.2. EPR and PELDOR Theory

In this chapter a brief summary of the interactions underlying EPR-spectra is given, followed by a more detailed review of the basic theory of the PELDOR experiment, together with methods for data analysis. A short introduction to pulse EPR methods used to measure nanometer distances concludes this chapter.

1.2.1. Spin Hamiltonian

In the following the terms of the spin Hamiltonian will be summarized. For a more detailed discussion see standard text books.[7, 24-26]

Unpaired electrons possess a magnetic moment $\mathbf{\mu}_e$. The corresponding operator is described by eq. 1.1.

$$\hat{\mathbf{\mu}}_e = -\mu_B g_e \hat{\mathbf{S}} \tag{1.1}$$

with μ_B being the Bohr magneton, g_e the free electron g-factor and $\hat{\mathbf{S}}$ the electron spin vector operator. For unpaired electrons in molecules g_e is replaced by the **g**-tensor, taking the orientational dependence of the g-value into account.

A nucleus with the spin I has the magnetic moment $\mathbf{\mu}_N$, its corresponding operator being described by eq. 1.2.

$$\hat{\mathbf{\mu}}_N = \mu_N g_N \hat{\mathbf{I}} \tag{1.2}$$

where μ_N is the nuclear magneton, g_N the nuclear g-value, and $\hat{\mathbf{I}}$ the nuclear spin vector operator.

The interaction of one electron spin with an external magnetic field vector **B** and i nuclear magnetic moments can be described by the effective spin Hamiltonian (eq. 1.3):

$$\hat{\mathcal{H}}_S = \mu_B \mathbf{B} \mathbf{g} \hat{\mathbf{S}} - \sum_i \left(g_{N_i} \mu_N \mathbf{B} \hat{\mathbf{I}}_i \right) + \sum_i \left(\hat{\mathbf{S}} \mathbf{A}_i \hat{\mathbf{I}}_i \right) + \sum_i \left(\hat{\mathbf{I}}_i \mathbf{Q}_i \hat{\mathbf{I}}_i \right) + \hat{\mathbf{S}} \mathbf{D} \hat{\mathbf{S}} \tag{1.3}$$

The first term describes the electron Zeeman splitting, the second term sums the nuclear Zeeman splittings of i nuclei. The hyperfine interaction with all nuclei is given in the third term. For nuclear spins $I > 1/2$ the nuclear quadrupole interaction has to be considered by the fourth term, and for electron spins $S > 1/2$ the zero-field splitting is described by the last term. **A** is the hyperfine coupling tensor of one nucleus, **Q** the quadrupole coupling tensor of one nucleus and **D** the zero-field splitting tensor. Eq. 1.3 neglects the anisotropy of the nuclear Zeeman interactions as well as nuclei-nuclei interactions.

The main part of this work is concerned with the interactions between two or more paramagnetic centers (e.g. electron spins). In the following two electronic spins are considered, as indicated by the subscripts A and B. In case of short distances or conjugated spin orbitals an electron-electron exchange interaction J can occur (interaction Hamiltonian given in eq. 1.4). It is usually considered isotropic, but can have anisotropic contributions from spin-orbit coupling.

$$\hat{\mathcal{H}}_J = J\hat{\mathbf{S}}_A\hat{\mathbf{S}}_B \tag{1.4}$$

In addition, the two electron magnetic moments will exhibit a distance and orientation dependent dipolar interaction, the Hamiltonian determining the interaction energy is given in eq. 1.5.

$$\hat{\mathcal{H}}_{dd} = \hat{\mathbf{S}}_A\mathbf{d}\hat{\mathbf{S}}_B \tag{1.5}$$

with **d** as dipole-dipole coupling tensor. This tensor can be derived from the classic interaction energy (E) of two magnetic dipoles with magnetic moments $\boldsymbol{\mu}_A$ and $\boldsymbol{\mu}_B$, which is given in eq. 1.6.

$$E = \frac{\mu_0}{4\pi}\left[\frac{\boldsymbol{\mu}_A\boldsymbol{\mu}_B}{|\mathbf{R}|^3} - \frac{3(\boldsymbol{\mu}_A\mathbf{R})(\boldsymbol{\mu}_B\mathbf{R})}{|\mathbf{R}|^5}\right] \tag{1.6}$$

where **R** is the distance vector interconnecting $\boldsymbol{\mu}_A$ and $\boldsymbol{\mu}_B$. If the magnetic moments in eq. 1.6 are substituted by the corresponding quantum mechanic operators, the dipolar Hamiltonian can be written in the following form (eq. 1.7):

$$\hat{\mathcal{H}}_{dd} = -\frac{g_A g_B \mu_B^2 \mu_0}{4\pi\hbar|\mathbf{R}|^3}\left(A + B + C + D + E + F\right) \tag{1.7}$$

where g_A and g_B are the g-values of the two coupled spins and assumed to be isotropic, μ_0 is the vacuum permeability, $\hbar$ is the Planck constant divided by 2π. The terms A-F represent the 'dipolar alphabet' and give products of spin operators and angular expressions in spherical coordinates θ, φ and R describing the orientation of the molecule with respect to $\mathbf{B}$ (eq. 1.8).

$$\begin{aligned}
A &= \hat{S}_{zA}\hat{S}_{zB}\left(3\cos^2\theta - 1\right) \\
B &= -1/4\left(\hat{S}_{+A}\hat{S}_{-B} + \hat{S}_{-A}\hat{S}_{+B}\right)\left(3\cos^2\theta - 1\right) \\
C &= 3/2\left(\hat{S}_{+A}\hat{S}_{zB} + \hat{S}_{zA}\hat{S}_{+B}\right)\sin\theta\cos\theta\cdot e^{-i\varphi} \\
D &= 3/2\left(\hat{S}_{-A}\hat{S}_{zB} + \hat{S}_{zA}\hat{S}_{-B}\right)\sin\theta\cos\theta\cdot e^{i\varphi} \\
E &= 3/4\,\hat{S}_{+A}\hat{S}_{+B}\sin^2\theta\cdot e^{-2i\varphi} \\
F &= 3/4\,\hat{S}_{-A}\hat{S}_{-B}\sin^2\theta\cdot e^{2i\varphi}
\end{aligned} \tag{1.8}$$

In eq. 1.8 $\hat{S}_z$ are the z-magnetization operators, $\hat{S}_+$, the raising operators and $\hat{S}_-$ the lowering operators of the two spins. In the high field approximation (meaning the spins are quantized along $\mathbf{B}$) only the terms A and B need to be retained.

It will be useful to define the parameters ω_{dd}, ν_{dd}, $\omega_\perp$, and $\nu_\perp$ here (eq. 1.9).

$$\begin{aligned}
\omega_{dd} &= 2\pi\nu_{dd} = -\frac{\mu_0\mu_B^2}{4\pi\hbar}\frac{g_A g_B}{R^3}\left(3\cos^2\theta - 1\right) \\
|\omega_\perp| &= 2\pi|\nu_\perp| = \frac{\mu_0\mu_B^2}{4\pi\hbar}\frac{g_A g_B}{R^3} \\
\omega_{dd} &= \omega_\perp\left(3\cos^2\theta - 1\right)
\end{aligned} \tag{1.9}$$

R is the length of the distance vector.

For a pair of radicals with $g_A = g_B = 2.005$, this leads to (eq. 1.10):

$$|v_\perp|[\text{MHz}] = \frac{52.18}{R^3[\text{nm}]}$$

$$R[\text{nm}] = \left(\frac{52.18}{|v_\perp|[\text{MHz}]}\right)^{\frac{1}{3}}$$

(1.10)

The spin Hamiltonian for two coupled electron spins can be written as the sum of three terms (eq. 1.11).

$$\hat{\mathcal{H}} = \hat{\mathcal{H}}_Z + \hat{\mathcal{H}}_J + \hat{\mathcal{H}}_{dd}$$

(1.11)

The first term accounts for the Zeemann interaction of the electrons with the magnetic field (along the z-axis) and magnetic nuclei in the high field approximation (eq. 1.12):

$$\hat{\mathcal{H}}_Z = \omega_A \hat{S}_{zA} + \omega_B \hat{S}_{zB}$$

(1.12)

ω_A and ω_B are the resonance frequencies of the two spins in the absence of the electron-electron coupling and are determined by g-values and hyperfine coupling constants. The second term in eq. 1.11 is describing the exchange interaction between the two electrons (eq. 1.13)

$$\hat{\mathcal{H}}_J = J\hat{\mathbf{S}}_A \hat{\mathbf{S}}_B = J\hat{S}_{zA}\hat{S}_{zB} + \frac{1}{2}J\left(\hat{S}_{+A}\hat{S}_{-B} + \hat{S}_{-A}\hat{S}_{+B}\right)$$

(1.13)

The third term is the dipolar Hamiltonian (eq. 1.14).

$$\hat{\mathcal{H}}_{dd} = \omega_{dd}\hat{S}_{zA}\hat{S}_{zB} - \frac{1}{4}\omega_{dd}\left(\hat{S}_{+A}\hat{S}_{-B} + \hat{S}_{-A}\hat{S}_{+B}\right)$$

(1.14)

Using the basis states $|\alpha_A\alpha_B\rangle$, $|\alpha_A\beta_B\rangle$, $|\beta_A\alpha_B\rangle$, $|\beta_A\beta_B\rangle$ and the matrix representations of the operators given in appendix B one finds (eq. 1.15):

$$\hat{\mathcal{H}}_Z = \frac{1}{2} \begin{pmatrix} +(\omega_A + \omega_B) & 0 & 0 & 0 \\ 0 & +(\omega_A - \omega_B) & 0 & 0 \\ 0 & 0 & -(\omega_A - \omega_B) & 0 \\ 0 & 0 & 0 & -(\omega_A + \omega_B) \end{pmatrix}$$

(1.15)

$$\hat{\mathcal{H}}_J = \frac{1}{4} J \begin{pmatrix} 1 & 0 & 0 & 0 \\ 0 & -1 & 2 & 0 \\ 0 & 2 & -1 & 0 \\ 0 & 0 & 0 & 1 \end{pmatrix} \qquad \hat{\mathcal{H}}_{dd} = \frac{1}{4} \omega_{dd} \begin{pmatrix} 1 & 0 & 0 & 0 \\ 0 & -1 & -1 & 0 \\ 0 & -1 & -1 & 0 \\ 0 & 0 & 0 & 1 \end{pmatrix}$$

The 'weak coupling limit' is met, if the off-diagonal elements in eq. 1.15 are much smaller than the corresponding diagonal elements, i.e. if the coupling strength is much smaller than the difference in Lamor frequencies of the two electron spins. In this limit the secular approximation allows ignoring the non-secular off-diagonal terms in the dipolar and the exchange Hamiltonian, so that the eigenvalues (in radians per second) are the diagonal matrix elements of the Hamiltonian and the eigenstates are the basis states (eq. 1.16).

$$\varepsilon_{|\alpha_A \alpha_B\rangle} = +\frac{1}{2}(\omega_A + \omega_B) + \frac{1}{4}(J + \omega_{dd})$$

$$\varepsilon_{|\alpha_A \beta_B\rangle} = +\frac{1}{2}(\omega_A - \omega_B) - \frac{1}{4}(J + \omega_{dd})$$

(1.16)

$$\varepsilon_{|\beta_A \alpha_B\rangle} = -\frac{1}{2}(\omega_A - \omega_B) - \frac{1}{4}(J + \omega_{dd})$$

$$\varepsilon_{|\beta_A \beta_B\rangle} = -\frac{1}{2}(\omega_A + \omega_B) + \frac{1}{4}(J + \omega_{dd})$$

Therefore, considering only allowed EPR transitions, the spectrum consists of a pair of doublets centered at ω_A and ω_B and split by $\omega_{AB} = |J + \omega_{dd}|$.

If the weak coupling limit is not met, the $|\alpha_A \beta_B\rangle$ and $|\beta_A \alpha_B\rangle$ states will mix. However, the coupling (ω_{AB}) is usually smaller than the difference in resonance frequencies in pulse EPR distance measurements. If, as in a spin-echo experiment, the evolution arising from the Zeemann Hamiltonian is refocused, in practice ω_A and ω_B in eq. 1.16 can be simply dropped, so that for a given θ a pair of lines of equal intensity split by ω_{AB} is expected. This splitting only depends on the exchange coupling, the dipolar angle θ and the length of the distance vector $\mathbf{R}$ (Figure 1.2.1).
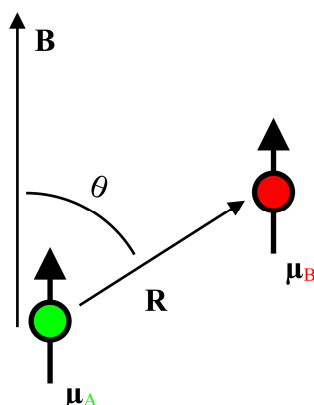
Figure 1.2.1. Two coupled magnetic dipoles.

It is worth mentioning here that the dipole-dipole coupling is the interaction of the spin Hamiltonian, which is easiest to interpret in terms of molecular structure. If the magnetic moments are known and *z*-quantization is assumed (which is valid for Zeemann interactions with small anisotropies), the only variable determining the strength of these interactions is **R**, which is of direct structural significance. This holds for dipolar couplings between electron spins as well as between electron and nuclear spins, as it is comprised in the anisotropic part of the hyperfine coupling tensor.

1.2.2. PELDOR

In this chapter the PELDOR experiment is introduced, based on several reviews[13, 15-17, 27] and text books.[7, 28] The 3-pulse PELDOR pulse sequence (Figure 1.2.2 A) has been invented already in 1981 by Milov *et al.*,[18] it is identical to Hahn's spin echo double resonance (SEDOR) experiment to detect the coupling between nuclear spins.[29]

In PELDOR a 2-pulse Hahn echo sequence with a fixed pulse separation τ is applied selectively to probe the A spin species of the A-B spin pair (at the frequency ν_A). An additional microwave inversion pulse at the resonance frequency of the B spins (ν_B), often called pump pulse, is employed to flip these spins. This spin flip induces a change in the Lamor frequency of the A spins by $\pm\omega_{AB}$. As a result the A spins precess with this altered frequency in the transversal plane and accumulate a phase factor depending on the time delay (*t*) of the pump pulse. The transversal magnetization is projected onto the *y*-axis (assuming the pulses along *x*) by recording an echo. This projection of the periodic change of the

dephasing angle in dependence of t, leads to a modulation of the echo intensity of the A spins (V_0) in dependence of the coupling strength (eq. 1.17).

$$V(t) = V_0 \cos\left(\omega_{AB} t\right) \tag{1.17}$$

In this ideal case the echo is fully inverted leading to a modulation depth of 200%. In most applications the resonance frequencies of A and B spins overlap and the spectral width is broader than the pulse excitation bandwidth achievable with commercially available microwave sources and amplifiers. This induces orientation selection, only subensembles of A and B spins with distinct orientations towards the magnetic field vector are excited and thus the modulation depth reduces.
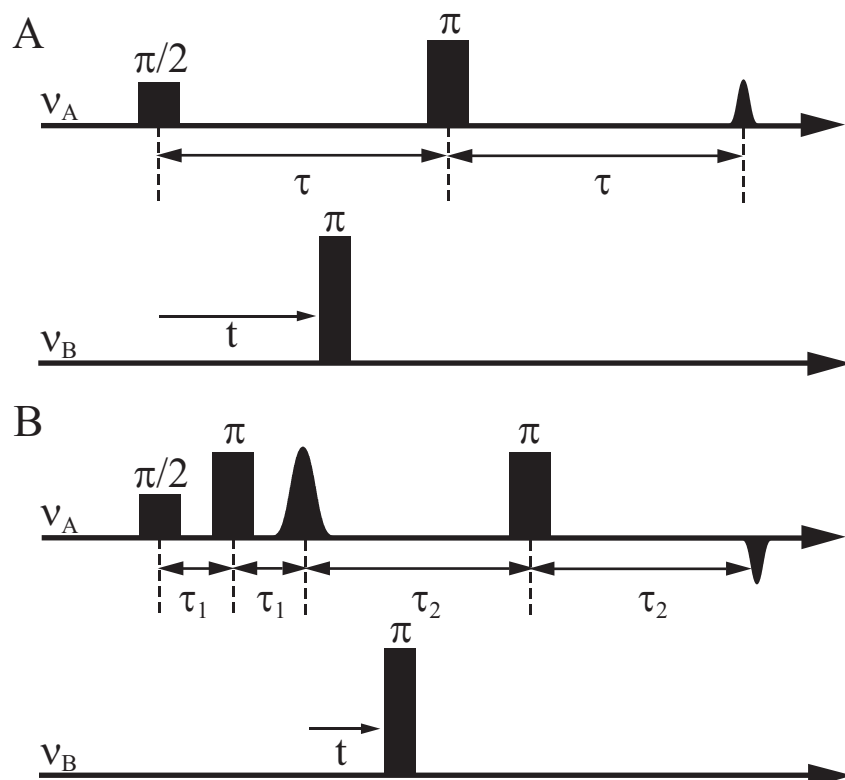

Figure 1.2.2. Pulse Sequences for PELDOR.
A: 3-pulse-PELDOR; B: 4-pulse-PELDOR.

The general technical problem of the 3-pulse PELDOR experiment is the significant dead-time to avoid the overlap of two microwave pulses within one amplifier for $t = 0$. This overlap either leads to strong distortions in the output power level or to the necessity to use unfavorably low microwave power levels. This problem has been solved by the invention of

the 4-pulse PELDOR sequence (Figure 1.2.2 B).[30] In this experiment the Hahn echo is refocused after an additional time τ ($\tau_1 = \tau_2 = \tau$) leading to the formation of a refocused echo at the time 4τ after the first pulse. The time t can be incremented between the second and the third pulse of the detection sequence. The position of the Hahn echo, 2τ after the first two pulses, corresponds to $t = 0$. The major disadvantage of this dead-time free experiment is that the detection sequence is twice as long as the three pulse sequence, so that transverse relaxation leads to a decrease in signal intensity, in addition to losses from incomplete refocusing. The effects of transversal relaxation can be partially circumvented by introducing an asymmetry between the evolution period τ_1 of the primary Hahn echo, and the evolution period τ_2 prior to the refocusing pulse.[31] Especially for slow relaxing species τ_2 can be chosen much larger than τ_1, leading to small differences in the overall lengths of the 3- and 4-pulse PELDOR detection time windows. This time window also determines the maximum length of the dipolar evolution that can be recorded as a function of t. To increase sensitivity, a variable time PELDOR experiment was proposed,[32] but it is unreliable for samples with an inhomogeneous distribution in transversal relaxation times, which hampers the internal normalization.[27]

In the most common case two nitroxide spin-labels are used as paramagnetic probes. At X-band frequencies (9 GHz) their spectra are dominated by the anisotropic ^{14}N hyperfine coupling. The **g**-anisotropy is unresolved within the inhomogeneous linewidth. The discrimination of A and B spins is usually achieved via the large A_{zz} hyperfine component of ~100 MHz. A typical frequency offset ($\Delta \nu_{AB}$) of 70 MHz corresponds to the average difference in Lamor frequencies and thus the weak coupling approximation is valid for distances larger than 1.5 nm, meaning dipolar splittings ($\nu_\perp$) smaller than 16 MHz. Usually, the maximum of the nitroxide spectrum is pumped with the inversion pulse at ν_B to achieve large effects in modulation depth, whereas the low-field maximum of the nitroxide spectrum is chosen for the detection frequency (ν_A) for optimum sensitivity. To maximize the wanted modulation effect relative to noise the pump pulse is usually chosen as short as possible still maintaining the flip angle of π. Pulse lengths down to 12 ns are feasible, shorter pulses lead to an increased overlap of the excitation profiles of pump and detection pulses. The pulse lengths at ν_A are usually chosen 32 ns to minimize this overlap and still excite a substantial part of the spin system. The effects of pulse lengths are extensively discussed in literature.[33-35]

The optimum temperature for PELDOR experiments depends on the transversal and longitudinal relaxation times (T_2 and T_1 respectively) of the spin probes as well as on the polarization of the spin system, the longer T_2 and the higher the polarization, the larger the signal becomes. On the other hand, short T_1 allows faster averaging. Hence a temperature of 40 to 60 K yields a good compromise between long T_2, short T_1, and reasonable Boltzmann polarization for nitroxides.

An increase in sample concentration also enhances signal intensity, but is limited due to instantaneous diffusion reducing the phase memory time of the spins. Biradical concentrations of 100 µM are feasible for distances up to 6 nm and still give reasonable signals. Also, matrix deuteration and solvents without methyl groups cause a reduced transverse relaxation rate and an increased signal.

A two-step phase cycle of the $\pi/2$ pulse eliminates receiver offsets making sure the signal tends to zero for large t.

To analyze experimental data obtained from PELDOR experiments on spin pairs in disordered powder samples, two different limiting cases can be considered accounting for selective pulse excitation and the resulting orientation selection. The first limit is strong angular correlation between the spin centers. Here, the Euler angles describing the transformation from the A spin principle axis system (PAS) to the PAS of the B spin have to be explicitly treated (section 1.2.2.1). The second limit is the neglection of angular correlations between the two spin centers, leading to a random distribution of Euler angles, which is often a fairly good approximation for systems containing flexible spin-labels (section 1.2.2.2). If there is more than one B spin coupled to the A spin, which is always true for samples at finite dilution, the theory can be extended to multiple spin centers (section 1.2.2.3). In the following the theory for both limits of correlation, as well as the extension to multiple spin centers in one molecule or cluster, will be summarized and discussed.

1.2.2.1.   Limit of Strong Angular Correlation

Considering a PELDOR experiment on a single spin pair in a fixed mutual orientation and in a unique orientation with respect to the magnetic field **B**, and assuming that the spin-orientations are not changed due to spin diffusion or spin-lattice relaxation, $V(t)$ can be described by eq. 1.18.[23]

$$V(t) = V_0 \left(1 - \lambda \left[1 - \cos(\omega_{AB} t) \right] \right) \qquad (1.18)$$

where V_0 is the A spin echo intensity at $t = 0$ as a fuction of ν_A and λ is the fraction of B spins which are coupled to the detected A spin and inverted by the pump pulse as a function of ν_A and ν_B. λ and ω_{AB} depend on the polar angles (ϕ and ψ) specifying **B** in the A spin molecular axis system, λ also depends on the set of Euler angles (Ω) describing the orientation of spin B in the axis system of spin A. For a definition of the angles see Figure 1.2.3.
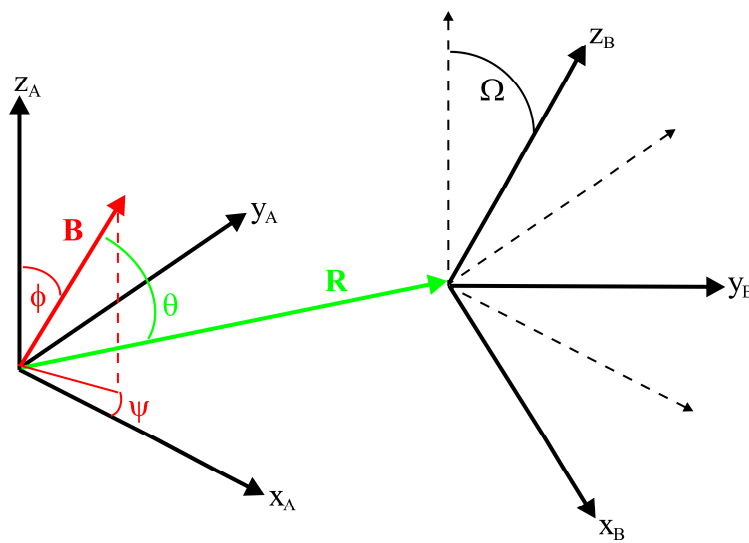

Figure 1.2.3. Graphical representations of the angles in eq. 1.18.
Ω is the set of Euler angles describing the transformation of the A spin PAS to the B spin PAS.

In principle, $V(t)$ and λ also depend on B_0, but the magnetic field is usually kept constant during PELDOR experiments. In the secular approximation, described in chapter 1.2.1, the spin-spin coupling is given by the sum of the dipolar and exchange coupling (eq. 1.19).

$$\omega_{AB} = \omega_{dd} + J \qquad (1.19)$$

For disordered powder samples, such as frozen solutions, eq. 1.18 has to be integrated over a sphere to represent all orientations of the A-B spin pair – which is still in a unique mutual orientation – with respect to the magnetic field (eq. 1.20).

$$V(t) = \int\limits_{0}^{2\pi} \int\limits_{0}^{\pi} V(t) \sin \phi \, d\phi \, d\psi \qquad (1.20)$$

The pump efficiency λ in eq. 1.18 is dependent on the relative orientation of the two paramagnetic centers A and B, described by Ω. Additionally, the orientation selectivity of the excitation of spin A described by V_0, in combination with the orientation selectivity of ν_B, will lead to a distribution function $P(\theta)^{[21]}$ of dipolar angles differing from the $\sin(\theta)$ distribution of a random distribution, which results in a spectrum resembling the Pake pattern (Figure 1.2.4).[36] The echo signal intensity for a given pump and detection frequency in such a general case is described by eq. 1.21.

$$V(t) = V_0 \left(1 - \left[\int\limits_{0}^{\pi/2} P(\theta) \left[1 - \cos(\omega_{AB} t) \right] d\theta \right] \right) \qquad (1.21)$$

with

$$P(\theta) = \lambda(\theta) \sin \theta \qquad (1.22)$$
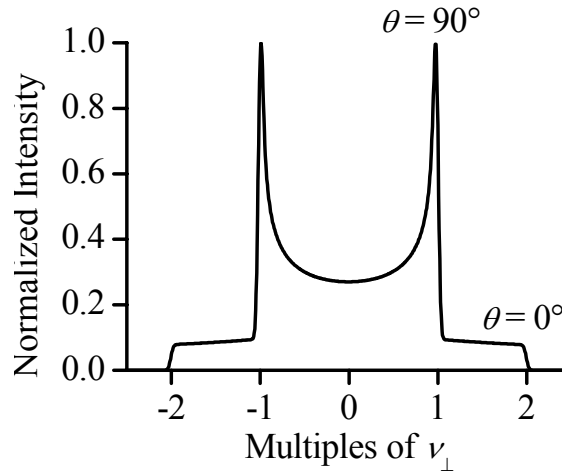

Figure 1.2.4. Pake pattern for disordered powder samples.
This pattern resembles the pattern observed after Fourier transformation of PELDOR data. In case of cw spectra the peak-to-peak distance corresponds to $\nu_\perp$ and the edge-to-edge distance to $2\nu_\perp$.

Presuming that the spin Hamiltonian parameters of A and B, their mutual orientation, and the distance vector are known, the signal response can be calculated from the experimental parameters according to eq. 1.21.

In case of spin-density distributions the dipolar interaction tensor is averaged over all spin bearing centers leading to a rhombic interaction matrix. Its elements d_{ij} in the A spin PAS are described by eq. 1.23:[37-40]

$$d_{ij} = -\frac{\mu_0 \mu_B^2}{4\pi\hbar} g_A g_B \sum_m \sum_n \rho_m \rho_n \frac{R_{mn}^2 \delta_{ij} - 3R_{mni} R_{mnj}}{R_{mn}^5} \qquad (1.23)$$

where δ_{ij} is the Kronecker delta, m and n are the spin bearing atoms at centers A and B respectively, ρ are their respective spin densities, R_{mn} the respective interatomic distances, and R_{mni} and R_{mnj} are the i and j components of the interatomic distance vectors in the A spin PAS. The sums extend over all point-charges that constitute the interacting spins. In this logical extension of the point-dipole approximation the **g**-tensors are still assumed to be isotropic.

1.2.2.2.   Uncorrelated Spin Centers

For flexible biradical systems, as often achieved by spin-labeling biomolecules, the situation simplifies due to full averaging of the mutual orientations, so that integration over Ω will diminish the orientation dependence of λ. Within this limit the integration over all magnetic field orientations, as given in eq. 1.20, can be converted into integration over all dipolar angles θ (eq. 1.24).[21]

$$V(t) = V_0 \left(1 - \lambda \left[1 - \int_0^{\pi/2} \cos(\omega_{AB} t) \sin\theta d\theta \right] \right) \qquad (1.24)$$

The modulation frequency of the signal described by eq. 1.24 only depends on the spin-spin coupling and therefore on the dipolar coupling constant and the exchange coupling. If the latter can be neglected, as usually approximated, only the spin-spin distance and **g** are contributing to the oscillation frequency. In the common case of two identical nitroxide spin probes, **g** is well known and thus the distance is the only variable in the analysis of the data.

This is the basis of data analysis via cosine Fourier Transformation (FT) and data inversion using Tikhonov regularization methods, as described in sections 1.2.2.4 and 1.2.2.5, respectively.

Godt and coworkers introduced 'orientational averaging' by adding several time traces with different pump and detection frequencies. This should essentially lower the effect of angular correlations, even in the case of strongly correlated biradicals, but it has not been proven that the resulting form factor corresponds to the one of a Pake pattern.[22]

1.2.2.3.   Multiple Spin Centers

PELDOR experiments are performed at sample concentrations demanding explicit treatment of intermolecular spin-spin couplings, as the coupling to other biradicals present in the sample will affect the intramolecularly coupled A-B pairs. The additional intermolecular contributions are multiplicative for all additional coupling partners[41] and cause a decay of the echo. For a homogeneous three-dimensional distribution of radicals without angular correlations or excluded volumes the signal exhibits a monoexponential decay (eq. 1.25).[42]

$$
\begin{aligned}
V_{\text{inter}}\left(t\right) &= V_0 \exp\left(C \cdot f\left(t\right)\right) \\
f\left(t\right) &= \lambda \int_0^\pi 2\pi \sin\theta \, d\theta \int_0^\infty \left[1 - \cos\left(\omega_{\text{AB}} t\right)\right] R^2 dR
\end{aligned}
\tag{1.25}
$$

Here C is the volume concentration of spins. The integration over R can be performed approximating the intermolecular exchange coupling to be negligible versus the intermolecular dipolar coupling, which results in eq. 1.26.

$$
f\left(t\right) = -\frac{2\pi g^2 \mu_B^2 \mu_0}{9\sqrt{3}\hbar} \lambda t
\tag{1.26}
$$

If the distribution is homogeneous in a lower dimensionality, as for example two-dimensional distributions in membranes, the signal will exhibit a stretched exponential decay.[43] The overall signal arising from the finite sample concentration (eq. 1.25), and the response of the specific A-B pair (eq. 1.20), is the product of both contributions (eq. 1.27).[42-44]

$$V(t) = V_{\text{intra}}(t) V_{\text{inter}}(t) \tag{1.27}$$

In case of a homogeneous, disordered sample, the intermolecular contributions (V_{inter}) can be approximated monoexponentially and deconvoluted from the intramolecular signal. In the following, only the latter is discussed and the index 'intra' is omitted.

If more than two spins are coupled with specific distances and relative orientations, eq. 1.21 can be extended to n coupled spins.

$$V(t) = \frac{V_0}{n} \sum_{A=1}^{n} \int_0^{\pi/2} \prod_{\substack{B=1 \\ B \neq A}}^{n} \left\{ 1 - P_{AB}(\theta) \left[1 - \cos(\omega_{AB} t) \right] \right\} d\theta \tag{1.28}$$

The resulting signal is the sum of products of all A-B pairs, with their respective Euler angles Ω_{AB}, geometrical form factors P_{AB}, and spin-spin couplings ω_{AB}. The product of dipolar modulations for all B-spins is integrated over the dipolar angle θ, and summing all possible A spins tributes to asymmetry in relative orientations and distances. In the limit of uncorrelated spin centers $P_{AB}(\theta)$ can again be substituted by $\lambda \sin\theta$. Furthermore, a broad distribution of ω_{AB} values exists in disordered samples. Therefore, the $\cos(\omega_{AB} t)$ term in eq. 1.28 will interfere to zero for times $t \gg \omega_{AB}^{-1}$, and $V(t)$ will tend to its limit V_λ, which is the value of $V(t)$ where the signal oscillation is completely damped. Normalizing to $t = 0$ and assuming identical B spins, V_λ can be written in the form of (eq. 1.29).[20]

$$V_\lambda = V(t \to \infty) = (1 - \lambda)^{(n-1)} \tag{1.29}$$

From eq. 1.29 follows that the number of radicals (n) in a cluster is (eq. 1.30):

$$n = \frac{\ln V_\lambda}{\ln(1 - \lambda)} + 1 \tag{1.30}$$

Thus, V_λ values factorize for uncorrelated, similar B-spins. For example, V_λ of a triradical can be described as the square of V_λ of a biradical, and V_λ of a tetraradical as the cube of V_λ of a biradical. This approximation will not be valid if the coupling spins belong to radicals with different spectral widths. In that case, the different λ values have to be explicitly taken

into account. If $\lambda \ll 1$, then eq. 1.29 can be expanded in a power series and all terms nonlinear in λ can be neglected, leading to eq. 1.31, which is also named 'linear approximation'.[20]

$$V_\lambda = 1 - \lambda(n-1) \tag{1.31}$$

The only free parameter in the calculation of n is λ, which can be determined experimentally using a standard biradical.

1.2.2.4. Fourier Transformation

Fourier transformation (FT) is the common approach to analyze the frequency responses in time domain spectroscopy. This transformation is based on the unique correspondence between time and frequency domain signals. A given signal in the time domain ($s(t)$) can be directly transformed to the frequency domain signal ($S(\omega)$) by eq. 1.32.

$$S(\omega) = \int_{-\infty}^{\infty} s(t) \cdot e^{-i\omega t} \cdot dt \tag{1.32}$$

The inverse transformation is given by eq. 1.33.

$$s(t) = \frac{1}{2\pi} \int_{-\infty}^{\infty} S(\omega) \cdot e^{i\omega t} \cdot d\omega \tag{1.33}$$

These two transformations are fully symmetric and allow extraction of the spin-spin coupling frequencies (ω_{AB}) contributing to the PELDOR time domain signal. Several fundamental theorems, like the 'Similarity Theorem', the 'Shift Theorem', the 'Sampling Theorem', and the 'Convolution Theorem', underlie the processing of time domain data in the frequency domain and vice versa.[7] This is especially important for filtering and deconvolution of spectra. In general, V_{inter} is removed from PELDOR time traces, then they are 'windowed' with an apodisation function to modify the envelope of the truncated signal, and zero filled to increase the frequency resolution. The real part of the Fourier transformed

(of the real part of the quadrature detected complex dataset) corresponds to the cosine Fourier transformed, resembling the spin-spin couplings contributing to the time trace.

Several remarks have to be made concerning data acquisition and reliability of the spectra obtained. The highest frequency that can be retrieved is the 'Nyquist frequency' (f_N), which is determined by the sampling rate (f_s), or in other words, by the resolution in the time domain.

$$f_s = \frac{1}{\Delta t} = 2 f_N \tag{1.34}$$

The frequency resolution Δf is given by the length of the time trace t_{max}

$$\Delta f = \frac{1}{t_{max}} \tag{1.35}$$

Within these boundaries all frequencies can be resolved. If, as most common, only one sharp peak is resolved after FT, and only weak angular correlation is expected, this peak is taken to correspond to the singularity of the Pake pattern at $\theta = 90°$ (Figure 1.2.4), which is usually the most prominent feature.

Angular correlation does not hamper spectral analysis in the frequency domain, but distance distributions lead to a nonlinearity in the broadening of the frequency peaks, due to the inverse cubic dependence between spin-spin distance and dipolar frequency.

1.2.2.5. Tikhonov Regularization

In the limit of negligible angular correlation the modulation depth parameter λ is independent of the dipolar angle θ. Thus, frequencies contributing to the signal in eq. 1.24 only depend on ω_{AB} and can be calculated, if the dipolar coupling $\nu_\perp$ and the exchange coupling J are known. If J is approximated to be zero, only the distance R between the two spins will alter the frequency contributions to the time domain signal. In the case of distributions of distances, FTs exhibit broad peaks, and the distance information obtained from FT are rather unreliable. However, a known distance distribution function $P(R)$ allows straightforward calculation of the signal $V(t)$. The inverse problem is ill-posed and the inversion is becoming highly unstable with experimental noise. One way to circumvent this problem is the use of regularization methods, such as Tikhonov regularization.[45]

These methods have been implemented into several computer programs for the analysis of PELDOR data.[46-50] In these approaches, the simulated signal $S(t)$ is described by a Kernel function $K(t, R)$ and the distance distribution function $P(R)$ (eq. 1.36):

$$S(t) = \int_{R_{min}}^{R_{max}} K(t,R)P(R)dR$$

$$K(t,R) = \int_0^1 \cos\left[(3x^2 - 1)\omega_\perp t\right]dx \qquad (1.36)$$

$$x = \cos\theta$$

Minimizing the square deviation between the simulated and the experimental data leads to a solution of the inverse problem. Assuming that physically reasonable distance distributions are smooth, the function is weighted with the smoothness of the distance distribution (η), given by the square norm of its second derivative, multiplied by the regularization parameter α (eq. 1.37).

$$G_\alpha\left(P(R)\right) = \left\|V(t) - S(t)\right\|^2 + \alpha\left\|\frac{\partial^2}{\partial r^2}\left(P(R)\right)\right\|^2$$

$$\rho_\alpha = \left\|V(t) - S(t)\right\|_\alpha^2 \qquad (1.37)$$

$$\eta_\alpha = \left\|\frac{\partial^2}{\partial R^2}\left(P(R)\right)\right\|_\alpha^2$$

Here, G_α is the overall function to be minimized, ρ is the quality of the fit in the time domain and the index α refers to the regularization parameter, because different α will lead to different results for ρ, η and thus G. α is optimized using the 'L-curve criterion'. By inverting the data for different values of α and plotting η_α versus ρ_α on a double logarithmic scale, the so-called L-curve can be constructed. The optimum α-value corresponds to the kink of the L-curve (Figure 1.2.5).[47] At this point the fit of the data is not much improved upon reduction of α. On the other hand, the fit becomes much worse if α is enlarged, and thus the optimum compromise of a physically reasonable distance distribution fitting the experimental data is achieved. Subsequent maximum entropy regularization methods increase the tolerance

towards experimental noise and stabilize the output of the ill-posed inversion, usually the regularization is constrained to non-negative $P(R)$.[51]
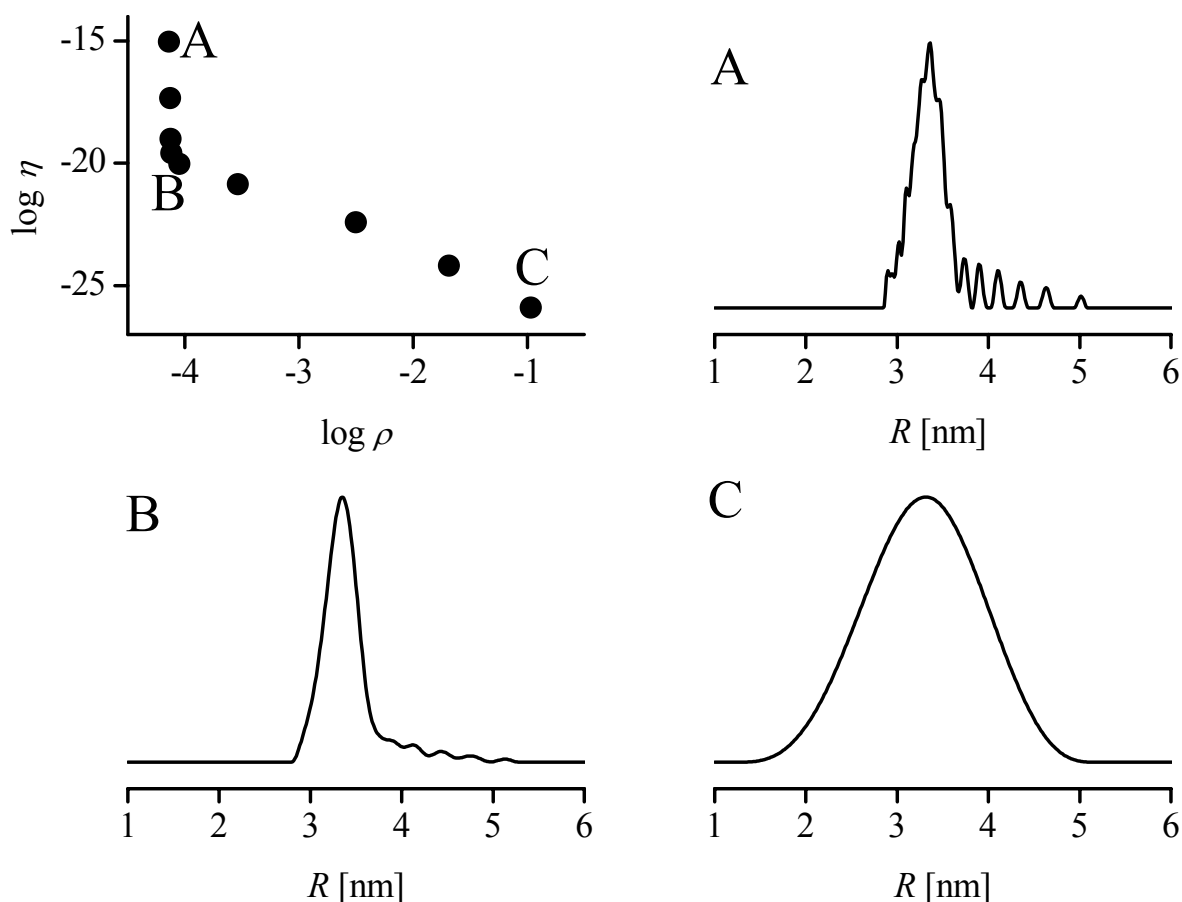

Figure 1.2.5. The so-called L-curve and three distance distributions as obtained by Tikhonov regularization. A ($\alpha = 0.001$) very good fit but unphysical, B ($\alpha = 10$) good fit and physically reasonable, C ($\alpha = 100000$) very broad distribution, very bad fit.

1.2.3. Further Pulse EPR Methods for Distance Measurements

In this chapter, a short summary of further pulsed methods used for nanometer distance measurements is given. For a more details concerning these methods and their applications, the interested reader is referred to several excellent reviews.[13, 15-17, 28]

Depending on the properties of the spin centers and instrumental aspects a variety of pulse sequences can be employed in pulse EPR distance measurements. A method similar to PELDOR, that only requires one microwave source and allows to work with more critical coupling of the resonator, is the '2+1' method (Figure 1.2.2 A; $\nu_A = \nu_B$).[52, 53] The major drawbacks of '2+1' in comparison with PELDOR is the loss of freedom to adjust the two

microwave frequencies independently and that high excitation bandwidths lead to strong superposition of dipolar and unwanted nuclear modulations.[54]
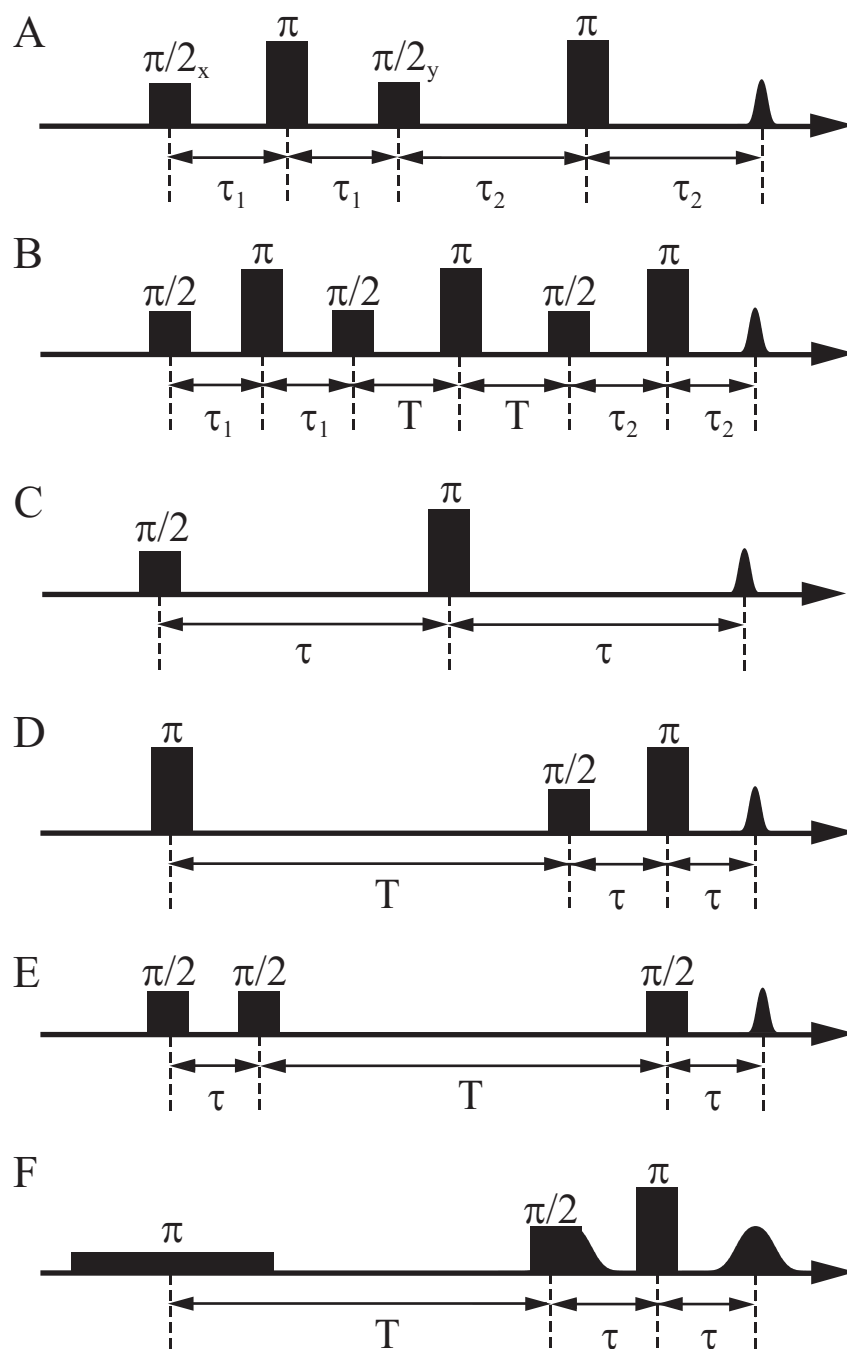

Figure 1.2.6. Further pulse EPR sequences for distance measurements.
A: Solid-Echo SIFTER; B: six-pulse DQC; C: Hahn-echo; D: Inversion and saturation recovery; E: stimulated echo; F: selective hole burning.

The use of the solid echo sequence known from NMR[29] has also been demonstrated for EPR (Figure 1.2.6 A). To efficiently refocus off-resonant spins, two π-pulses have been inserted to yield the single-frequency techniques for refocusing (SIFTER).[55] Here, the

dipolar coupling can be monitored as an echo modulation as a function of τ_2-τ_1. This experiment suffers from incomplete excitation, leading to unwanted contributions to the echo modulation. Due to these disadvantages, the method is not as established as PELDOR or double quantum coherence (DQC) [56] filtered EPR.

In DQC filtered EPR (Figure 1.2.6 D) the dipolar coupling is separated from other coherences by introducing a double quantum filter in analogy to liquid state NMR.[57] In principle, this experiment requires the complete excitation of the EPR line which is extremely challenging with common EPR signal widths. Borbat and Freed have shown that such an experiment can be successfully carried out using a home-built K-band (17 GHz) spectrometer with a sufficiently high B_1 field.[58] In a six-pulse sequence,[59] using an appropriate phase cycle, the dipolar coupling can be separated from other coherences. Unwanted nuclear modulations can only be partially suppressed with the commercially available microwave field strengths.[60] It is tempting to assume that the general success of this method will depend on the commercial availability of microwave field strengths an order of magnitude higher than today.

All single-frequency methods described so far require that the coupled spins exhibit slow relaxation rates and can be sufficiently exited by the microwave pulses at the detection frequency. In contrast, relaxation based methods, as described in the following, only need one of the spin centers to be relaxing slow enough to be detected, whereas the dipolar coupling is affecting the detected spin by relaxation. Theoretically, the mechanism altering the spin state of this coupled spin is not of importance – be it a microwave pulse or longitudinal relaxation. However, it is obvious that the B spin flip induced by relaxation cannot be coherent, in contrast to the inversion by a microwave pulse. On the other hand, relaxation based methods allow to investigate centers, which relax to fast to efficiently detect or invert them. If the relaxation processes of the two spins are not correlated, the total relaxation rate of the A spin will be a product of the intrinsic relaxation and the dipolar relaxation rate.[41] Thus, the dipolar relaxation can be isolated, in case that the intrinsic A spin relaxation can be studied independently.

For a B spin longitudinal relaxation rate ($1/T_1$) in the order of ω_{dd}, the enhancement of the A spin transverse relaxation will be maximum.[61] The dipolar coupling can be studied by monitoring the A spin transverse relaxation via a Hahn echo decay (Figure 1.2.6 C).[41, 62, 63] Temperature-dependent studies allow identification of the dipolar coupling, since relaxation is temperature dependent in contrast to ω_{dd}.

Furthermore, if the longitudinal relaxation rate of the B spin is in the same range as the Zeemann splitting of the A spin, the longitudinal relaxation rate of the latter will be enhanced via the dipolar coupling. This can be studied utilizing an inversion recovery or saturation recovery sequence (Figure 1.2.6 D).[64, 65] In inversion recovery experiments the first pulse is an unselective π-pulse inverting the M_z magnetization, whereas the first pulse will be replaced by a saturation pulse or pulse train, if saturation recovery is studied. Again, temperature-dependent studies permit finding the optimal temperature for the strongest relaxation enhancement, and thus identification of the dipolar coupling.

A further method for accessing dipolar couplings between a slow and a fast relaxing species is relaxation induced dipolar modulation enhancement (RIDME).[66] In a stimulated echo sequence (Figure 1.2.6 E) the first two $\pi/2$-pulses create an M_z magnetization that is grated with a periodicity of $1/\tau$ as a function of the resonance frequency offset $\Delta\omega_A$. The signal is recorded as an echo-like free induction signal, which forms at the time τ after the third $\pi/2$-pulse. If the Lamor frequency of the A spin changes due to a flip of the fast relaxing B spin during the evolution period T between the second and the third pulse, the echo will dephase. This will be most efficient if the A spin Lamor frequency jumps from a minimum of the grating to a maximum. Thus, the signal will be periodically modulated by the dipolar coupling in case of a variation of τ, assuming that T is chosen long enough for the B spin longitudinal relaxation to efficiently alter ω_A. Since this method is strongly susceptible to unwanted hyperfine modulations, it performs best at high fields, where these modulations are suppressed.[67] It also bears the drawback of a considerable dead-time.

An analogous, dead-time free method has been invented based on selective excitation.[68, 69] It relies on spectral hole burning in the A spin spectrum by a selective π-pulse, in the order of microseconds in length. During the evolution period T, spin flips of B spins will alter the Lamor frequency of spin-packets by $\pm\omega_{AB}$, thereby superimposing the spin-spin coupling with the spectral hole. A non-selective $\pi/2$-pulse allows recording the free induction decay (FID) of this spectral hole, which is modulated with ω_{AB}. To achieve a dead-time free measurement, the FID can be refocused by a non-selective π-pulse (Figure 1.2.6 F). By measurement with and without the hole-burning pulse, the overlapping Hahn echo can be subtracted from the refocused FID.

In a general case of a dipolar coupled A-B spin pair, a variety of methods can be used to determine the dipolar coupling. In the following their advantages and disadvantages are

summarized. PELDOR and '2+1' require the T_2 of the A spin to be long enough for reasonable detection time windows, and the T_1 of the B spin to permit efficient coherent inversion. DQC and SIFTER demand excitation of the whole spectrum, as well as transversal relaxation rates T_2 slow enough for detection of the signal. Relaxation-based measurements can be applied for fast and very fast relaxing B spins, but the experimentally observed effects, due to dipolar couplings are smaller and non-oscillating, as they rely on the statistic nature of B spin flips, and not on coherent inversion by microwave pulses. Only PELDOR and two-dimensional DQC[28] experiments give rise to studying arbitrary combinations of sub-ensembles of A and B spins, which are only limited by spectrometer hardware. The use of two microwave frequencies introduces an additional degree of freedom, even though this increases the experiment's technical demands.

1.3. Applications of PELDOR Spectroscopy in Literature

This chapter gives a review of PELDOR-studies that have been published in literature. As outlined in section 1.1.1, the number of publications, especially those involving biologically relevant systems, has dramatically increased in the past years. Section 1.3.1 describes the experimental calibration and technological development gained on model compounds. In section 1.3.2 applications in material science are summarized, followed by measurements on spin-labeled peptides and proteins (1.3.3), spin-labeled nucleic acids (1.3.4) and experiments involving metal centers (1.3.5).

1.3.1.   Nitroxide Model Systems

The PELDOR experiments have been initially calibrated and further methodological achievements have been evaluated employing model systems. In the very first work, the distance distribution between nascent hydrogen atoms and their parent hydroquinone radicals have been estimated.[18] Milov *et al.* have also been the first to use nitroxide biradicals, exhibiting well resolved dipolar modulations, allowing to estimate distances[19] and to deduce the number of coupled spins from the time domain signal.[20] They have also established the acronym DEER, which still splits the EPR community in the usage of DEER and PELDOR to describe one and the same method.

The first evaluation of orientation selection has been performed by Singel and Larsen on a twofold nitroxide labeled anthracene.[21]

The end-to-end distances in several alkyl-linked bisnitroxides have been compared quantitatively to a more rigid anthraquinone linked bisnitroxide in the Spiess group.[70] The same group has also invented the dead-time free version of the method, and has demonstrated it on five rigid nitroxide biradicals with spin-spin distances of 1.4 to 2.8 nm.[30] In 2000, the asymmetric four-pulse sequence commonly applied today has been introduced using rigid bisnitroxides and the adduct of a tetraalkylammonium-labeled poly(isoprene) with the potassium-carboxylate of 4-carboxy Tempo (2,2,6,6-tetramethyl-piperidine-1-oxyl) exhibiting a signal differing from a random distribution.[31] In the same year, the library of model systems has been extended to bisnitroxides with spin-spin distances of up to 5.1 nm and the first nitroxide triradical, but no experimental data was presented.[71] In 2002, the dipolar coupling has been separated for the first time from the exchange coupling by

PELDOR via a series of actetylene- and similar ester-bridged bisnitroxides measured at X-band and S-band (3 GHz) frequencies.[72]

In combination with the invention of the variable time PELDOR experiment the measurement of a 7.5 nm distance was reported by Jeschke and coworkers.[32] They also synthesized ^{15}N and ^{2}H isotope-labeled nitroxides and biradicals.[73] In mixtures of both systems, the individual distances have been separated by either choosing spectral positions, which preferentially select one nitrogen isotope or by applying a deuterium hyperfine filter on a 2-dimensional PELDOR dataset. A study on the relative orientations of a nitroxide bi- and triradical, measured by W-band (95 GHz) PELDOR and compared to MD predictions, has been reported by Polyhach *et al.*[74] Margraf *et al.* have determined the conformational flexibility of nitroxide biradicals by PELDOR measurements using different detection frequencies and explicit simulations of the time domain data.[75]

Until now, a large library of nitroxide model compounds exists, that allows benchmarking PELDOR for applications in material and biological sciences. Not only the accuracy and applicability of the experiment, but also the methods for inversion of the time domain data to the frequency domain have been evaluated and optimal experimental settings have been established using this pool of samples.

1.3.2. Material Science

Even though the majority of the published PELDOR studies concerns distance measurements in model systems, peptides, and proteins, there are several applications in material sciences. Some of the work on model systems can be considered to have an impact on material sciences, as the linkers of bisnitroxide model systems often represent building blocks of organic polymers. Already in 1996, the distances obtained from alkyl-linked bisnitroxides have been correlated with conformational statistics on alkyl chains.[70] Milov and Tsvetkov have derived the dimensionality of the pair distribution function of spin-labeled poly(4-vinyl) pyridine by concentration dependent measurements. Assuming a homogeneous intermolecular distribution, a fully extended linear conformation of the polymer was concluded.[76]

Above all the distribution of paramagnetic anions coordinated to ionic polymers is well studied. Milov *et al.* have examined the repulsion of ionic spin probes in solutions of low ionic strength, e.g. Fremy's salt in frozen glassy solution (a mixture of glycerol and water).[77] Pannier *et al.* have determined ion cluster sizes and cluster-to-cluster distances in ionomers

by PELDOR, and established the method for these samples referring to earlier small angle X-ray scattering (SAXS) data.[78] For ionically functionalized diblock copolymers, the same group has shown that the ion clusters do not depend on the topology of the ionomer and polymer chain length.[79]

The co-conformations of nanosized [2] catenanes were analyzed by Jeschke and Godt. Interestingly, except for small macrocycles, the aliphatic chains of the two interlocked ring systems have been found to be fully extended in frozen chloroform solution, but partially collapsed in glassy *ortho*-terphenyl.[80] Hinderberger *et al.* found that a polyelectrolyte solution of poly(diallyldimethylammonium chloride) mixed with low concentrations of Fremy's salt exhibits an equilibrium between 20% directly bound, and 80% not directly bound to the polyelectrolyte-coordinated divalent anions, by assuming the time domain signal decay to be a superposition of a homogeneous bulk distribution and a linear distribution along the polyelectrolyte chain.[81] Applying the same principle, Fremy's salt has been attached electrostatically to rodlike Ru^{2+} coordination polymers. Due to the choice of non-coordinating anions of the polymer and the interaction of divalent anions with divalent cations, the attachment is almost quantitative. The distances measured between the anions of Fremy's salt reflect the Ru^{2+}-Ru^{2+} distances in the polymer.[82]

In an oligomerization study of coiled-coil copolymers, consisting of an α-helical peptide conjugated to a poly(ethylene glycol), the peptide could be spin-labeled, and thus a parallel arrangement of α-helices upon oligomerization of these nanoobjects has been concluded from PELDOR data.[83] In a study of polymer-clay nanocomposites employing surfactant spin probes, the slow-down of the exponential intermolecular PELDOR decay showed that the clay intercalated into the polymer.[84] Recently, a structural picture of such composites has been derived from PELDOR, electron spin echo envelope modulation (ESEEM) and electron nuclear double resonance (ENDOR) data.[85]

A very detailed study of micelles built from copolymers of poly(ethylene oxide) and poly(propylene oxide) has been published by the Goldfarb group. Nesting the hydrophobic 4-hydroxy-tempo-benzoate in the core of the micelles, the hydrophobic core radii and aggregation numbers for different polymers could be derived.[86]

The flexibility of doubly nitroxide labeled oligo(*para*-phenyleneethylenes) has been derived from PELDOR data in combination with MD and time trace simulations. Noteworthy, the analysis of the time domain data points to a backbone bending potential that is only half of the value expected from MD studies.[22] By a combination of PELDOR and

EPR imaging, Jeschke and Schlick have studied the nitroxide radical formation from stabilizers during the thermal degradation of poly(acrylonitrile-butadiene-styrene) copolymers. The spatial profiles of radical concentrations have been characterized, and a significant formation of biradicals could not be concluded from the PELDOR signal.[87]

The lateral diffusion of thiols on gold nanoparticles has been monitored via PELDOR on thiol functionalized nitroxides attached to the surface of the nanoparticles. Initially the nitroxides were covalently linked to biradicals. After cleavage of the ester linker, diffusion of the thiols was monitored, and no lateral mobility was found at room temperature.[88]

1.3.3. Peptides and Proteins

1.3.3.1. Spin-Labeled Peptides

A first example of the application of PELDOR on spin-labeled peptides was published in 1999. Milov *et al.* studied the peptabiol antibiotic trichogin, which had been doubly labeled with 2,2,6,6-tetramethyl-piperidine-1-oxyl-4-amino-4-caboxylic acid (TOAC).[42] The distance of 1.97±0.1 nm indicates a 2_7-helix formed in frozen chloroform/dimethylsulfoxide solution. To test whether the antibiotic activity is, as proposed, due to self assembly in the membrane, trichogin GA IV was labeled with TOAC at three different positions. In a chloroform/toluene mixture these peptides formed helix bundles with an aggregation number of $n = 4.0\pm0.3$, as determined from the modulation depth parameter V_λ, whereas addition of ethanol led to monoexponential decays, indicating dissociation of the complex. In combination with distance constraints, a structural model has been obtained that consists of tetrameric helix bundles of 3_{10}-helices.[89, 90] This was confirmed one year later by mixing the doubly labeled peptide with unlabeled trichogin.[44] Additionally, the helicity strongly depends on the used solvent.[91] Using head-to-tail linked dimeric trichogin constructs, the aggregation to dimers of dimers or dimers of trimers occurred in dependence of concentration in chloroform/toluene, whereas aggregation could not be observed in methanol. Interestingly, the covalently linked dimers exhibit α-helical secondary structures.[92] Monitoring concentration dependence led to a proposed mechanism of preformed dimers, aggregating to dimers of dimers. Both equilibrium constants could be estimated.[93] It has been further demonstrated that trichogin only oligomerizes in dipalmitoyl phosphatidylcholine membranes at higher concentrations to dimers,[94-96] doubly labeled peptides, however, are partly α-helical and partly extended 3_{10}-helical in these membranes as inferred from distance

measurements.[97] The aggregation states and secondary structures of two other antibiotics of fungal origin, zervamicin IIA[98, 99] and alamethicin,[100-102] have been investigated by the same authors.

The lengths and flexibilities of five end-labeled bis-peptide nanostructures have been determined using PELDOR by Pornsuwan *et al*. The distance distributions centered at 2.4 to 3.5 nm exhibit widths increasing with the distance.[103] The distances are smaller than predicted from MD, leading the authors to conclude that MD progressively underestimates the flexibility of these structures. A systematic study employing a geometric model and optimizing force field parameters has been published.[104]

The neurotoxicity of the 42-mer and 40-mer amyloid β peptides is closely related to radical formation at tyrosyl 10 and subsequent reaction with methionine 35. PELDOR measurements on double cysteine mutants indicate that the two amino acids are closer in space in the 42-mer, which could partly explain its stronger neurotoxicity.[105]

1.3.3.2. Paramagnetic Protein Cofactors

Paramagnetic cofactors in proteins have been extensively investigated by distance measurements: (experiments involving metal centers are discussed in section 1.3.5) In particular trapped non-polarized radical pairs in Photosystem II (PS II) have been characterized, initially using the '2+1' pulse train. For spin-polarized radical pairs the reader is referred to reference [15]. By '2+1', the distances between the cation radicals of tyrosine D ($Y_D^{+\bullet}$) and tyrosine Z ($Y_Z^{+\bullet}$),[106] and the angle of the distance vector with respect to the membrane normal have been determined.[107] Also the distance between $Y_D^{+\bullet}$ and the quinone radical anion $Q_A^{-\bullet}$, as well as the orientation of **R** have been measured by '2+1'.[108] For the chlorophyll *Chl Z*$^{+\bullet}$/$Y_D^{+\bullet}$-pair, the distance[109] and orientation of **R**[110] have been derived by the same method. Using the PELDOR experiment, the distance between $Y_Z^{+\bullet}$ and $Q_A^{-\bullet}$ has been proven to be 3.45 nm.[111] The three spin systems $Y_D^{+\bullet}$/$Y_Z^{+\bullet}$/$Q_A^{-\bullet}$ and $Y_D^{+\bullet}$/$Q_A^{-\bullet}$/*Chl Z*$^{+\bullet}$ have been studied by PELDOR allowing to extract the previously unknown $Q_A^{-\bullet}$/*Chl Z*$^{+\bullet}$ distance of 3.4 nm.[112] The so-called 'doublet signal' in PS II has also been subjected to PELDOR measurements concerning the radical center's orientation and distance with respect to $Y_D^{+\bullet}$.[113]

Another subject of PELDOR studies is the enzyme ribonucleotide reductase (RNR), which catalyzes the reduction of nucleotides to 2'-deoxynucleotides in all organisms. The

initial radical is localized on a tyrosyl in subunit R2, from which the electron is transferred to the active site in R2. Initial work by Bennati *et al.* on RNR from *Escherichia coli* (*E. coli*) has proven the presence of two radicals in an R2 homodimer and the distance was found to be 3.31±0.02 nm.[114] The setup of a high frequency PELDOR spectrometer working at G-band (180 GHz)[115-117] has yielded orientation-selective measurements by Denysenkov *et al.*, revealing the relative orientation of the two R2 subunits in the homodimer.[118] The mutual orientation indicates a slight rearrangement of the tyrosyls with respect to the orientation of the unreduced tyrosyls as present in the crystal structure. The same measurements were also performed on the mammalian mouse RNR, allowing to deduce the distance[119] and the orientation[120] of the two tyrosyl radicals, indicating that at least some mammalian R2 subunits are homodimers. Inhibition of the active site in R1 gave rise to the distance measurement of the radical initiation pathway, supporting the model of long range electron transfer initiation in *E. coli*.[121] Recently, the electron transfer pathway has been studied by site-specific incorporation of the radical traps 3-hydroxy-tyrosine (DOPA) and 2-amino-tyrosine (NH_2Y).[122]

Furthermore, by inducing two neutral flavin radicals in Augmenter of Liver Regeneration the distance between the two monomers in the homodimer has been obtained by PELDOR.[123]

Recently, the distance and relative orientation of the spin polarized radical pair of $P_{865}^{+\bullet}$ and $Q_A^{-\bullet}$ from *Rhodobacter sphaeroides* has been gained from W-Band PELDOR, based on a stimulated echo sequence.[124, 125]

1.3.3.3. Spin-Labeled Proteins

A quantitative comparison of EPR methods for distance measurements on doubly MTSSL ((1-Oxyl-2,2,5,5-tetramethylpyrroline-3-methyl) methanethiosulfonate) labeled human carbonic anhydrase II was performed in the group of Eaton and Eaton. It has been concluded that distances measured by PELDOR bear more information than those from Fourier deconvolution or line shape simulation of cw spectra. This was the first example of a PELDOR measurement on a doubly spin-labeled protein.[126]

PELDOR and cw EPR was applied to the doubly MTSSL labeled inhibitory region of troponin. Even though only one PELDOR distance was obtained, it allowed to identify the region as α-helical in combination with dipolar constraints from cw EPR and MD, opposing theoretical models of a β-hairpin inhibitory region.[127] Structural changes induced by Ca^{2+}

binding have been quantified within the same system.[128] In human cardiac troponin C this change is predominantly observed in reconstituted fibers, as compared to the monomeric protein.[129]

The arrangement of the b-subunits of F_0F_1-ATP synthase from *E. coli* was studied by cw EPR at X- and W-band, and PELDOR. A parallel arrangement of helices in the tether domain was confirmed, and a previously proposed coiled-coil model expelled, by the obtained distance of 2.9 nm irrespective of labeling site.[130]

Accessibility and mobility studies by cw EPR in combination with PELDOR were performed on singly labeled mutants of the cytoplasmic domain of erythrocyte band 3 protein, an anion exchange protein stabilizing the erythrocyte membrane. The central dimer has been proven to be similar to the crystal structure by time traces exhibiting several clearly resolved dipolar modulations.[131] The mutant P327R of this protein, known as band 3 Tuscaloosa, causes hemolytic anemia. The cw EPR and PELDOR experiments performed on this mutant indicate that the arrangement of the central dimer is the same, but subtle changes occur close to the mutation site, increasing the structural heterogeneity by the population of subensembles.[132]

The manganese(II)-activated anthracis repressor from *Bacillus anthracis* regulates transcription. Metal binding was characterized by a combination of cw EPR and PELDOR studies. The formation of specific homodimers in absence of metal(II) ions was indicated by dipolar modulations in samples of singly nitroxide labeled protein.[133] Recently, the dimeric form has been investigated attaching three different spin-labels on three different cysteine mutants in presence and absence of Zn^{2+}. Mobility studies by cw EPR in combination with PELDOR distance measurements have shown that metal binding leads to a more rigid conformation as deduced from narrowed distance distributions. Higher rigidity was found especially in the DNA binding regions.[134]

The chemotaxis receptor-kinase assembly of *Termotoga maritime* has been structurally characterized by the Freed group using a combined PELDOR/DQC approach. The CheA domain P5 arrangement in complex with CheW subdomain 2, the individual structures had been derived from X-ray and NMR studies, has been calculated from 40 different long range constraints based upon dipolar couplings. A remarkable agreement with the crystal structure of the CheA(P4,P5):CheW complex was achieved.[135] Using a large number of constraints overcompensates deviations of single constraints. PELDOR and DQC measurements on spin-labeled histidine kinases are extensively reviewed regarding experimental and instrumental

aspects,[136] as well as the use of long range restraints for rigid body refinement of proteins.[137] A quantitative comparison of PELDOR and DQC has also been performed on twofold labeled human ubiquitin.[138] A proof of principle study by Sale *et al.* demonstrated that the accuracy of EPR constraints measured by cw EPR, T_1 relaxation enhancement, or PELDOR can be improved by explicit modeling of the spin-label.[139]

The characterization of the oligomerization of a von Willebrand Factor A domain proved a previously unknown, noncovalent protein-protein complex in solution.[140]

A human immunodeficiency virus type 1 (HIV-1) protease mutant has been studied by SDSL and PELDOR. A mutant known to stabilize dimer formation and bearing a single cysteine residue was labeled with two different nitroxides. Distance measurements on the protein in its inhibited and uninhibited states give evidence that the protein locks in the inhibited state in a conformation that covers the active site. In contrast, the uninhibited protease exhibits a wide distance distribution, corresponding to a range of conformations and a partially uncovered active site. This opens a framework for testing drug resistant mutants of HIV-1.[141]

Several mutants of the influenza hemaglutinin fusion domain have been studied by magnetic resonance and biochemical methods. PELDOR data obtained on four doubly spin-labeled double cysteine mutants in lipid bilayers indicate that mutants lacking large hydrophobic residues cause a fusion domain with higher flexibility, which is in agreement with NMR data. Therefore, the authors conclude that the kink in the helical fusion domain is locked by these residues.[142]

The Hubbell group performed PELDOR experiments on the arrestin oligomer found in the visual system. Eight spin-labeled cysteine mutants were subjected to PELDOR measurements after tetramerization of the protein. Deviations between the distance distributions obtained by Tikhonov regularization and the predictions obtained by modeling the spin-labels into the crystal structure guided the authors to the conclusion, that the crystal state is different from the native solution state. Indications for tetramerization from the modulation depth are not discussed.[143]

Distance measurements on a spin-labeled double mutant of the *Dictyostelium discoidicum* myosin II motor domain as a function of nucleotide state and actin binding revealed distances of 1.6 to 1.8 nm with distribution widths of 0.9 to 1.2 nm by cw EPR, and 2.3 to 2.5 nm with distribution widths of 1.7 to 2.3 nm by PELDOR.[144]

Based on cw EPR mobility studies and PELDOR distance measurements, Banham *et al.* found evidence that nitroxide spin-labels alter their conformation upon freezing in doubly labeled human hemoglobin.[145]

PELDOR data on spin-labeled proteins reconstituted in membranes or vesicles is sparse and modulations are often shallow. Nevertheless, there is an increasing number of studies on membrane proteins, as for example measurements on the flexible N-terminal domain in light harvesting chlorophyll a/b protein,[146] the Na^+/proline transporter PutP[147], the Na^+/H^+ antiporter NhaA[148], and the vitamin B_{12} transporter BtuB[149] all of *E. coli*, or lysophospholipid bound α-synuclein.[150] Recent studies on NhaA allowed modeling a high-resolution structure from the previously known monomer structure and a set of nine distance constraints obtained on dimers of the singly labeled protein.[151] BtuB distance distributions narrowed significantly upon binding of Ca^{2+} or Ca^{2+} and vitamin B_{12}.[152]

The mechanism of the receptor-catalyzed activation of the heterotrimeric G protein α subunit has been structurally investigated using cw EPR and PELDOR. Activation-dependent conformational changes in the α5 helix have been found. Based on this dynamic movement the authors discuss possible mechanisms of G protein activation.[153]

Another interesting system also studied by EPR is an F-BAR module from mouse. This homodimeric protein exhibits an antiparallel all-helical structure. The complex is curved and binds liposomes at the concave site, deforming them into tubules with variable diameters of up to 0.13 μm. The question of interest was whether the crystal structure obtained without liposomes reflects the membrane-bound state. PELDOR studies on dimers of singly labeled mutants revealed that the distance of 2.9 nm is the same in the soluble and membrane bound form, which is in good agreement with predictions based on the X-ray structure, suggesting a crystal-like dimer retained in both forms. The distance distribution is narrow, as evident from clearly modulated time traces.[154]

Borbat *et al.* observed a large-scale movement of the ATP-binding cassette (ABC) transporter MsbA from *E. coli* upon lipopolysaccharide binding and following ATP turnover. Distance changes of up to 3.3 nm between the two ABCs are involved. The authors discuss mechanistic implications of the conformational changes in ATP-powered transport.[155]

Light-induced conformational changes of *Natronomonas pharaonis* phoborhodopsin have been studied by Hayashi *et al.* Although the structure of the HAMP domain could not be clarified by PELDOR measurements, significant distance differences were observed between solubilized and reconstituted samples, indicating structural differences.[156] The importance of

membranes for the native structure has recently been found also for voltage dependent potassium channels.[157]

Conformational changes by effector binding were studied using nine doubly spin-labeled constructs of the lactose permease of *E. coli*. Changes in interspin distances of up to 2.1 nm measured by PELDOR indicate opposite movements of the cytoplasmic and the periplasmic end of transmembrane helices upon sugar binding.[158]

Phospholamban (PLN) regulates calcium translocation. It is known to form a monomeric and a pentameric form. Several membrane architectures have been proposed for the PLN pentamer. Based on liquid and solid-state NMR, cw EPR dynamics and PELDOR in micelles and membranes the so called 'pinwheel' conformation was proposed to be predominant in rabbit PLN, but that the sampling of all conformations and mediation by lipids is necessary for the molecular recognition by the interaction partners.[159]

Oligomerization studies on human and rat monoamine oxidase in membranes and detergent have yielded dimers in the membrane and ~50% dimer-like structures in detergent.[160]

By a combination of PELDOR distances and EPR accessibility studies high resolution atomic-detail computer simulation models of T4-lysozyme and αA-crystallin could be obtained with less than one constraint per four residues.[161]

In one example SDSL was combined with a natural cofactor, namely $Q_A^{-\bullet}$ of the reaction center of *Rhodobacter sphaeroides*. The measured distance of 3.05 nm is slightly longer than predicted from MD studies (2.8 nm), but this approach might allow to study electron transfer induced structural changes of the protein.[162]

1.3.4. Nucleic Acids

Recently, also nitroxide spin-labeled oligonucleotides have become subject of PELDOR studies. In a first experiment using nitroxides covalently bound to the 2'-carbon via an urea linker, a shallow modulation was observed, nicely matching the 3.5 nm distance from the structural modeling.[163] Bowman *et al.* performed PELDOR distance measurements also on 2'-labeled RNA duplexes using amide groups as linkers. A distance of 2.4 nm has been extracted via Fourier transformation for one duplex, and a peak at 1.8 nm in the distance distribution was acquired for the second duplex, all distances agree with the predictions.[49]

Schiemann *et al.* established a nanometer distance ruler on five doubly 2,2,5,5-tetramethyl-pyrrolin-1-yloxyl-3-acetylene (TPA) labeled DNA duplexes via PELDOR and

MD studies, showing an excellent distance correlation coefficient of 0.99.[164] The labeling scheme involves Sonogashira-cross-coupling to 5-iodo-2'-desoxyuridine during automated synthesis. The same approach was later on transferred to three RNAs using 5-iodouridines.[165] An extension to 2-iodoadenosine and 5-iodocytidine has allowed to study further spin-labeling positions, which also correlate well with MD-studies.[166, 167] For a detailed description of spin-labeling and experimental settings a protocol has been published recently by the same authors.[168]

Cai *et al.* reported a set of measurements of distances between 2.0 and 4.0 nm on duplex DNA dodecamers labeled via the phosphate backbone and also on a 68 base-pair DNA. One drawback of this labeling procedure is the presence of two diasteriomeric label configurations, which complicates data analysis. Comparison with molecular modeling resulted in a good agreement explicitly treating the spin-labels.[169] A more detailed computation of the nitroxide-nitroxide distances using MD studies and conformer search algorithms have been reported recently for two of the DNA systems.[170] The labeling method has been further optimized[171] and extended to six RNA duplexes. Distance from 2.5 to 4.7 nm have been measured and the correlation with the structural model exhibits an RMSD of only 0.17 nm.[172] Also for this labeling scheme a protocol has been published.[173]

Recently, Ward *et al.* have examined five doubly labeled DNA duplexes with spin-spin distances of 2.8 to 6.8 nm, and mixtures of the duplexes. The agreement of the distances with generic B-DNA models is good and the deconvolution of the distance distributions of simple mixtures was found to be quantitative.[174]

The structural transition from DNA B-form to A-form by high concentrations (> 70%) of trifluoroethanol was studied by Sicoli *et al.* The distance distributions obtained from PELDOR data on A- and B-form was quantitatively correlated to MD calculations.[175]

Bowman *et al.* estimated the spatial distribution of radicals in the ion tracks of heavy atom irradiated DNA.[176]

1.3.5. Metal Centers

In early experiments, the distance between the manganese cluster of the oxygen-evolving complex in the S_2 state ($S = 1/2$) and $Y_D^{+\bullet}$ of PS II was determined to be 2.7 nm from deeply modulated PELDOR time traces.[113, 177] Measurements in oriented membranes have confirmed the distance and provided an angle of 110° between the membrane normal and the distance vector.[107] In contrast, the same measurement performed on the manganese cluster in

the S_0 state gave a distance of 3.4 nm.[178] Both distances disagree with the distance of 3.0 nm from the crystal structure,[179] which is probably due to the failure of the point-dipole approximation. In the case of several high-spin centers, which couple to a total spin $S = 1/2$, the spin projection factors have to be taken into account, since the latter change upon double oxidation of the cluster.[180] The distance between the quinone radical $Q_A^{-\bullet}$ and the heme Fe^{3+}, located between the two subunits of cytochrome b_{559} in PS II, was 4.0 nm according to PEDLOR experiments. The large g-anisotropy of the heme allows orientation selective measurements at X-band. By performing measurements on oriented membranes and in frozen solution, the angle of 78° between the distance vector and the membrane normal was extracted.[181] The crystal structure revealed a larger distance of 4.8 nm.[179]

The first PELDOR experiment between two metal sites has been reported by Elsässer *et al.* for the [NiFe]-hydrogenase from *Desulfovibrio vulgaris* Miyazaki F. Time traces were obtained by detecting the broad [NiFe] signal and inverting parts of the [3Fe4S]$^+$ signal. The authors assign the spin projection factors obtained by Mössbauer spectroscopy, and explicitly treat them in the simulation. In the proper assignment the distance between the [NiFe] center ($S = 1/2$) and the [3Fe4S]$^+$ cluster ($S = 1/2$) matches the 2.1 nm found in the crystal. Finally, also the two different paramagnetic states of the [NiFe]-center could be differentiated on the basis of these simulations.[182] The effects of spin projection factors and orientation selection have been discussed by the same authors.[183] An earlier work on the Mo(V)/Fe(III)-state of sulfite oxidase from chicken liver did not resolve any dipolar modulation between the $S = 1/2$; $S = 1/2$ spin pair.[184] The authors attribute this to intrinsic flexibility, but by working at C-band (6 GHz) dipolar oscillations are difficult to separate from hyperfine modulation, which is present to a high degree in the experimental data presented.

In 2003, a Cu^{2+}-Cu^{2+} distance of 2.6 nm was estimated by PELDOR.[185] This distance was obtained on a covalently linked azurin dimer, whereas a more flexibly linked dimer did not bear any dipolar modulation. The authors claim that the latter corresponds to an expected short distance of 1.4 nm, superimposed by a large distance distribution. The distance between the metal ion binding sites in dicupric human transferrin and lactoferrin have been determined to 4.16 and 4.24 nm, respectively.[186] Both are shorter than the expected values from the X-ray structure, but orientation selection has not been considered in evaluating these spectra. Recently, a Cu^{2+}-Cu^{2+} PELDOR measurement in a model peptide has been reported[187] and correlated with earlier DQC data.[188] Surprisungly, the authors did not observe the predicted orientation selection. They explain this via either an unfortunate relative orientation between the copper centers, or a significant conformational flexibility.

The paramagnetic intermediates in pyruvate ferredoxin reductase (PFOR) from *M. thermoacetica* have been identified by PELDOR and RIDME.[37] Distance measurements between a hydroxyl-ethylidene thiamine pyrophosphate and a $[4Fe4S]^+$ cluster allowed identifying the reduced FeS cluster among the three clusters present in PFOR, explicitly treating the spin projection factors.

A report from the Goldfarb group proves that PELDOR can be extended to high-spin systems.[189] Shallow modulations were obtained on a complex containing two Gd^{3+} ($S = 7/2$) ions. The authors show that the application of PELDOR to high-spin ions is feasible at K- and W-band.

Only one example of a copper-nitroxide distance measurement has been published so far. The complex composed of two nitroxide labeled terpyridines and a Cu^{2+}-ion was generated *in situ* and thus not isolated. Even though modulations are shallow, a dipolar coupling has been determined for the two copper nitroxide pairs, as well as for the nitroxide-nitroxide pair, all three in good agreement with structural modeling.[190]

2. Results and Discussion

2.1. Counting the Monomers in Nanometer-Sized Oligomers with PELDOR

2.1.1. Model Systems

Suitable model systems for PELDOR spin counting should be chemically stable, rigid and should have a spin-spin distance that is well within the limit of the method (1.5 – 8.0 nm).[16] The poly-nitroxide radicals **1 - 5** (Figure 2.1.1) containing fairly rigid aromatic spacers fulfill these requirements. In addition, the use of these spacers allowed synthesizing molecules **1 - 5** from a small pool of building blocks. **6** and **7** (Figure 2.1.1) were used as reference monoradical and biradical, respectively to calibrate the modulation depth parameter λ.
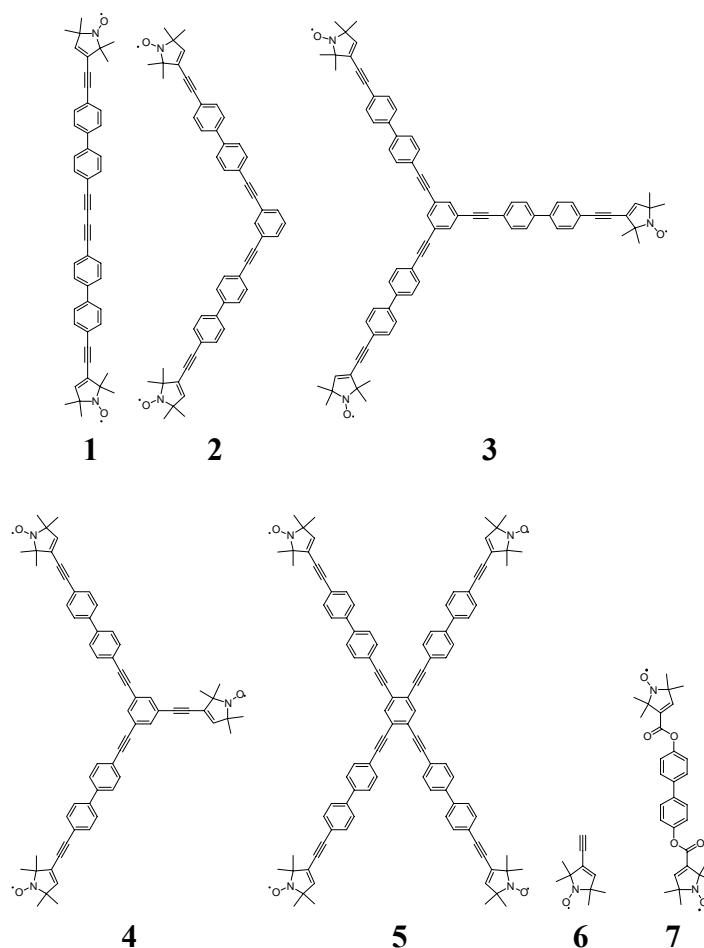
Figure 2.1.1. Poly-nitroxide model compounds **1 - 7**.

2.1.2. Distance Measurements

The 4-pulse PELDOR time traces of model systems **1** - **5** and the corresponding distances obtained by data inversion are shown in Figure 2.1.2.
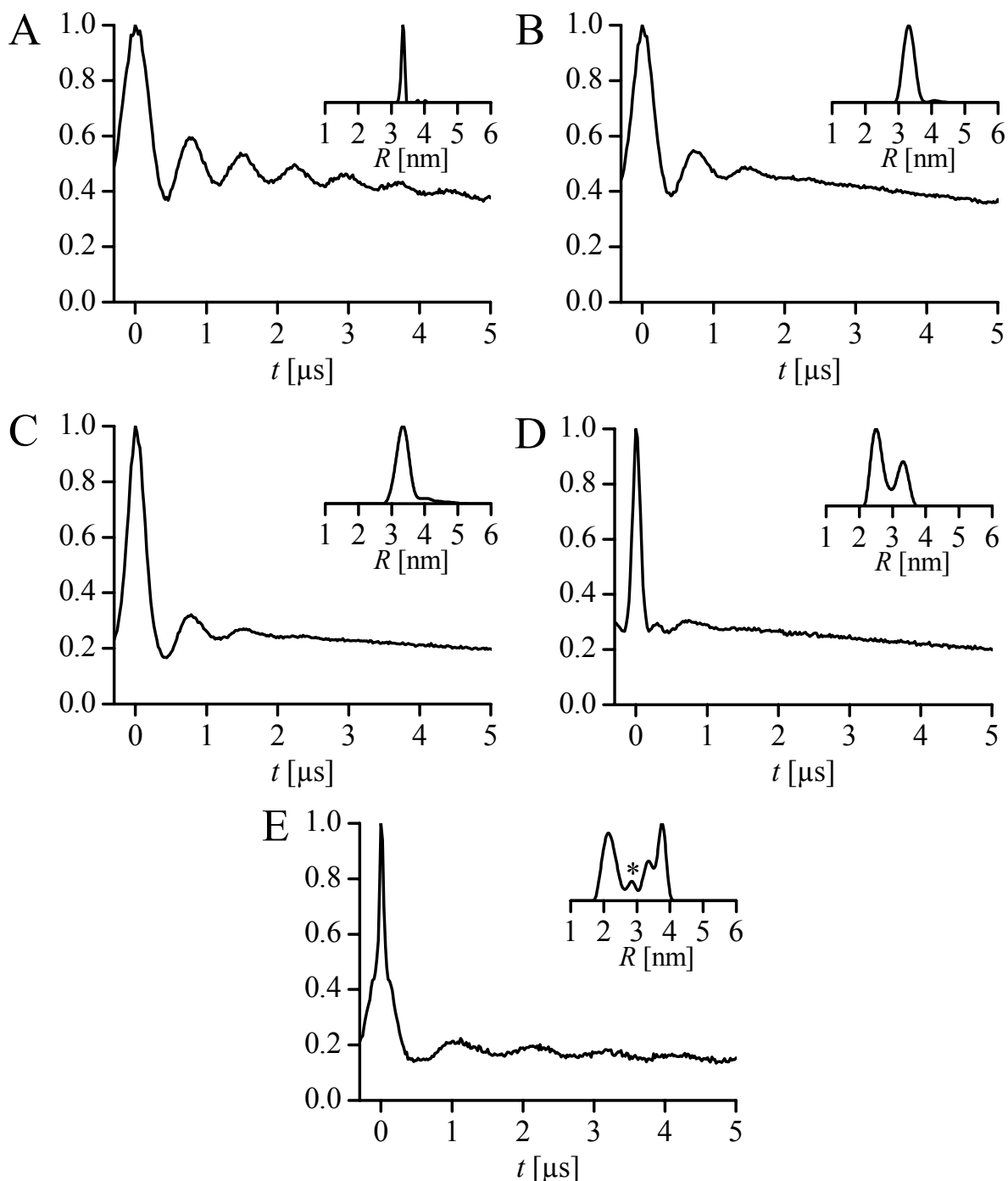
Figure 2.1.2. 4-Pulse PELDOR time traces of compounds **1** - **5.**
The normalized traces are given in A-E, respectively. Distance distributions by time domain data inversion are shown as insets. The asterisk (*) in E marks a Tikhonov regularization artifact.

The obtained distances agree well with the ones predicted from modeling and are summarized in Table 2.1.1. To ensure the reproducibility and significance, the regularization was also performed on longer time traces with higher resolution than shown in Figure 2.1.2. Changes in the dominant peaks in the distance domain were not observed.

Table 2.1.1. Distances R [nm] in molecules **1** - **5** from modelling and Tikhonov regularization.

Molecule[a]	Modeled R [nm]	PELDOR R [nm][b]
1	3.4	3.4(0.1)
2	3.4	3.3(0.4)
3	3.4	3.3(0.4)
4 [1,3/1,5]	2.5	2.5(0.4)
4 [3,5]	3.4	3.3(0.4)
5 [ortho]	2.0	2.2(0.5)
5 [meta]	3.4	3.3(0.4)
5 [para]	3.9	3.8(0.3)

[a]The numbers in square brackets give the positions at the benzene ring to which the nitroxide bearing moieties are linked.
[b]The number in brackets is the full width at half maximum of the corresponding peak.

The linear biradical **1** (Figure 2.1.2 A) exhibits the largest number of visible oscillations, leading to a narrow peak in the distance distribution. In contrast, the bent, *meta*-substituted molecules **2** and **3** display faster damping of the oscillations and in consequence broader peaks in the distance domain (Figure 2.1.2 B and C). The different widths of the peaks in the distance domain can be qualitatively related to the molecular structure. In a linear, stretched structure, as in **1**, the spin-spin distance can only be reduced by molecular bending motions. Whereas in bent structures, as in **2** and **3**, bending motions can increase and decrease the end-to-end distance around the equilibrium structure. Furthermore, the same angular deviations cause larger distance deviations in a bent structure than in a linear structure based on simple geometric considerations. In consequence, the asymmetric triradical **4** shows peaks of approximately the same widths as the radicals **2** and **3** (Figure 2.1.2 D). The faster damping of the modulation of **4** is due to the interfering dipolar frequencies. The approximately 2-fold higher intensity of the peak at 2.5 nm in the distance domain of **4** may also be rationalized by the molecular geometry; the shorter distance can be extracted twice, the longer distance only once. However, tetraradical **5** does not show this correlation. According to structural symmetry, all three distances appear two times, but the intensities of the peaks differ. On the other hand, the decreasing widths of the peaks at 2.2 (*ortho*), 3.4 (*meta*), and 3.8 (*para*) nm

are in agreement with the above considerations about molecular structure and bending motions (Figure 2.1.2 E).
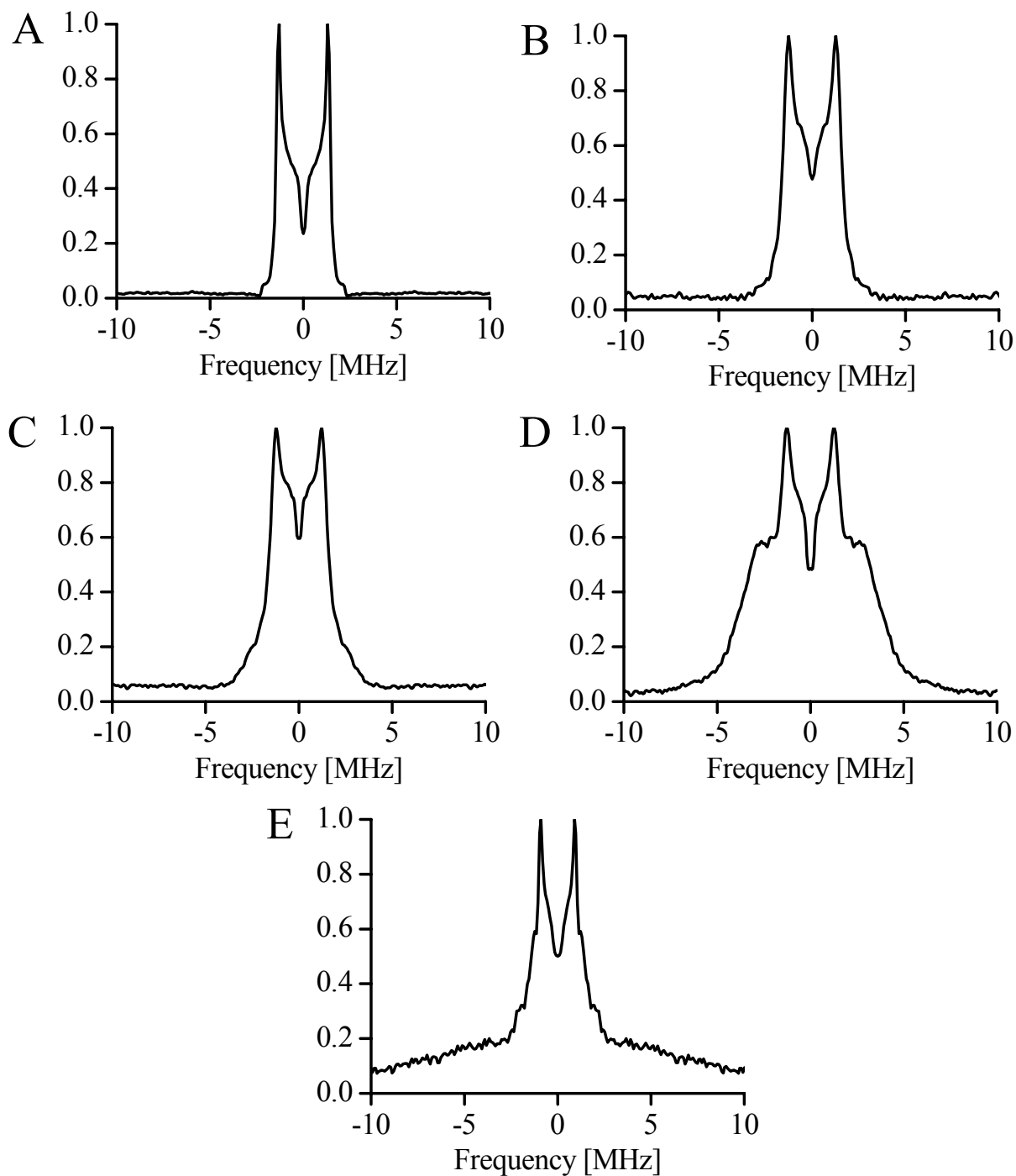
Figure 2.1.3. Normalized, Fourier transformations of time traces of compounds **1 - 5** in A-E, respectively.

Cosine Fourier transformation, as an alternative method to extract distances from the time domain data, did not resolve all individual dipolar frequencies in **4** and **5** as strong peaks (see

Figure 2.1.3). Especially in **5**, the full set of three predicted distances could only be recovered by data inversion utilizing Tikhonov regularization. Provided a high signal-to-noise ratio is given and V_{inter} can be determined precisely, this procedure is a valuable tool to extract distances. In **4** and **5** all different distances within the molecules could be disentangled, even though two distances in **5** differ by 5 Å only.

Although this data inversion nicely yields the mean distances, a quantitative analysis of the distance distributions should be treated with care: In current state-of-the-art software implementations, the time domain data is only simulated as a sum of pairs and not as a sum of products of triples or quadruples (see eq. 1.28). Therefore, cross-terms of higher order in λ arising from the simultaneous pumping of several B spins in tri- and tetraradicals are not properly treated. Especially, in tetraradical **5** the probability of multiple, coherent B spin-flips is fairly high (~35%), which might cause the observed regularization artifact and improper amplitudes in the distance distribution. The 2.8 nm peak in the inset of trace E (Figure 2.1.2) was checked for significance by simulating the time domain data suppressing that peak. It was confirmed that this peak does not result from deuterium modulation (free Lamor frequency 2.3 MHz at 350 mT) by measuring the sample in non-deuterated toluene. In Figure 2.1.4 simulations of the time domain signal are shown, with the distribution generated from data inversion by Tikhonov regularization and with a distribution in which the peak at 2.8 nm is suppressed. Within experimental signal-to-noise ratio the peak is found to be insignificant.
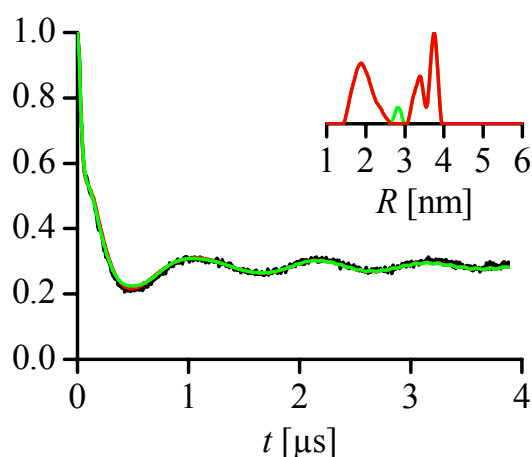
Figure 2.1.4. Significance of the peak at 2.8 nm in the distance distribution of **5**.
Normalized, background-corrected time domain data in black. $P(R)$ from data inversion (inset) and resulting PELDOR trace in green, $P(R)$ suppressing the peak at 2.8 nm (inset) and resulting time trace in red.

2.1.3. PELDOR Spin counting

To prove that the number n of coupled nitroxides can be determined from the PELDOR time traces, using the analytical expressions derived for geometrically uncorrelated radical centers, molecules **1** - **6** have been investigated. On the basis of the considerations of Milov *et al.*[20] spectra in Figure 2.1.2 were corrected for the intermolecular contributions to the echo decay by division by a monoexponential decay and normalized to $t = 0$. The processed spectra are shown in Figure 2.1.5.
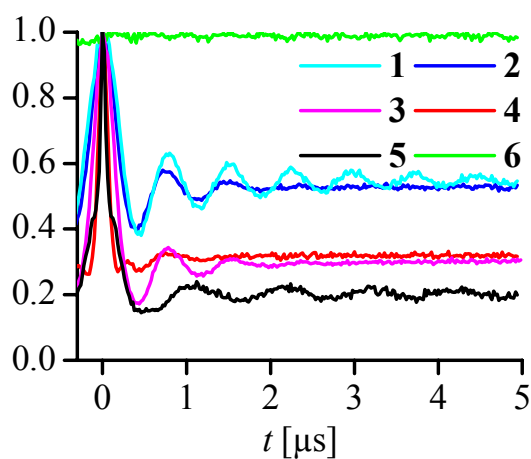
Figure 2.1.5. Background-corrected and normalized time domain signal for determination of n in **1** - **6**.

Figure 2.1.5 clearly demonstrates that the modulation depth increases from a mono- to a tetraradical. Reading off the modulation depth V_λ at the end of the respective time traces, and substituting the value into eq. 1.30 (see chapter 1.2.2.3), allows direct determination of the number of spins n. The spin counting results are compared to the actual number of spins in the corresponding molecules in Table 2.1.2.

Table 2.1.2. Number of spins n from processed time domain data.

Molecule	N	V_λ	n_{found}[a]
1	2	0.54	2.1(1)
2	2	0.53	2.1(1)
3	3	0.30	3.1(2)
4	3	0.32	3.0(2)
5	4	0.20	3.9(2)

[a]The number in brackets is the error in the last digit, determined from a ΔV_λ of 0.02.

The experimental results nicely reproduce the nominal number of spin centers in the model systems. The accuracy in n is determined by the error in V_λ. The observed experimental reproducibility of the individual V_λ values is within 0.02 leading to an error in n of about 5%. To achieve this accuracy, a high signal-to-noise ratio (here > 100:1) and a precise value for λ are important. In this study, λ was calibrated with **7**. Phase cycling of the $\pi/2$-pulse is mandatory to eliminate receiver offsets, because the applied deconvolution of intra- and intermolecular contributions to the echo decay implies that the experimental trace is zero at infinity.

In addition, the measured number of spins was independent of the sample concentration in a range from 13 to 500 µM, even though high concentrations lead to strong intermolecular contribution, and thus to a decreased signal-to-noise ratio after the deconvolution of V_{inter} (Figure 2.1.6).
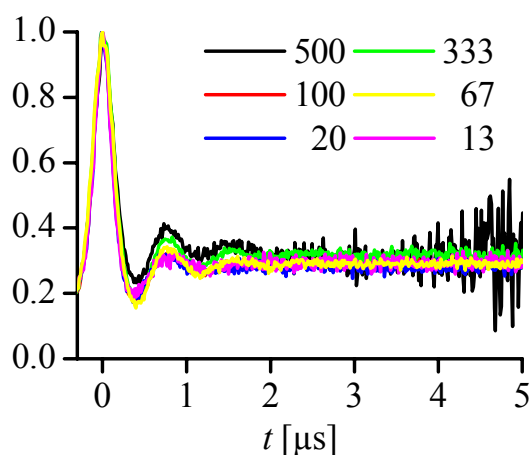
Figure 2.1.6. Background-corrected and normalized time traces of **3** for different concentrations given in µM.

Suppression of unwanted nuclear modulations was performed to test whether the addition of time traces with different τ_1-values influences the modulation depths. The results presented in Figure 2.1.7 and Table 2.1.3 are, within the given error, identical to those performed without modulation averaging.

The results clearly show that monomers, dimers, trimers, and tetramers can be readily distinguished. Within these limits a pentamer can still be identified, but for $n > 5$ a strong decrease in accuracy is proposed, since V_λ will come closer to zero, which lowers the signal-to-noise ratio and the differences in V_λ decrease with the potency of n.
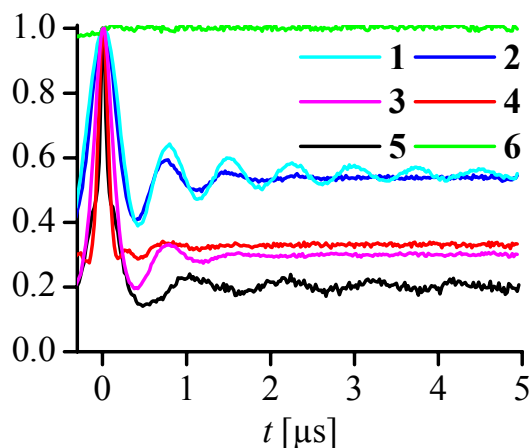
Figure 2.1.7. Background-corrected and normalized time traces suppressing nuclear modulations.

Table 2.1.3. Number of spins n from modulation averaged time domain data.

Molecule	V_λ	N	n_{found}[a]
1	0.55	2	2.1(1)
2	0.53	2	2.1(1)
3	0.30	3	3.1(2)
4	0.32	3	3.0(2)
5	0.20	4	3.9(2)

[a]The number in brackets is the error determined from an ΔV_λ of 0.02.

As mentioned in section 1.2.2.3, V_λ is described as a product of the contributions of all coupled spins (eq. 1.29). Figure 2.1.8 shows the applicability of eq. 1.29. The cube root of tetraradical **5** and the square roots of triradicals **3** and **4** give within the error the same V_λ as biradicals **1** and **2**.
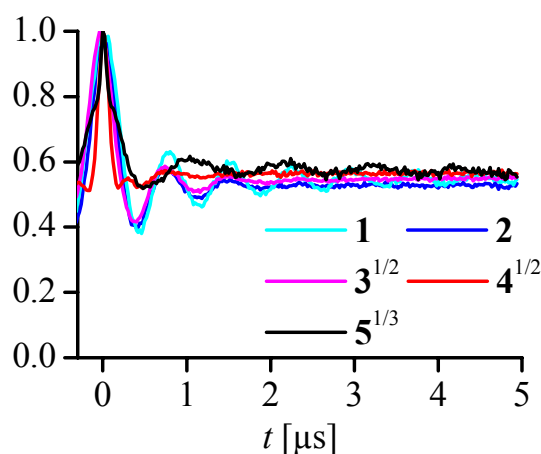
Figure 2.1.8. Background-corrected and normalized time traces to the power of $1/(n-1)$.

In this work, λ was approximated to be identical in radicals **1 - 6**, which is valid in case the orientations of the nitroxide labels within one molecule, and thus their respective hyperfine and **g**-tensor orientations, are not correlated. If this assumption was not fulfilled, λ would depend on the relative orientation (see also sections 1.2.2.1 and 1.2.2.2). To verify the assumption of negligible angular correlation, numerical simulations of the time domain signals of linear biradical **1** and bent triradical **3**, exhibiting different geometries, were performed. Assuming some degree of backbone bending (±10°) and full rotational freedom about the acetylene linkers, a set of 10 000 structures was generated. The simulations were obtained by explicit calculation of λ for each structure and random orientation with respect to the external magnetic field. The result depicted in Figure 2.1.9 shows that especially the modulation depth parameters λ of the experimental data are very well reproduced. Thus, it is feasible to estimate equal λ values.
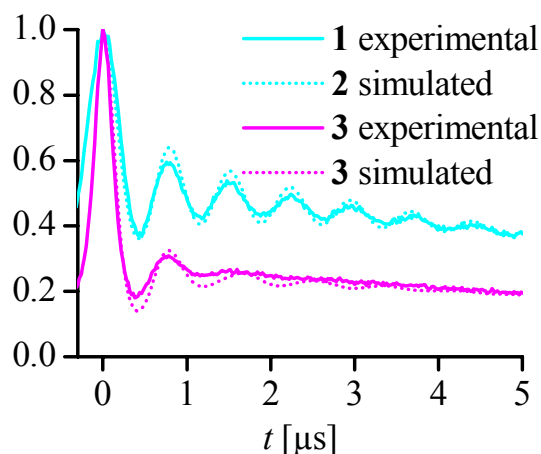
Figure 2.1.9. Normalized experimental PELDOR data and simulations for **1** and **3**.

Even though weak angular correlations are present,[75] they are not observed to affect V_λ within the error of the experiment. Recent work by Jeschke and co-workers on similar biradical model systems exhibited high flexibility and also weak correlations in label orientations.[22] In biological systems, spin-labels are usually even more flexible than in this study, therefore their angular correlation will be even weaker. Thus, it is possible to count the number of monomers in samples of pure oligomeric states, using eq. 1.30. A more detailed study of angular correlation, orientation selection and motional flexibility of **1** and **2** has been published lately.[75]

To verify the linear approximation, leading to eq. 1.31, the inversion pulse length was increased, decreasing λ to about 0.12. Figure 2.1.10 shows the time traces of molecules **1 - 6**

using an inversion pulse of 92 ns length. These data do not meet the accuracy of the 12 ns pulse, even within the factorization approach (eq. 1.30).
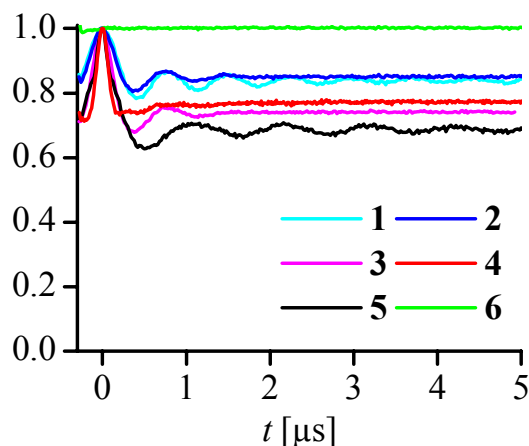
Figure 2.1.10. Background-corrected and normalized time traces utilzing a 92 ns inversion pulse.

Table 2.1.4 shows a comparison of the linear approximation (eq. 1.31) with the factorization approach (eq. 1.30) for data obtained with selective (92 ns) and non-selective (12 ns) inversion pulses. For the 12 ns pump pulse eq. 1.31 is not applicable, but eq. 1.30 reproduces the number of spins per molecule. For the 92 ns pulse, significant differences between the calculations arise with increasing n. It is obvious that λ is still not small enough to apply eq. 1.31 to clusters with more than two spins. Comparison of the results obtained with a 12 ns and a 92 ns pump pulse shows, that the experimental error in n increases, because differences in the individual V_λ become smaller with decreasing λ. The results of the 12 ns pulse and the 92 ns pulse, using eq. 1.30, demonstrate that the results gained with the 92 ns pulse bear a larger deviation to the real n. In addition to calibrating λ to the standard **7**, it was also calibrated to the model compounds **1 - 5**. The results indicate that the 92 ns pulse is much more prone to errors from calibration than the 12 ns pulse, with occurring deviations in the given experimental error. This is attributed to the fact that the application of selective pump pulses implies a calibration of λ with a biradical mimicking geometry and a dipolar coupling similar to the investigated system, as the more selective inversion pulse introduces several problems. First, its small excitation bandwidth leads to an orientation selectivity of the pumped species causing the absolute error to increase, as compared to the short pulse, by amplifying the effects of small angular correlations. Second, the differences in V_λ become smaller with decreasing λ, which raises the overall uncertainty in n. Finally, in the case of

different dipolar coupling strengths, as present in the model systems, λ will show a dependence on the coupling.[46] This dependence can only be neglected if the microwave field strength B_1 is much larger than the dipolar coupling, which is here fulfilled better for the 12 ns pulse as compared to the 92 ns pulse.

Table 2.1.4. Number of spins n from processed time domain data for 92 ns and 12 ns inversion pulses using six different molecules for the calibration of λ.

Molecule/ Calibration[a]	n	V_λ 92 ns	n_{found}[b,c] 92 ns	n_{found}[b,d] 92 ns	V_λ 12 ns	n_{found}[b,c] 12 ns	n_{found}[b,d] 12 ns
1 / 7	2	0.85	2.4(2)	2.3(2)	0.54	2.1(1)	2.1(1)
2 / 7	2	0.84	2.3(2)	2.3(2)	0.53	2.1(1)	2.0(1)
3 / 7	3	0.74	3.4(3)	3.2(2)	0.30	3.1(2)	2.6(1)
4 / 7	3	0.77	3.0(3)	2.9(2)	0.32	3.0(2)	2.6(1)
5 / 7	4	0.69	3.9(3)	3.6(2)	0.20	3.9(2)	2.9(1)
1 / 1	2	0.85	2.0(2)	2.0(2)	0.54	2.0(1)	2.0(1)
2 / 1	2	0.84	1.9(2)	1.9(2)	0.53	2.1(1)	2.0(1)
3 / 1	3	0.74	2.7(2)	2.6(2)	0.30	3.0(2)	2.6(1)
4 / 1	3	0.77	2.5(2)	2.4(2)	0.32	2.9(2)	2.5(1)
5 / 1	4	0.69	3.1(2)	2.9(2)	0.20	3.7(2)	2.8(1)
1 / 2	2	0.85	2.1(2)	2.1(2)	0.54	1.9(1)	2.0(1)
2 / 2	2	0.84	2.0(2)	2.0(2)	0.53	2.0(1)	2.0(1)
3 / 2	3	0.74	2.9(2)	2.7(2)	0.30	2.9(2)	2.5(1)
4 / 2	3	0.77	2.6(2)	2.5(2)	0.32	2.8(2)	2.4(1)
5 / 2	4	0.69	3.3(2)	3.1(2)	0.20	3.5(2)	2.7(1)
1 / 3	2	0.85	2.2(2)	2.1(2)	0.54	2.0(1)	2.0(1)
2 / 3	2	0.84	2.1(2)	2.1(2)	0.53	2.1(1)	2.0(1)
3 / 3	3	0.74	3.0(2)	2.9(2)	0.30	3.0(2)	2.5(1)
4 / 3	3	0.77	2.7(2)	2.7(2)	0.32	2.9(2)	2.5(1)
5 / 3	4	0.69	3.5(2)	3.2(2)	0.20	3.7(2)	2.8(1)
1 / 4	2	0.85	2.3(2)	2.3(2)	0.54	2.1(1)	2.0(1)
2 / 4	2	0.84	2.2(2)	2.2(2)	0.53	2.1(1)	2.1(1)
3 / 4	3	0.74	3.3(3)	3.1(2)	0.30	3.1(2)	2.6(1)
4 / 4	3	0.77	3.0(3)	2.9(2)	0.32	3.0(2)	2.6(1)
5 / 4	4	0.69	3.8(3)	3.5(2)	0.20	3.8(2)	2.8(1)
1 / 5	2	0.85	2.4(2)	2.4(2)	0.54	2.1(1)	2.1(1)
2 / 5	2	0.84	2.3(2)	2.3(2)	0.53	2.2(1)	2.1(1)
3 / 5	3	0.74	3.4(3)	3.2(2)	0.30	3.2(2)	2.7(1)
4 / 5	3	0.77	3.1(3)	3.0(2)	0.32	3.1(2)	2.6(1)
5 / 5	4	0.69	4.0(3)	3.7(2)	0.20	4.0(2)	2.9(1)
1 average[e]	2	0.85	2.2(2)	2.2(2)	0.54	2.0(1)	2.0(1)
2 average[e]	2	0.84	2.1(2)	2.1(2)	0.53	2.1(1)	2.1(1)
3 average[e]	3	0.74	3.1(3)	3.0(3)	0.30	3.1(2)	2.6(1)
4 average[e]	3	0.77	2.9(3)	2.7(3)	0.32	3.0(2)	2.5(1)
5 average[e]	4	0.69	3.6(4)	3.3(3)	0.20	3.8(2)	2.8(1)

[a]The first number is the molecule studied, the second number is the molecule used for calibrating λ.
[b]The number in brackets is the experimental error in the last digit, determined from a ΔV_λ of 0.02.
[c]Values are calculated according to eq. 1.30.
[d]Values are calculated according to eq. 1.31.
[e]Values averaged over all six λ, the number in brackets is the standard deviation in the last digit.

Thus, spin counting becomes less accurate with selective pump pulses in unknown samples. However, a long inversion pulse might be useful for aggregates with a large number of spin-bearing centers.[176]

2.1.4. Mixtures of Oligomeric States

Since biological systems may exhibit equilibriums between monomers, dimers, and higher oligomers, various mixtures of mono-, bi-, tri-, and tetraradicals equimolar in spin concentrations were prepared, and the resulting PELDOR spectra were measured (Figure 2.1.11 and Table 2.1.5).
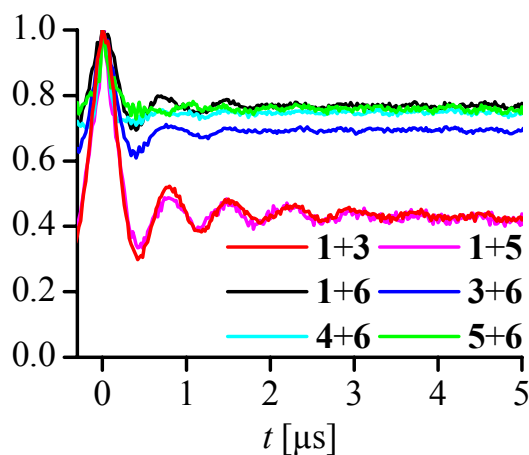
Figure 2.1.11. Background-corrected and nomalized time traces for mixtures of oligomers.

Table 2.1.5. Mixtures and the corresponding measured and calculated V_λ.

Mixture[a]	V_λ measured[b]	V_λ calculated[c]	V_λ calculated[d]
1+6 (1)	0.77(2)	0.77	0.79
3+6 (2)	0.69(2)	0.65	0.68
4+6 (2)	0.75(2)	0.65	0.74
5+6 (3)	0.76(2)	0.61	0.74
1+3 (1)	0.43(2)	0.42	0.42
1+5 (2)	0.43(2)	0.37	0.41

[a]The number in brackets gives the difference in *n* between the two molecules.
[b]The number in brackets gives the error in the last digit.
[c]These numbers are calculated with eq. 2.1, see below.
[d]These numbers are calculated with eq. 2.2, see below.

The analysis of these data is complicated, because *n* in eq. 1.30 cannot simply be substituted by the average number of spins ($\bar{n}$). The substitution with $\bar{n}$ will only be valid, if the linear approximation leading to eq. 1.31 is fulfilled. Instead, the resulting signal is the

sum of responses of different species, and eq. 1.29 transforms to eq. 2.1, where x_i is the fraction of spins in the respective oligomer, giving the signal $V_{\lambda i}$.

$$V_\lambda = \sum_i x_i V_{\lambda i} \tag{2.1}$$

In column 3 of Table 2.1.5 the V_λ of each mixture is calculated using eq. 2.1, which are the weighted sums of the signals of the pure molecules. Comparison with experimental results shows that the data are not reproduced for mixtures with large differences in the number of coupled spins per molecule. This can be explained by considering different transversal relaxation behavior, induced by the dipolar couplings within the oligomers (see section 1.2.3). Therefore, the proper weighting factors also have to contain the contribution of each oligomer to the refocused echo intensity in the constant time PELDOR experiment. This difference in transversal relaxation rates is taken explicitly into account by the scaling factor s_i, weighting the contribution of the individual oligomers to the refocused echo in the constant time experiment (eq. 2.2).

$$V_\lambda = \frac{\sum_i s_i x_i V_{\lambda i}}{\sum_i s_i x_i} \tag{2.2}$$

The factor s_i depends on the observation time window $2(\tau_1 + \tau_2)$ and the transverse relaxation time constant T_{2i} of the individual oligomer. The s_i-values of the oligomers relative to the monomer are given in eq. 2.3, where $T_{2\mathbf{6}}$ is the transverse relaxation time constant of monoradical **6**.

$$s_i\left(\tau_1 + \tau_2\right) = \frac{e^{-\frac{2(\tau_1+\tau_2)}{T_{2_i}}}}{e^{-\frac{2(\tau_1+\tau_2)}{T_{2\mathbf{6}}}}} \tag{2.3}$$

Column 4 in Table 2.1.5 shows the results for the six mixtures according to eq. 2.2. The calculated values are now in agreement with the experimental data, indicating the importance of relaxation for mixtures.

To estimate the relaxation scaling factors, the ratio between the refocused echo (A_{REi}) and the Hahn echo (A_{HEi}) for each pure oligomer was divided by the ratio between the refocused echo (A_{RE6}) and the Hahn echo (A_{HE6}) for the monomer (eq. 2.4). The amplitudes of the Hahn echo and the refocused echo were measured using the 3-pulse detection sequence of the PELDOR experiment.

$$s_i = \frac{A_{RE_i}/A_{HE_i}}{A_{RE_6}/A_{HE_6}} \tag{2.4}$$

The scaling factors are given in Table 2.1.6.

Table 2.1.6. Scaling factors s_i for dipolar relaxation and $V_{\lambda i}$ of the pure oligomers.

Molecule	s_i	$V_{\lambda i}$
1	0.82	0.54
3	0.83	0.30
4	0.61	0.32
5	0.48	0.20
6	1.00	1.00

Table 2.1.7 summarizes the results in $\bar{n}$ that would be obtained if eq. 1.30 was valid for mixtures. Eq. 1.30 is clearly not applicable for mixtures measured with strong pump pulses, as Table 2.1.7 implies.

Table 2.1.7. Number of spins $\bar{n}$ from mixtures assuming the linear approximation (eq. 1.31) to be valid.

Mixture[a]	$\bar{n}$ in mixture	$\bar{n}$ calculated
1+6 (1)	1.5	1.5
3+6 (2)	2.0	1.7
4+6 (2)	2.0	1.5
5+6 (3)	2.5	1.5
1+3 (1)	2.5	2.5
1+5 (2)	3	2.5

[a]The number in brackets gives the difference in n between the two molecules.

In samples of unknown composition, this analysis becomes more demanding, because the fraction of each oligomer and its respective dipolar relaxation enhancement are unknown. In this case, studying V_λ as a function of λ might allow an extraction of the constituents of the

mixture, assuming a sufficiently high signal-to-noise ratio. Furthermore, deducing V_λ as a function of the observation time window τ_2 might give rise to extrapolation of the dipolar relaxation scaling factors of the different oligomers. Therefore, with a series of measurements, the dependencies of V_λ on λ and τ_2 might be determined and the composition of unknown mixtures derived. Since only V_λ has to be determined solely the points $t = 0$ and $t \rightarrow \infty$ of V_{intra} need to be determined. To allow precise experimental deconvolution of V_{inter} several points at long t are needed. However, this should allow using larger or nonlinear time increments as compared to regular PELDOR experiments, thus obtaining high signal-to-noise ratio in short time. Working with small B_1 introduces the problem of operating the traveling-wave-tube (TWT) amplifier out of saturation, which leads to pulse amplitude noise and worse reproducibility of B_1-fields. This might be circumvented by operating two TWT amplifiers in saturation, but will be experimentally more demanding than the commercial PELDOR setup.

Prior to this experimental validation of spin counting, the method had already been applied to biological systems of known oligomerization states, but the data did in neither case reproduce the oligomeric states found in crystal structures or by biochemical methods. These discrepancies might be attributed to experimental noise, incomplete spin-labeling, and/or mixtures of oligomeric states.[140, 146, 148]

2.2. PELDOR measurements on a Nitroxide Labeled Cu(II) Porphyrin

2.2.1. Copper(II)-Nitroxide System

Molecule **8** was chosen as a suitable model system to study the effects of spin-density delocalization, orientation selection and conformational flexibility on Cu^{2+}/nitroxide PELDOR measurements. The copper(II)octaethylporphyrin (OEP) moiety resembles binding motives found in proteins, ensures considerable amount of spin density delocalization into the coordinating ligand, and the interconnecting bridge allows some degree of structural flexibility. In addition, the synthesis scheme involves the selective covalent attachment of only one nitroxide group to the copper complex, in contrast to the previously reported *in situ*-synthesis of a copper(II)-bis(terpyridyl) derivative.[190]

8   **9**   **10**
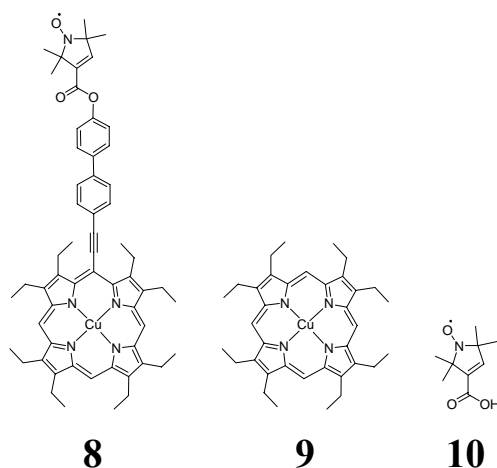
Figure 2.2.1. Chemical structures of complexes **8** and **9** and the monoradical **10**.

2.2.2. PELDOR Measurements

A 2-pulse field swept spectrum of model compound **8** is depicted in Figure 2.2.2. The PELDOR experiments were performed choosing the frequency of the pump pulse to be resonant with the central line of the nitroxide (position P), in order to achieve large modulation depths. The detection pulses were applied at higher frequency (positions A and B), to solely select spectral contributions from the Cu^{2+} ion. The PELDOR time trace recorded at detection position A (corresponding to a frequency offset $\Delta \nu_{AB}$ of 226 MHz) is given in Figure 2.2.3 in combination with the time trace of a reference sample composed of an equimolar mixture of **9** and **10**. The PELDOR time trace of **8** exhibits three clearly resolved periods of modulation, whereas the reference measurement does not, proving that

the modulation is only caused by intramolecular dipolar coupling and not arising from intermolecular interactions or experimental artifacts.
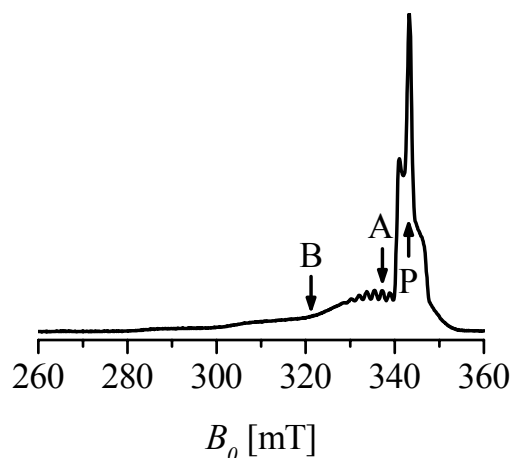
Figure 2.2.2. 2-Pulse field swept spectrum of **8**.
A and B indicating 226 MHz and 603 MHz offset, repectively, to the pumping position (P).
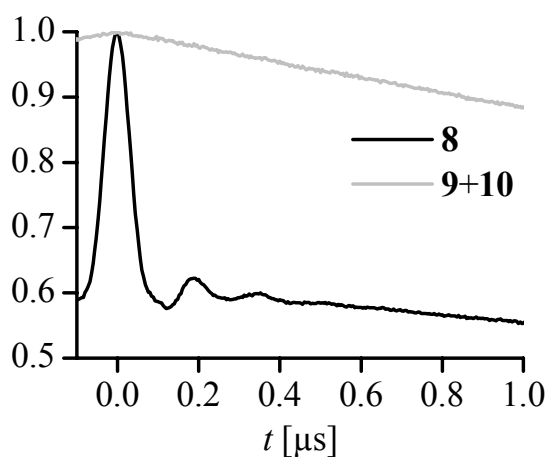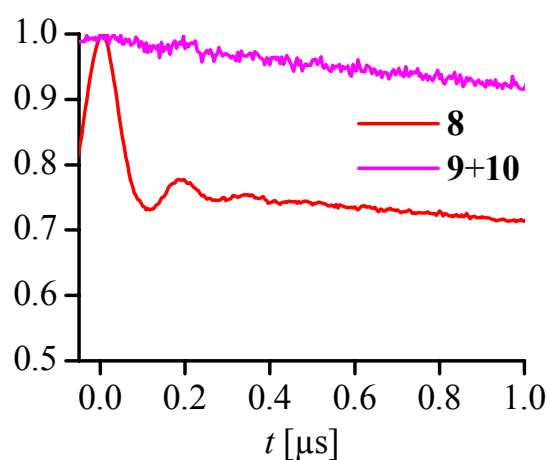

Figure 2.2.3. Normalized 4-pulse PELDOR time trace of **8** and of a reference sample composed of **9** and **10** recorded at a frequency offset $\Delta \nu_{AB}$ of 226 MHz.

The modulation depth of 0.40 is comparable to those found in time trace of bisnitroxide systems using identical conditions for the pump pulse. However, the damping of the modulation is much faster compared to structurally analogous bisnitroxide model compounds, as for example **7** (see Figure 2.2.4).
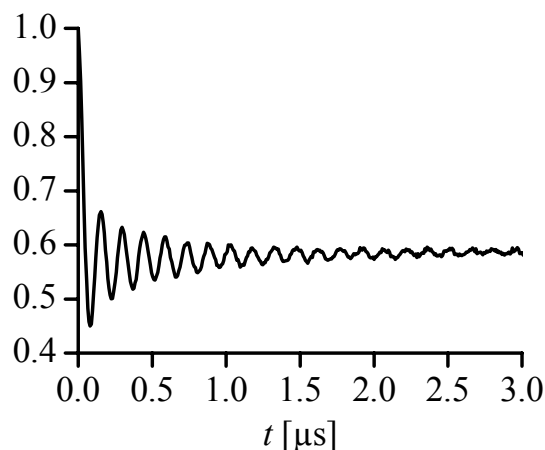
Figure 2.2.4. 4-Pulse PELDOR time trace of **7** recorded with a frequency offset $\Delta\nu_{AB}$ of 70 MHz. The trace is background-corrected and normalized.

First, the spin density distribution in the porphyrin moiety might induce a pronounced rhombicity in the spin-spin interaction. Second, the spectral selection on copper might correspond to a selection of distance vector orientations that causes rapid interference of frequencies. Third, the g-anisotropy of the copper-spin might cause a significant orientation dependence of g_A in eq. 1.9, which leads to a dependence of the coupling strength not only on the orientation of the distance vector but also on the orientation of the Cu(OEP) moiety with respect to the external magnetic field. Fourth, a high conformational flexibility of the porphyrin fragment might lead to a wide distance distribution. A high conformational flexibility of the biphenyl linker and the nitroxide spin-label in **8** is excluded, since this bridge is the same as in structural analogous bis-nitroxide systems such as **7**. Fifth, an exchange coupling contribution J, which is, according to cw EPR data and simulations, small, might occur. In the experimental cw EPR spectra, even the ^{1}H hyperfine coupling of the twelve methyl-protons is resolved (Figure 2.2.5). The spectra were simulated with EasySpin,[191] using the spin Hamiltonian parameters from literature[192] and an isotropic ^{1}H hyperfine coupling of 0.65 MHz for 12 equivalent methyl protons, and 1.3 MHz for the vinylic proton, an isotropic ^{13}C hyperfine coupling constant of 16.5 MHz for the α- and methyl-carbons in natural abundance, all in good agreement with literature values for nitroxides.[193, 194] The residual Lorentzian linewidth is 0.3 MHz. An axial diffusion tensor with $D_{xy} = 1$ GHz and $D_{zz} = 100$ GHz was assumed. The simulations are in good accordance with the experiment and give an upper limit for the exchange coupling of 0.2 MHz.
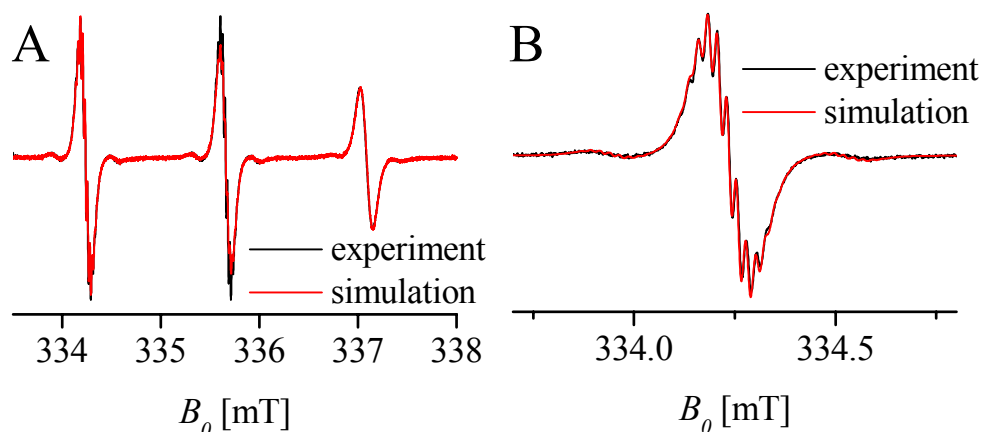
Figure 2.2.5. Experimental and simulated fast motion cw X-band spectrum of **8**.
Nitroxide spectrum is depicted in A. Enlarged view of the low field ^{14}N hyperfine line is shown in B.

To investigate the effect of spectral selectivity on the PELDOR time traces, spectra of **8** were recorded with different frequency offsets $\Delta\nu_{AB}$. The one with maximum detection frequency offset of $\Delta\nu_{AB} = 603$ MHz (position B in Figure 2.2.2) is depicted in Figure 2.2.6, in combination with the measurement on the reference sample under the same conditions. Offsets larger than 603 MHz are not feasible due to limited B_1 and signal-to-noise ratio.

Figure 2.2.6. 4-Pulse PELDOR time trace of **8** and of a reference sample composed of **9** and **10** recorded with a frequency offset $\Delta\nu_{AB}$ of 603 MHz.

The time trace shows three well-resolved modulation periods, which are not present in the reference sample. Interestingly, slight changes in the shape of the modulation pattern, especially in the first minimum, can be observed compared to the measurement at $\Delta\nu_{AB} = 226$ MHz, indicating different orientation selections. The smaller modulation depth λ of 0.23 compared to 0.40 at 226 MHz is due to the more selective pump π-pulse of 32 ns

compared to the 12 ns pulse length used at 226 MHz. The reason for applying a longer pump pulse is the limited resonator bandwidth, and thus the limited B_1-field.

Time traces recorded with an offset of 226 MHz and 32 ns pump pulse length gave similar modulation depths. Figure 2.2.7 indicates that the residual deviation in λ of 0.015 lies within the experimental error of 0.02.
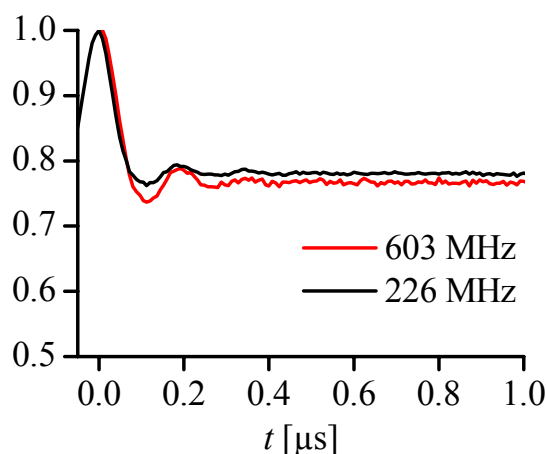
Figure 2.2.7. Experimental 4-Pulse PELDOR time traces of **8**.
Pump pulse length of 32 ns, frequency offsets given in the legend.

The excitation efficiencies on copper and on the nitroxide for the pumping and detection frequencies corresponding to the frequency offsets $\Delta \nu_{AB} = 226$ MHz and $\Delta \nu_{AB} = 603$ MHz were calculated, to explore the influence of the spectral selection on the PELDOR spectra in more detail. Figure 2.2.8 shows the resulting normalized excitation probabilities in dependence of the magnetic field orientation in the principle axis system of the respective molecule.

Whereas all orientations of the nitroxide are pumped by the inversion pulse independent of its length of either 12 or 32 ns, the observed selection on copper is more specific. Detecting at position A (corresponding to $\Delta \nu_{AB} = 226$ MHz), mainly Cu(OEP)-moieties with the molecular x- and y-axes (within the porphyrin plane) parallel to the magnetic field axis are selected, whereas those with the z-axis parallel to **B** are not excited. In contrast, detecting at position B ($\Delta \nu_{AB} = 603$ MHz), the probability of Cu(OEP)-rings with the molecular z-axis parallel to the field increases, whereas x and y are deselected. Since the **g**-tensor is collinear to the molecular axis system, detecting at A mainly selects g_{xx} and g_{yy}; detecting at B mainly selects non-canonical orientations.
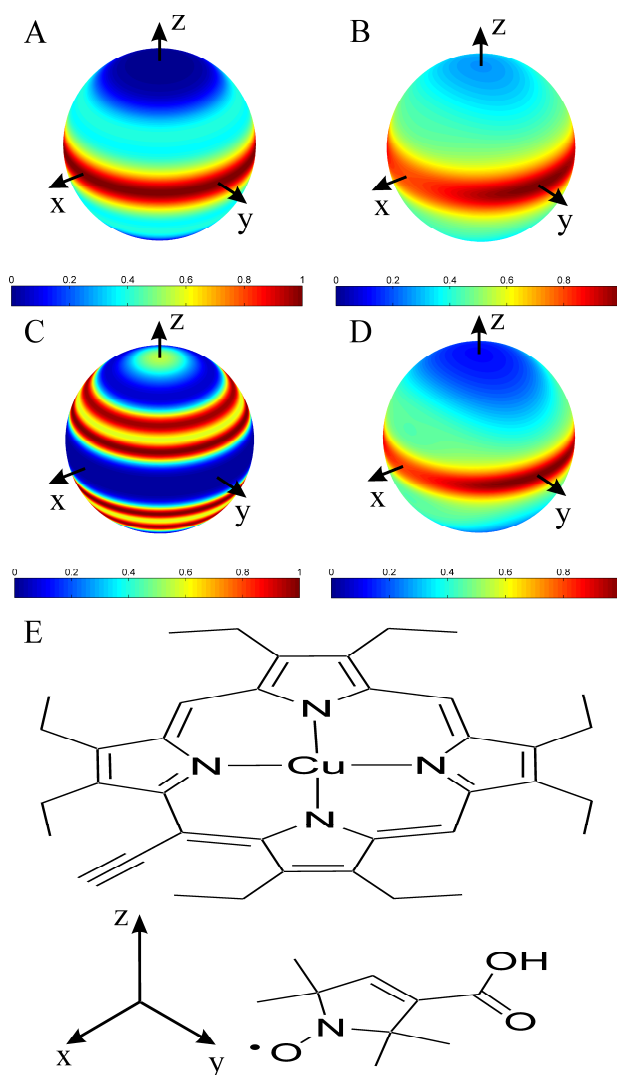
Figure 2.2.8. Orientation selection on copper and nitroxide.
Frequency offsets of $\Delta\nu_{AB}$ = 226 MHz (A and B) and $\Delta\nu_{AB}$ = 603 MHz (C and D); copper shown in A and C (t_{PA} = 32 ns) nitroxide shown in B and D (t_{PB} = 12 ns and t_{PB} = 32 ns, respectively). The molecular axis systems are defined in E.

To estimate the effect of the different selections on the PELDOR time traces, the form factors $P(\theta)$ were calculated (Figure 2.2.9), they describe the probabilities of excitation in dependence of the dipolar angle. The calculation has been performed by connecting the axis systems of the two spins, and thus the two excitation profiles, via the molecular structure, which is known from X-ray diffraction. To properly treat the effect of capturing a range of different conformations adopted by **8** at room temperature via freezing, a geometric/dynamic model was built, taking into account the mean distance of 2.07 nm between the copper and the nitroxide, a single, harmonic bending motion with a standard deviation of ±15° centered at the mid-point of the biphenyl bridge, and free rotation of the nitroxide group around the phenolic bond on a cone of 31.4°. Based on this model, which has already been used to

describe structurally analogous bisnitroxides, a conformational ensemble typically containing 1000 different conformers was generated.
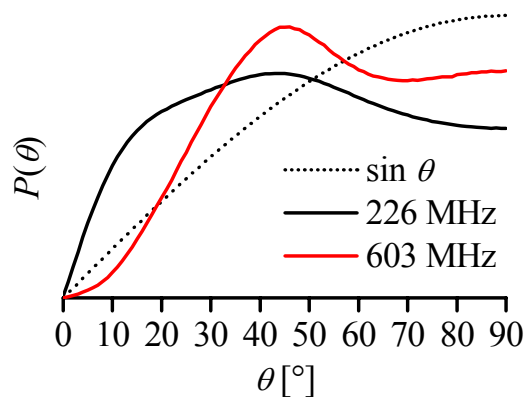
Figure 2.2.9. Calculated form factors $P(\theta)$ with normalized integrals.
The different frequency offsets are given in the legend, a $\sin(\theta)$ distribution for uncorrelated centers is shown for comparison.

The calculated form factors of these ensembles show in either case significant deviations from the classical $\sin(\theta)$ probability distribution function of a Pake pattern valid for orientational uncorrelated spin centers. For $\Delta\nu_{AB} = 226$ MHz, distance vectors parallel to **B** ($\theta = 0°$) gain in probability, and those perpendicular to **B** ($\theta = 90°$) become less probable than expected for a $\sin(\theta)$ distribution. In case of $\Delta\nu_{AB} = 603$ MHz the intensity of both singularities is smaller than compared to the $\sin(\theta)$ function, whereas intermediate angles increase. Thus, both form factors differ significantly from each other close to $\theta = 0°$. This effect can also be observed experimentally, as the double frequency (corresponding to $\theta = 0°$) contributes to the first modulation minimum in Figure 2.2.3. On the other hand, both form factors have maxima at approximately 45° and still strong intensity at $\theta = 90°$, which causes the similarity of the time traces. It is interesting to note, that even though the form factors are quite different, this is not translated into a strong change in the experimental PELDOR time traces, but can be visualized by Fourier Transformation, as depicted in Figure 2.2.10.
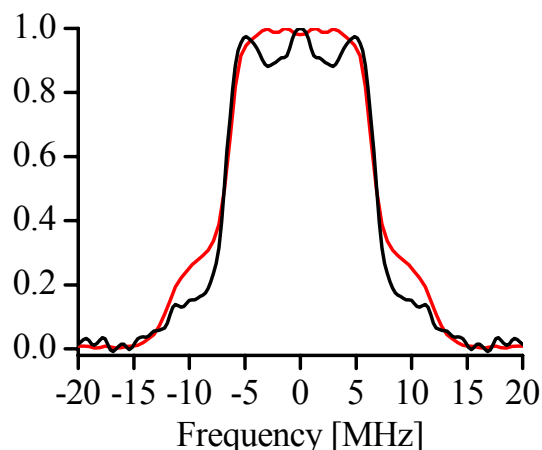
Figure 2.2.10. Normalized FTs of time traces of **8.**
$\Delta\nu_{AB}$ = 226 MHz 12 ns pump pulse (red) and $\Delta\nu_{AB}$ = 603 MHz 32 ns pump pulse (black).

Assuming the damping to be due to the flexibility of the copper nucleus in the porphyrin moiety, the time traces have been simulated employing the form factors as calculated above, and the explicit distance vector has been extracted from the geometric model. All calculated spectra are based on the identical geometric models, and spin Hamiltonian parameters. Pulse lengths, frequencies and magnetic field values were taken from the corresponding experiments. The flexibility of the copper was assumed to be described by a normal distribution in the porphyrin plane. If the width of this function was set to 0.1 nm (standard deviation) the simulation could be made to fit the experimental data (Figure 2.2.11). However, this flexibility model implies a large deformation of the porphyrin moiety with a standard deviation of ~30 % of the porphyrin radius (0.35 nm). This and especially the implied significant elongation of the minimum energy structure are physically unreasonable.
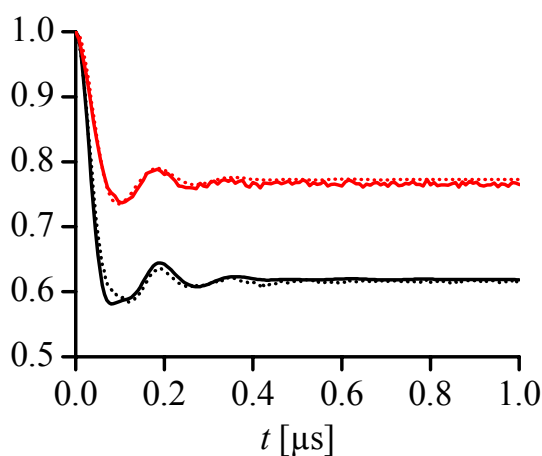
Figure 2.2.11. Simulations of the PELDOR data of **8** assuming a Gaussian distribution of the copper nucleus in the porphyrin plane.
The background-corrected and normalized experimental time trace with $\Delta\nu_{AB}$ = 226 MHz is shown in black and the one with $\Delta\nu_{AB}$ = 603 MHz in red. Their simulations are overlaid as dotted lines.

Spin-density distribution in the Cu(OEP)-moiety may be an additional reason for the damping of the dipolar oscillation, since it induces a rhombicity in the dipolar tensor. To estimate the significance of the spin-density distribution, density functional theory (DFT) calculations were performed of the smaller, but already asymmetric meso-ethinyl-Cu(OEP), and the Mulliken atomic spin densities were computed. The atomic spin densities are to 56% localized on the copper atom, 42% are equally distributed among the four nitrogen atoms (10.6% each) and 2% are delocalized within the rest of the porphyrin ring (Figure 2.2.12).
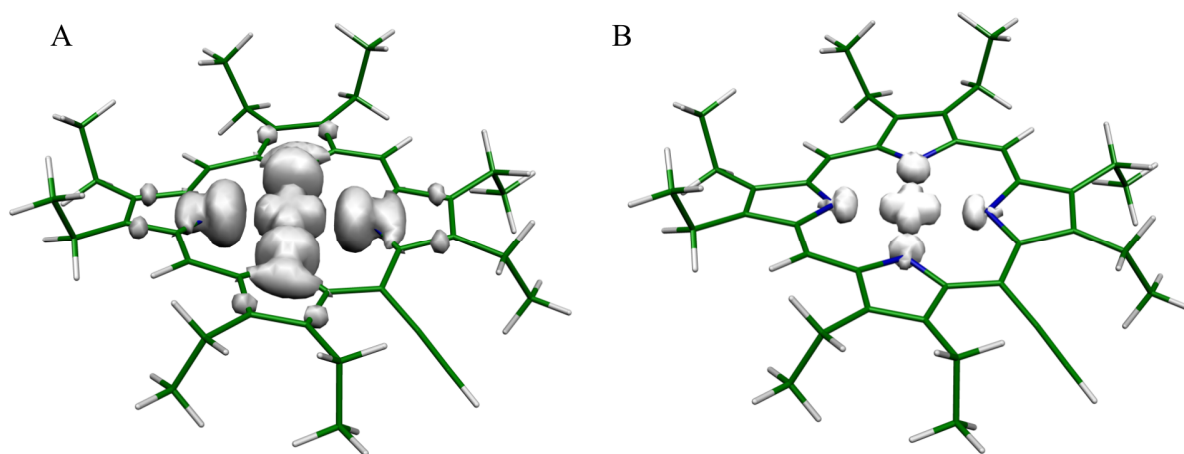
Figure 2.2.12. Calculated spin-density of meso-ethinyl-Cu(OEP) with cutoff values of 0.001 (A) and 0.01 (B).

These values are in very good agreement with other calculations.[195] Experimental estimates from ENDOR data show slightly smaller spin densities on the porphyrin nitrogens (~ 8%).[196, 197] Thus, the spin-density is strongly delocalized from the copper center into the porphyrin ring.

Similar calculations for nitroxide **10** revealed that the spin-density is localized to 50% on oxygen, to 45% on nitrogen and that the remaining 5% are delocalized among the α-carbons and methyl-groups (Figure 2.2.13).
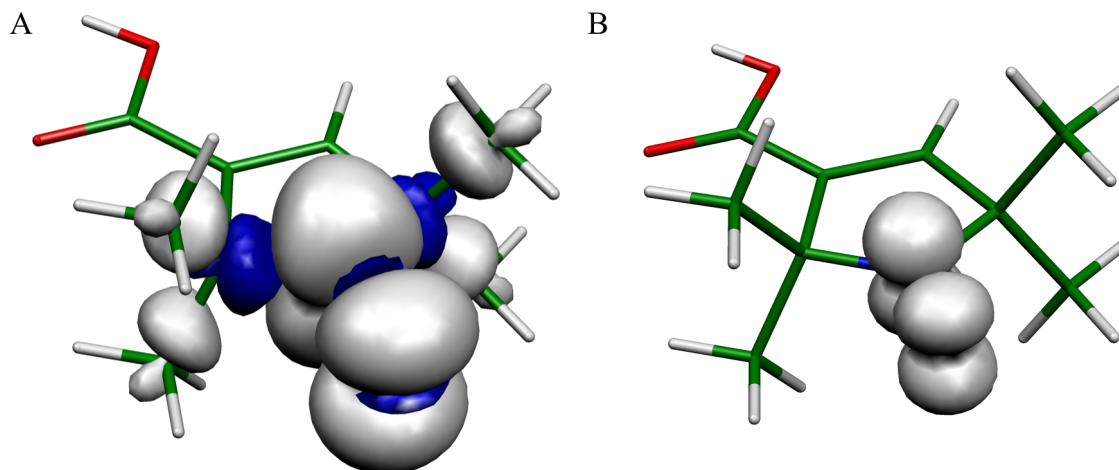
Figure 2.2.13. Calculated spin-density of **10** with cutoff values of 0.001 (A) and 0.01 (B).

The PELDOR time traces have been simulated to specify the effect of the form factor in combination with the spin-density distribution. The dipolar interaction tensor was calculated as specified in eq. 1.23, considering the copper nucleus to be fixed in the center of the porphyrin. Figure 2.2.14 demonstrates that despite the rather large spin-density distribution, its effect on the PELDOR time trace is only marginal.
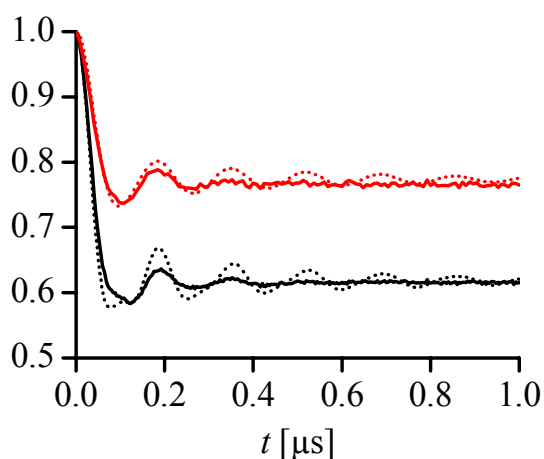
Figure 2.2.14. Simulations of the PELDOR time traces of **8** treating the spin-density distribution explicitly. The background-corrected and normalized experimental time trace with $\Delta \nu_{AB} = 226$ MHz is shown in black and the one with $\Delta \nu_{AB} = 603$ MHz in red. The respective simulations are overlaid as dotted lines.

On the other hand distortions of the porphyrin lead to different spin-density distributions, especially the meso-carbon nuclei exhibit up to 5% spin-density each in saddled porphyrins.[195] Possible asymmetric deformations were simulated by assigning 5% spin-density on C_{meso}, 12 % to the vicinal N, 9 % to the remaining two N and 50% on copper. In

addition, the copper nucleus was set 20 pm closer to C_{meso}. This polarization of the spin-density leads to a slightly faster modulation period. Applying the inverse polarization and averaging those two signals to mimic an ensemble of asymmetrically distorted porphyrins leads to an increased damping, but does still not reproduce the experiment (Figure 2.2.15).
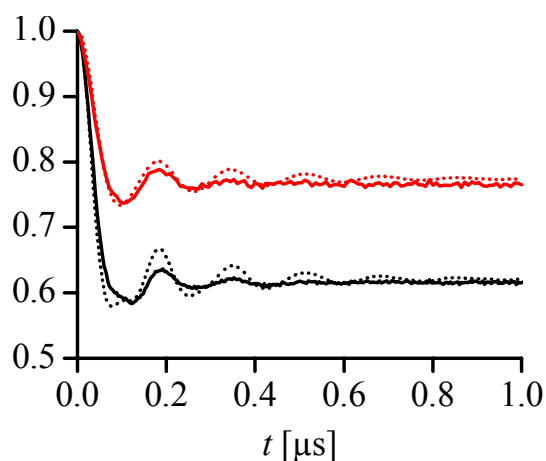
Figure 2.2.15. Simulations of the PELDOR traces of **8** assuming asymmetrically distorted porphyrins. The background-corrected and normalized experimental time trace with $\Delta\nu_{AB} = 226$ MHz is shown in black and the one with $\Delta\nu_{AB} = 603$ MHz in red. The respective simulations are overlaid as dotted lines.

To test for the influence of the flexibility of the backbone and the two spin centers additional simulations were performed. The motional degrees of freedom are depicted in Figure 2.2.16.
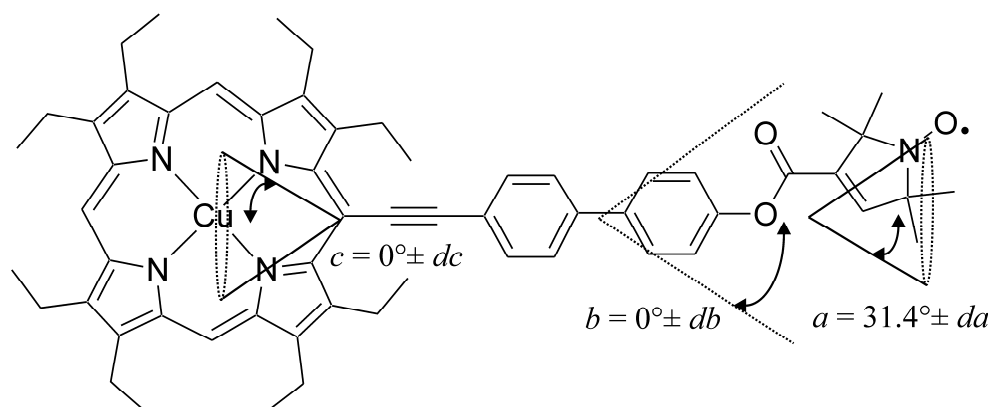
Figure 2.2.16. Definition of the geometric model.
a is the connection angle of the nitroxide, b the is the backbone bending angle, and c is the connection angle of the porphyrin moiety.

The standard deviations of the angles defined in Figure 2.2.16 (da, db and dc) were varied individually from 15° to 45° to study the impact on the distance distribution and on angular

correlations and thus the modulation damping. In Figure 2.2.17 the influence of the nitroxide flexibility on time traces of **8** is shown by simulations. Even a standard deviation of 45° in the connection angle (*da*) does not reproduce the experimental damping of modulations. Therefore, the influence of the nitroxide conformational flexibility is small.
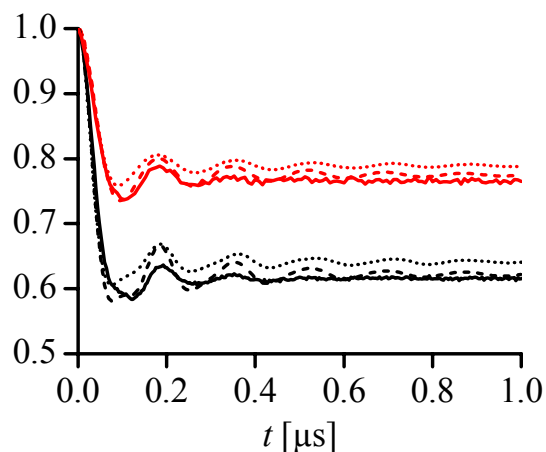
Figure 2.2.17. PELDOR simulations systematically varying the nitroxide flexibility (*da*). The background-corrected and normalized experimental data are given as solid lines with $\Delta \nu_{AB} = 226$ MHz (black) and $\Delta \nu_{AB} = 603$ MHz (red). For clarity only the simulations with *da* = 15° (dashed) and *da* = 45° (dotted) are overlaid.

In Figure 2.2.18 the results obtained by systematically increasing the conformational flexibility of the biphenyl-bridge (*db*) are depicted. Despite a slight shift to higher frequency also the damping increases with increased flexibility. A standard deviation of 45° does still not yield the experimental damping of modulations. Thus, increased backbone flexibility can not explain the experimental data.
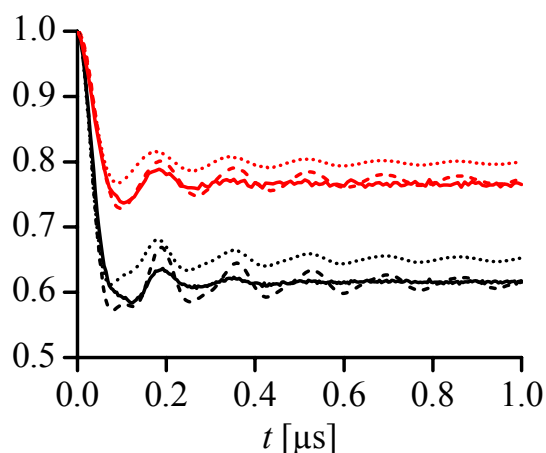
Figure 2.2.18. PELDOR simulations systematically varying the backbone flexibility (*db*).

The background-corrected and normalized experimental data are given as solid lines with $\Delta\nu_{AB} = 226$ MHz (black) and $\Delta\nu_{AB} = 603$ MHz (red). For clarity only the simulations with $db = 15°$ (dashed) and $db = 45°$ (dotted) are overlaid.

The influence of the conformational flexibility of the porphyrin, described by the standard deviation of its connection angle (dc) is shown in Figure 2.2.19. This conformational degree of freedom has the strongest effect on the modulation damping.
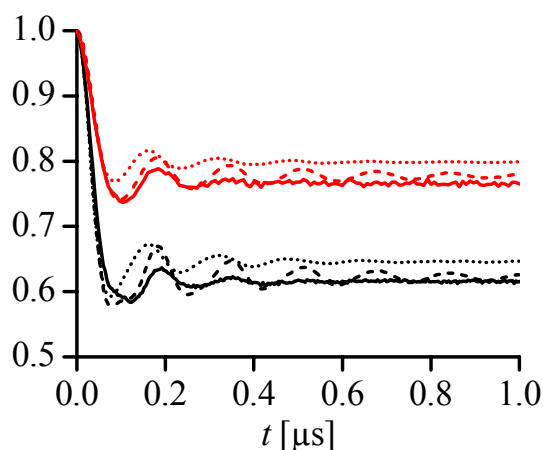
Figure 2.2.19. PELDOR simulations systematically varying the porphyrin flexibility (dc). The background-corrected and normalized experimental data are given as solid lines with $\Delta\nu_{AB} = 226$ MHz (black) and $\Delta\nu_{AB} = 603$ MHz (red). For clarity only the simulations with $dc = 15°$ (dashed) and $dc = 45°$ (dotted) are overlaid.

On the other hand, an increase in flexibility leads to a significantly increased modulation frequency. A standard deviation of 45° does almost reproduce the experimental damping, but the modulation depth and frequency are not met. Thus, increasing the flexibility in the geometric model also led to pronounced damping, but the conformational distributions needed to match the experiment contradict the findings on structurally analogous bis-nitroxides and make no physical sense.

However, the delocalization of spin-density into the porphyrin-bridge system could lead to a small exchange coupling constant J[192, 198] for which simulations of room temperature cw EPR spectra set an upper limit of ~0.2 MHz. Thus, freezing out a conformational ensemble might lead to a distribution in exchange couplings, which is small on average. Good agreement of the data with the experiment was found for a normal distribution in J centered at 0 with a standard deviation of 0.8 MHz (Figure 2.2.20).
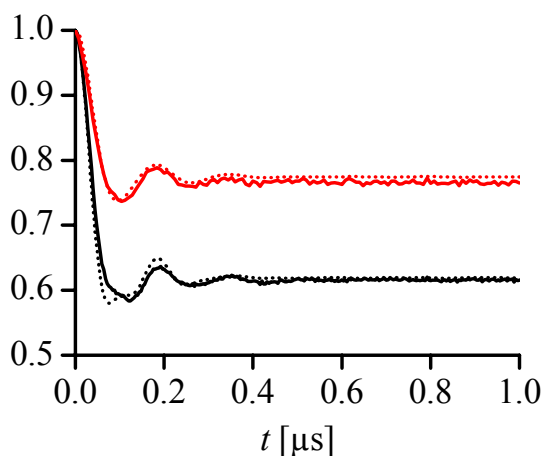
Figure 2.2.20. Simulations of the PELDOR traces of **8** assuming a small distribution in *J*.
The background-corrected and normalized experimental data with $\Delta\nu_{AB} = 226$ MHz is shown in black and the one with $\Delta\nu_{AB} = 603$ MHz in red. The respective simulations are overlaid as dotted lines.

In the case of the bisnitroxide systems, the localization of the spin-density on the two NO groups and the two ester linkages prevent an exchange coupling. These simulations indicate that the damping of the modulation induced by the conformational flexibility itself is not sufficient to reproduce the experimentally observed damping, but that the time domain signal is a convolution of distributions in distances, spin densities and exchange couplings induced by conformational heterogeneity. In addition, it is important to note, that not only the damping and modulation pattern is reproduced, but that also the modulation depth is met for both pump pulse lengths (12 ns and 32 ns) using the same geometric model for both frequency offsets, and thus indicating that the calculated form factors are reasonable.

Further simulations revealed that the shape of the first minimum strongly depends on mutual orientation of the spin-label with respect to the porphyrin ring (data not shown). Even though the assumption of full rotational freedom of the bridging acetylene and phenolic bonds works considerably well, deviations from this model may be the reason for the observed imperfection.

A convolution of the resonance frequencies of the two spins with the spin-spin coupling, to treat the different pulse selectivity in coupled systems, did not show significant effects on the simulations. Also the different influences of the **g**-anisotropy of the Cu-center and from **g**-strains up to 1 % on the dipolar coupling have been examined by simulations, but were found to be negligible.

Finally, decreasing the frequency offset $\Delta\nu_{AB}$ in the simulations down to 100 MHz does not lead to a more pronounced appearance of the parallel component, as also observed experimentally (data not shown). The reason for the latter effect is probably due to

"orientational smearing" caused by the isotropic nitrogen hyperfine coupling (~45 MHz). Thus, spectral selectivity on copper contributes to PELDOR at X-band but the effects are shallow.

2.2.3. Comparison with data inversion by Tikhonov regularization

For the extraction of distance distributions ($P(R)$) in the limit of uncorrelated spin centers time domain data inversion by Tikhonov regularization based on eq. 1.24 is the method of choice. Even though this limit is not met in our case, the results of this procedure were investigated. Figure 2.2.21 shows the simulations based on the distance distributions obtained by inversion of both time traces of **8**. The distance distributions are depicted in Figure 2.2.22. The main peak at 20.6 Å in both distributions nicely matches the distance inferred from the crystal structure and the fit of the time domain data is exceptional. However, additional distances appear at much higher and smaller distance, without any structural basics. The reason for these artifacts are the deviations of the form factors from $\sin\theta$, which is compensated by taking additional distances into account, because the distance distribution is a best fit of $P(R)$ with $P(\theta) \sim \sin\theta$.
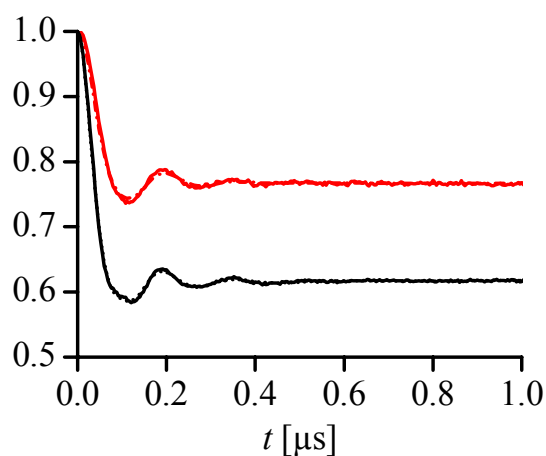
Figure 2.2.21. Simulations based on P(R) from data inversion by Tikhonov regularization. Background-corrected and normalized experimental time traces with $\Delta\nu_{AB} = 226$ MHz (black curve) and $\Delta\nu_{AB} = 603$ MHz (red curve) and their simulations (dotted lines).

This approach, as implemented in recent PELDOR simulation programs, fails in case of fixed mutual orientations as present in protein cofactors[114, 123] in combination with strong spectral selection.[74, 118, 120, 124] Additionally, the width of these peaks is commonly interpreted to represent the conformational distribution of a biradical. Yet, in the present case

this distribution does not stand for the conformational flexibility of the molecule, but for a convolution of different spin-density delocalizations, for a distribution in exchange couplings, and for mobility.
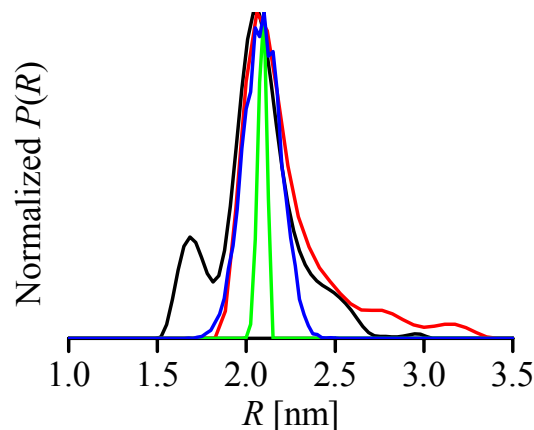

Figure 2.2.22. Distance distributions from data inversion by Tikhonov regularization.
Inverted data with $\Delta \nu_{AB} = 226$ MHz (black curve) and with $\Delta \nu_{AB} = 603$ MHz (red curve) are shown together with the distribution of spin-spin distances obtained from a Gaussian distribution of the copper nucleus in the porphyrin plane (blue curve) and the distribution of copper-nitroxide distances from the same model without the Gaussian distribution (green curve).

The simulating approach used here, allows deconvolution of different contributions. Indeed, the width of $P(R)$ from the structural dynamics of the model (Figure 2.2.22, green curve) is in good agreement with data from Tikhonov Regularization obtained on a structurally analogous bis-nitroxide (Figure 2.2.23).
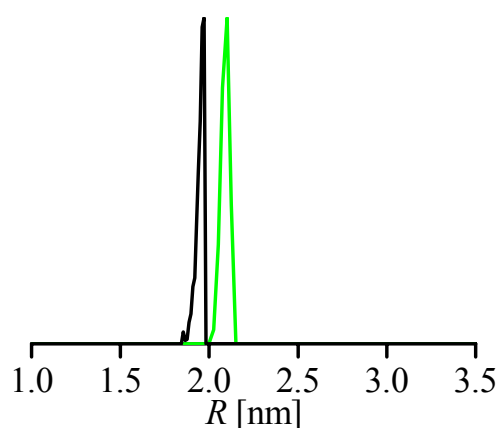
Figure 2.2.23. Comparison of distance distributions.
The narrow distribution form Figure 2.2.22 (green) is similar the distance distribution obtained from data inversion on **7** (black).

The chosen simulation approach allows the deconvolution of effects contributing to the shape of PELDOR time traces: Starting from the angular correlations the form factors can be

calculated, thus disentangling distance distributions from spectral selectivity, spin-density distributions and exchange couplings. Therefore, in case of a high degree of similarity between experimental data and simulation, and if the experimental and Spin Hamiltonian parameters are known, more information than mere distances can be extracted from PELDOR measurements and structural models can easily be verified or disproved.

3. Conclusions and Outlook

In the last years PELDOR has been widely applied. In contrast to other pulsed EPR experiments for nanometer distance measurements, it allows to easily extract distances. It is technically less demanding than DQC EPR, and less prone to artifacts than other single frequency techniques. The instrumentation is commercially available and, in combination with site directed mutagenesis and SDSL, protein structure and folding can be studied. The method has also been employed in materials, nucleic acids, and paramagnetic cofactors and metal centers in proteins.

This thesis shows on a set of newly synthesized polyradicals that a single PELDOR data set does not only yield distances, and thereby precise geometric information on the nanometer scale, but also the number of spins n in a molecule. The first experimental calibration of the method presented herein determines the overall error of 5% in n for up to four spins, provided that the spin-labeling is complete, and that the error of the excitation probability factor λ does not exceed 0.02, which can be readily achieved. In complexes with more than five spins or incomplete labeling, or in presence of mixtures of oligomeric states, this accuracy strongly decreases. It is evident from experiments that the modulation depth of mixtures of oligomeric states is nonlinearly dependent on the average number of coupled spins, when measured at high microwave field strengths. But, with the afore discussed limitations, mixtures can be analyzed in terms of measuring V_λ as a function of λ. Additionally, the significance of dipolar relaxation in these mixtures could be proven, which further complicates the analysis of such heterogeneous systems. Thus, the oligomeric state of biologically relevant complexes can be evaluated by the PELDOR method down to concentrations of ~50 μM at a volume of 80 μL, given that the monomers carry a spin center, and that the spin-spin distances are within the PELDOR limit (1.5 – 8.0 nm).

Furthermore, this work demonstrates on a copper(II)porphyrin-nitroxide model system that orientation selectivity on copper affects PELDOR time traces at X-band frequencies. However, that the experimentally observable differences are shallow. The time domain data is simulated by a home-written Matlab® program. This approach allows the deconvolution of effects contributing to the shape of PELDOR time traces. Treating angular correlations of the molecular frames of the two spin centers, the form factors can be calculated. This disentangles distance distributions from spectral selectivity. Moreover, the knowledge of spin-density distributions and exchange couplings allows differentiating dynamics from other mechanisms of dipolar broadening. This simulation approach gives a framework for the

testing of structural/dynamic models on the basis of the experimental PELDOR time domain data and spin Hamiltonian parameters.

Both major topics of this work – spin counting and metal nitroxide distance measurements – offer new opportunities for applications to biological systems, oligomerization studies, metal ion localization, and constraints for structural modeling.

In addition, to deconvolute mixtures of oligomeric states and to quantitatively derive the constituents, multidimensional PELDOR will have to be set up and optimized to find experimental parameters, which allow sampling of further dimensions in a reasonable measurement time. Temperature-dependent studies or varying the lengths of the constant time experiments will give access to dipolar relaxation to quantitatively interpret the data, and thus the system under study.

Experiments on metal-nitroxide spin pairs, especially rigid systems with fixed mutual orientations, give rise to the determination of angular constraints, as well as distances and conformational flexibility. It will be utmost interesting to investigate the effect of strong **g**-anisotropy on the coupling strength and strongly delocalized or localized spins centered on metal ions with respect to the damping of dipolar modulations. Especially, the latter effects need to be investigated further for the physical interpretation of the distance distribution obtained by inversion of the time domain data by regularization methods. These distributions are commonly interpreted to reflect the conformational space that is sampled by the system. Influences of delocalization, exchange coupling and strains of the spin Hamiltonian are commonly neglected in the interpretation.

The results presented in this thesis together with further systematic investigations will strengthen PELDOR as a (bio)physical method. Insight into structure and dynamics for structural chemistry and biology is provided by the extension to oligomerization studies and quantitative interpretation of metal nitroxide distances allowing triangulation of metal ions in the native fold of biopolymers.

4. Deutsche Zusammenfassung

Puls Elektron-Elektron Doppelresonanz (PELDOR)[18] ist die etablierteste EPR-Methode für Abstandsmessungen zwischen paramagnetischen Zentren im Bereich von 2 - 8 nm.[16, 17] In den letzten Jahren hat sich die Anwendung von PELDOR auf biologisch relevante Systeme rasant entwickelt.[15] In Verbindung mit Weiterentwicklungen im Bereich der Datenanalyse wie der Verwendung von Regularisierungsmethoden[46, 47, 51] wandelt sich PELDOR gerade zu einer etablierten Methode zur Komplementierung der biophysikalischen Strukturforschung. In der vorliegenden Arbeit wird die experimentelle Anwendbarkeit dieser Methode zum Zählen von Spins anhand von Modellverbindungen getestet und PELDOR Daten einer Kupfer-Nitroxid Modellverbindung quantitativ analysiert.

Instrumentell wird die Doppelresonanzmethode PELDOR durch die Verwendung zweier Mikrowellenfrequenzen umgesetzt, wobei der technische Aufbau kommerziell erhältlich ist und als solcher in dieser Arbeit verwendet wurde. In biomolekularer Forschung wird die PELDOR Methode bereits sehr erfolgreich zur Bestimmung von Strukturen von Proteinen und Proteinkomplexen verwendet. Im Vergleich zu kernmagnetischer Resonanz[2] und Röntgenkristallographie[1] kann mit Elektronen Paramagnetischer Resonanz[6, 7] keine atomare Auflösung für das gesamte Biomolekül erreicht werden, PELDOR liefert jedoch für Biopolymere, die sich nicht kristallisieren lassen und zu groß für hochauflösende kernmagnetische Resoananz sind, Abstandsrestriktionen im Nanometerbereich. Von Vorteil ist auch, dass im Unterschied zu optischen Methoden, wie Fluoreszens-Rresonanz-Energietransfer-(FRET) Experimenten,[5] für PELDOR zwei identische Spinsonden oder native Metallzentren[182] verwendet werden können. Die verwendeten Spinsonden sind zudem im Allgemeinen kleiner als Fluorophore und die Datenanalyse ist modellfrei, sodass sich die erhaltenen Daten leichter in eine Molekülstruktur übersetzen lassen.

Die in dieser Arbeit vorgestellten Ergebnisse können grob in zwei Hauptteile gegliedert werden. Während der erste Teil die Erweiterung der Methode auf Multispinsysteme behandelt, werden im zweiten Teil Abstandsmessungen zwischen paramagnetischen Metallionen und Nitroxiden am Beispiel eines spinmarkierten Kupfer(II)porphyrins diskutiert.

‚Spin Counting'

‚Spin Counting' erlaubt, die Beobachtung der Bildung von Homo- und Heterooligomeren aus einfach markierten Monomeren, diese Oligomerisierungsstudien sind speziell für biologisch relevante Protein- und Protein-Oligonukleotid-Komplexe interessant. Angewendet wurde PELDOR bereits auf oligomere Proteinkomplexe. Zum Beispiel wurde die Oligomerisierung einer von-Willebrand-Faktor-A Domäne anhand von Abstandsmessungen und Strukturmodellierung auf Basis der Struktur des Monomers gezeigt.[140] Allerdings ließ sich die Trimerisierung nicht eindeutig aus der Modulationstiefe ableiten. Anologe Ergebnisse wurden an anderen oligomeren Proteinen erzielt.[143, 146, 157, 159] Der Na^+/H^+ Antiporter NhaA aus *E. coli*, zeigte pH-abhängige Änderungen des Oligomerisierungsgrades,[148] es konnte aber keine vollständige Bildung von Monomer oder Dimer beoachtet werden. Unvollständige Dimerisierung lag auch in Monoamin Oxidasen aus Mensch und Maus vor.[160] Zur Kalibrierung des ‚Spin Counting' mittels PELDOR wurden in dieser Arbeit Modellverbindungen, die ein bis vier Nitroxidradikale enthalten, verwendet. Die Ergebnisse dieser Arbeit zeigen, dass Monomere, Dimere, Trimere und Tetramere mit einem Fehler von nur 5% unterschieden werden können. Der jeweilige Oligomerisierungsgrad *n* zweier Dimere, eines asymmetrischen und eines symmetrischen Trimers und eines Tetramers wurde zu 2,1; 2,1; 3,0; 3,1 und 3,9 bestimmt. Es wurde experimentell nachgewiesen, dass die Verwendung selektiver, weicher Mikrowellenpulse, wie in vorhergehenden Arbeiten empfohlen, mit einer Verringerung der Genauigkeit einhergeht.

Der Modulationshub des Signals in der Zeitdomäne hängt sowohl von der Zahl der Spinzentren als auch von deren relativer Orientierung ab. Anhand von Simulationen wurde gezeigt, dass auch für Systeme mit schwacher Winkelkorrelationen bereits die Vernachlässigung des Einflusses relativer Orientierungen auf den Modulationshub und somit modellfreie Anwendung des 'Spin-Counting' in guter Näherung zulässig ist.

Eine detaillierte Analyse der Abstandsverteilungen der Modellkomplexe zeigt außerdem, dass mehr als ein Abstand innerhalb eines Moleküls, das mehrere Spinzentren trägt, extrahiert werden kann, selbst bei Abstandsunterschieden von lediglich 0,5 nm. Es wurden zum Beispiel die drei unterschiedlichen Abstände des Modelltetramers bestimmt. Die anderen möglichen Abstände sind symmetrieäquivalent. Weiterhin kann auch die Breite der Abstandsverteilungen der Modellverbindungen qualitativ interpretiert werden.

Mischungen oligomerer Zustände komplizieren die Analyse, da die Anzahl der Radikalzentren nichtlinear in das Signal eingeht und unterschiedliches Relaxationsverhalten der Oligomere berücksichtigt werden muss. Letzteres führt dazu, dass sich der Beitrag der Oligomere zum Signal nicht mehr durch den jeweiligen Molenbruch abbilden lässt. Jedoch lässt sich der Modulationshub einer bekannten Zusammensetztung mit bekanntem Relaxationsverhalten quantitativ vorhersagen. In der Arbeit werden Experimente zur Lösung dieser Problemstellung vorgeschlagen.

Somit wurde ‚Spin Counting' erstmals an vollständig charakterisierten Systemen, die bis zu vier Spinzentren tragen, kalibriert und das Verhalten von Mischungen oligomerer Zustande quantitativ interpretiert.[199] Das nichtlineare Verhalten von Mischungen erklärt auch experimentell nicht eindeutigen Ergebnisse in oligomeren Proteinkomplexen, die nicht vollständig in einem oligomeren Zutsand vorliegen.

Kupfer-Nitroxid Abstandsmessungen

Im zweiten Teil der Arbeit wurden PELDOR Messungen an einem spinmarkierten Kupfer(II)porphyrin quantitativ analysiert. Metallzentren sind strukturell oder teilweise auch funktionell wichtige Bestandteile in Metallproteinen und Nukleinsäuren. Die Kombination von ortsgerichteter Spinmarkierung und PELDOR könnte eine geeignete Methode zur Lokalisierung und Charakterisierung dieser Metallzentren sein. PELDOR ist bereits auf Kupferionen in Proteinen, wie Azurin,[185] humanem Serum Lactoferrin und Transferrin[186] sowie in Modellpeptiden[187] angewendet worden, allerdings wurde keine Orientierungsselektion beobachtet und der Einfluss von konformationeller Flexibilität und Spindichtedelokalisierung ist nach wie vor unklar. Hierzu wurden in dieser Arbeit X-Band PELDOR Experimente bei unterschiedlichen Kombinationen von Mikrowellenfrequenzen durchgeführt. Die erhaltenen Zeitsignale zeigen nur eine schwache Orientierungsselektion aber eine viel schnellere Dämpfung der dipolaren Modulationen als strukturell analoge Nitroxidbiradikale. Diese Dämpfung übersezt sich in eine Linienbreite im dipolaren Frequenzspektrum, die im Allgemeinen als Ausdruck von konformationeller Flexibilität und somit als Abstandsverteilung interpretiert wird.

Die experimentellen Daten wurden mithilfe von Simulationen quantitativ interpretiert. Hierbei wurde der Einfluss von Orientierungsselektion, konformationeller Flexibilität, Spindichtedelokalisierung, Austauschwechselwirkung J sowie Anisotropie und Verzerrungen des **g**-Tensors untersucht. Eine Abschätzung der Spindichtedelokalisierung erfolgte aus

dichtefunktionaltheoretischen Rechnungen. Die dipolaren Wechselwirkungstensoren wurden mit einem Punktladungsmodell, der logischen Erweiterung des Punkt-Dipol-Modells auf mehrere Spindichte tragende Zentren, berechnet. Über die Berechnung der Anregungsprofile der Mikrowellenpulse in den breiten, anisotropen Pulverspektren wurden die unterschiedlichen Molekülorientierungen, die zum Signal beitragen, bestimmt. Die dipolaren Vektoren wurden aus einem geometrischen Modell, das konformationelle Dynamik einschließt, extrahiert.

Selbst unter der Annahme asymmetrischer Spindichteverteilungen als Resultat eines Ensembles asymmetrisch deformierter Porphyrine trägt der Effekt der Delokalisierung nur schwach zum PELDOR Zeitsignal bei. Die Simulationen zeigen auch, dass die experimentell beobachtete, starke Dämpfung der PELDOR Modulationen nicht auf konformationelle Heterogenität des Moleküls zurückgeführt werden kann, da die konformationellen Veränderungen, die zur Anpassung führen würden, chemisch nicht vertretbar sind. Vielmehr kann die Dämpfung durch die Annahme einer kleinen Verteilung in J durch Simulationen reproduziert werden. Es konnte somit gezeigt werden, dass die Dämpfung der PELDOR Modulationen nicht ausschließlich auf konformationeller Heterogenität beruht. Die resultierende, schmale Abstandsverteilung, die einzig auf die konformationelle Flexibilität des Strukturmodells zurückgeht, stimmt mit der Breite der Abstandsverteilungen strukturell analoger Bis-Nitroxidradikale gut überein.[200]

Schlussfolgernd ist in dieser Arbeit die quantitative Interpretation der PELDOR Daten auf Kupfer-Nitroxid- und Multispinsysteme erweitert worden. Der Einfluss des mittleren Abstands, der Anzahl der gekoppelten Spins, der konformationellen Flexibilität, der Spindichteverteilung und der elektronischen Struktur der Spinzentren auf das PELDOR Signal wurde anhand von Modellverbindungen analysiert. Diese Erkenntnisse aus Modellsystemen, die oligomere oder metallgebundene Zustände imitieren, kalibrieren die Methode in Bezug auf die Information, die aus experimentellen Daten zugänglich ist. Das daraus resultierende grundlegende Verständnis erlaubt nun die Korrelation experimenteller Ergebnisse von z.B. biologischen Systemen mit Struktur- und Dynamikmodellen, und eröffnet neue Anwendungsfelder für die Methode, z.B. Triangulation von Metallzentren und Oligomerisierungsstudien. Generell hat diese Arbeit gezeigt, dass moderne gepulste Elektronen Paramagnetische Resonanzexperimente in Kombination mit quantitativer

Datenanalyse zu einem detaillierten Verständnis von Struktur und Dynamik beitragen können.

Appendix

A   Abbreviations Used

ABC	ATP-binding cassette
ATP	adenosine triphosphate
Chl_Z	chlorophyll Z
cw	continuous wave
DEER	double electron-electron resonance
DFT	density functional theory
DNA	2'-deoxy ribonucleic acid
DOPA	3-hydroxy-tyrosine
DQC	double quantum coherence
E. coli	Escherichia coli
ELDOR	electron-electron double resonance
ENDOR	electron nuclear double resonance
EPR	electron paramagnetic resonance
ESEEM	electron spin echo envelope modulation
FID	free induction decay
FRET	fluorescence resonance energy transfer
FT	Fourier transformation
HIV	human immunodeficiency virus
MD	molecular dynamics
MTSSL	(1-Oxyl-2,2,5,5-tetramethylpyrroline-3-methyl) methanethiosulfonate
NH_2Y	2-amino-tyrosine
NMR	nuclear magnetic resonance
OEP	2,3,7,8,12,13,17,18-octaethylporphyrin
P_{865}	primary donor of the bacterial reaction center
PAS	principle axis system
PELDOR	pulsed electron-electron double resonance
PFOR	pyruvate ferredoxin reductase
PLN	phospholamban
PS II	Photosystem II
Q_A	quinone A

RI	resolution-of-the-identity
RIDME	relaxation induced dipolar modulation enhancement
RMSD	root mean square deviation
RNA	ribonucleic acid
RNR	ribonucleotide reductase
SAXS	small angle X-ray scattering
SDSL	site-directed spin-labeling
SEDOR	spin echo double resonance
SIFTER	single frequency technique for refocusing
Tempo	2,2,6,6-tetramethyl-piperidine-1-oxyl
TOAC	2,2,6,6-tetramethyl-piperidine-1-oxyl-4-amino-4-caboxylic acid
TPA	2,2,5,5-tetramethyl-pyrrolin-1-yloxyl-3-acetylene
TWT	traveling wave tube
Y_D	tyrosine D
Y_Z	tyrosine Z

B   Mathematics and Constants

Avogadro number	$N_A = 6.022137 \cdot 10^{23}$ mol^{-1}
Bohr magneton	$\mu_B = 9.274015 \cdot 10^{-24}$ A m^2
Boltzmann constant	$k = 1.380658 \cdot 10^{-23}$ J K^{-1}
Electron rest mass	$m_e = 9.109390 \cdot 10^{-31}$ kg
Elementary charge	$e = 1.602177 \cdot 10^{-19}$ C
Free electron g-value	$g_e = 2.002319$
Nuclear magneton	$\mu_N = 5.050787 \cdot 10^{-27}$ A m^2
Permeability of vacuum	$\mu_0 = 1.256637 \cdot 10^{-6}$ V s A^{-1} m^{-1}
Permittivity of vacuum	$\varepsilon_0 = 8.854188 \cdot 10^{-12}$ A s V^{-1} m^{-1}
Planck constant	$h = 6.626076 \cdot 10^{-34}$ J s
	$\hbar = 1.054589 \cdot 10^{-34}$ J s
Proton rest mass	$m_p = 1.672623 \cdot 10^{-27}$ kg
Speed of light in vacuum	$c = 2.997926 \cdot 10^8$ m s^{-1}

Matrix representations of the 2 spin operators:

$$\hat{S}_{xA} = \frac{1}{2}\begin{pmatrix} 0 & 0 & 1 & 0 \\ 0 & 0 & 0 & 1 \\ 1 & 0 & 0 & 0 \\ 0 & 1 & 0 & 0 \end{pmatrix} \quad \hat{S}_{yA} = \frac{1}{2}\begin{pmatrix} 0 & 0 & -i & 0 \\ 0 & 0 & 0 & -i \\ i & 0 & 0 & 0 \\ 0 & i & 0 & 0 \end{pmatrix} \quad \hat{S}_{zA} = \frac{1}{2}\begin{pmatrix} 1 & 0 & 0 & 0 \\ 0 & 1 & 0 & 0 \\ 0 & 0 & -1 & 0 \\ 0 & 0 & 0 & -1 \end{pmatrix}$$

$$\hat{S}_{+A} = \begin{pmatrix} 0 & 0 & 1 & 0 \\ 0 & 0 & 0 & 1 \\ 0 & 0 & 0 & 0 \\ 0 & 0 & 0 & 0 \end{pmatrix} \quad \hat{S}_{-A} = \begin{pmatrix} 0 & 0 & 0 & 0 \\ 0 & 0 & 0 & 0 \\ 1 & 0 & 0 & 0 \\ 0 & 1 & 0 & 0 \end{pmatrix}$$

$$\hat{S}_{xB} = \frac{1}{2}\begin{pmatrix} 0 & 1 & 0 & 0 \\ 1 & 0 & 0 & 0 \\ 0 & 0 & 0 & 1 \\ 0 & 0 & 1 & 0 \end{pmatrix} \quad \hat{S}_{yB} = \frac{1}{2}\begin{pmatrix} 0 & -i & 0 & 0 \\ i & 0 & 0 & 0 \\ 0 & 0 & 0 & -i \\ 0 & 0 & i & 0 \end{pmatrix} \quad \hat{S}_{zB} = \frac{1}{2}\begin{pmatrix} 1 & 0 & 0 & 0 \\ 0 & -1 & 0 & 0 \\ 0 & 0 & 1 & 0 \\ 0 & 0 & 0 & -1 \end{pmatrix}$$

$$\hat{S}_{+B} = \begin{pmatrix} 0 & 1 & 0 & 0 \\ 0 & 0 & 0 & 0 \\ 0 & 0 & 0 & 1 \\ 0 & 0 & 0 & 0 \end{pmatrix} \quad \hat{S}_{-B} = \begin{pmatrix} 0 & 0 & 0 & 0 \\ 1 & 0 & 0 & 0 \\ 0 & 0 & 0 & 0 \\ 0 & 0 & 1 & 0 \end{pmatrix}$$

C   Experimental Section

C.1   CW X-Band EPR Measurements

The cw X-band EPR spectra were acquired on a Bruker ELEXSYS E500 cw X-band EPR spectrometer, equipped with a standard rectangular Bruker EPR cavity (ER4102T), operated with an Oxford helium cryostat (ESR900). The microwave frequency was determined by use of a Systron Donner (6054D) frequency counter. The magnetic field was measured with a Bruker gaussmeter (ER035M). Spectra of **8** were recorded at room temperature with a sampling time of 40 ms, a microwave power of 1 mW, and a modulation amplitude of 0.001 mT at a modulation frequency of 100 kHz.

C.2   Simulation of CW Spectra

The spectrum of **8** was simulated with EasySpin[191] with the spin Hamiltonian parameters from literature[192, 201-203] and an isotropic ^{1}H hyperfine coupling of 0.65 MHz for 12 equivalent methyl protons and 1.3 MHz for the vinylic proton, an isotropic ^{13}C hyperfine coupling constant of 16.5 MHz for the α- and methyl-carbons in natural abundance, all in accordance with literature values for nitroxides.[193, 194] The residual Lorentzian linewidth is 0.3 MHz. An axial diffusion tensor with $D_{xy} = 1$ GHz and $D_{zz} = 100$ GHz was assumed. The simulations show very good agreement with the experiment and an upper limit for the exchange coupling of 200 KHz.

C.3   Pulse X-Band EPR Measurements

Samples of **1** - **7** were prepared from solutions of the radicals in d_8-toluene (100 μM in spins, 80 μL). The samples were saturated with argon prior to rapid freezing and storage in liquid nitrogen. Mixtures of radicals were obtained by combining d_8-toluene solutions of the pure substances after determination of their concentrations by cw EPR. Samples of **8** - **10** were prepared from solutions of the radicals in d_8-toluene freshly distilled from sodium (200 μM in spins, 80 μL). The samples were degassed by several freeze-thaw cycles prior to sealing of the quartz tube and storage in liquid nitrogen. All PELDOR spectra were recorded on a Bruker ELEXSYS E580 pulsed X-band EPR spectrometer with a standard flex-line probe head housing a dielectric ring resonator (MD5 W1), equipped with a continuous flow helium cryostat (CF935) and temperature control system (ITC 502) both from Oxford instruments. The second microwave frequency was coupled into the microwave bridge by a commercially available setup (E580-400U) from Bruker. All pulses were amplified via a

pulsed traveling wave tube (TWT) amplifier (117X) from Applied Systems Engineering. The resonator was over-coupled to a quality factor Q of about 50. Four-pulse PELDOR experiments were performed with the pulse sequence $\pi/2(\nu_A)$-τ_1-$\pi(\nu_A)$-$(\tau_1 + t)$-$\pi(\nu_B)$-$(\tau_2 - t)$-$\pi(\nu_A)$-τ_2-echo. The detection pulses (ν_A) were set to 32 ns for both π and $\pi/2$ pulses and applied at a frequency 70 to 226 MHz higher than the resonance frequency of the resonator. The amplitude was chosen to optimize the refocused echo. The $\pi/2$-pulse was phase-cycled to eliminate receiver offsets. To achieve a frequency offset ($\Delta\nu_{AB}$) of 70 to 226 MHz, the pump pulse (ν_B) was set to 12 ns at the resonance frequency of the resonator. For $\Delta\nu_{AB} = 603$ MHz, ν_B was set to a frequency of 377 MHz lower than the resonance frequency of the resonator and the pump pulse length was adjusted to 32 ns. The magnetic field was set to apply the pump pulse to the maximum of the nitroxide spectrum in either case. There it selects the central $m_I = 0$ nuclear spin state of A_{zz} together with the $m_I = 0, \pm 1$ nuclear spin states of A_{xx} and A_{yy}. The pulse amplitude was optimized on maximum inversion of a Hahn-echo on the pump frequency. Time traces of **1 - 7** were recorded at 40 K with an experiment repetition time of 5 ms, time traces of **8** and of the mixture of **9** and **10** at 20 K with a shot repetition time of 3 ms. The video amplifier bandwidth was set to 25 MHz and the amplifier gain to 60 - 63 dB. For quantitative measurements of the modulation depth in **1** to **6** τ_1 was set to 400 ns and τ_2 to 5200 ns. Usually 1000 scans were accumulated with 272 data points and time increments Δt of 20 ns giving an approximate measurement time of 1 h. All spectra were acquired using the same experimental parameters as quality factor of the resonator, pulse amplitudes, and timings. Experiments with small λ were measured using the same conditions, but with an inversion pulse of 92 ns and a τ_2 of 4400 ns. Suppression of proton modulation by the addition of 8 spectra of variable τ_1 with Δt_1 of 8 ns was performed for comparative reasons. For time traces of **8** and of the mixture of **9** and **10** τ_1 was set to 400 ns and τ_2 to 1200 ns. Usually 150 scans were accumulated with 180 data points and time increments Δt of 8 ns giving an approximate measurement time of 3.5 hours. Typically 500 scans were accumulated for spectra with $\Delta\nu_{AB} = 603$ MHz giving an approximate measurement time of 10 hours. Proton modulation was suppressed by addition of 8 spectra of variable τ_1 with a $\Delta\tau_1$ of 8 ns. Transverse relaxation times and the corresponding scaling factors for **1 - 6** were estimated by comparing the Hahn echo and refocused echo amplitudes (40960 averages each) using the same 3-pulse sequence as for the detection sequence in the PELDOR measurements. Data inversion by Tikhonov regularizations for the extraction of $P(R)$ of **1 - 5**

and **7** were carried out on spectra with τ_2 of 6 - 8 µs with time increments (Δt) of 8 - 12 ns to increase the resolution of the distance transformations. All spectra were divided by a monoexponential decay and normalized to the point $t = 0$. These preprocessed datasets were also taken for cosine Fourier transformation. λ was calibrated using **7**; it was determined to be 0.43 and 0.12 for a 12 and a 92 ns inversion pulse, respectively.

C.4   Simulation of PELDOR Time Traces

Simulations were performed based on eq. 1.21, with detection and pumping efficiencies explicitly calculated for each orientation, each hyperfine state of the nitroxide nitrogen and each hyperfine state of the copper nucleus. The nitrogen hyperfine coupling of the porphyrin ring was assumed to be isotropic.[203] The respective resonance positions are computed using the **g**- and hyperfine tensors of TPA[192] and Cu(OEP),[201-203] and the experimental values for pulse lengths and microwave frequencies. A conformational ensemble typically containing 1000 different conformers was generated, each characterized by a distance vector **R**, with polar angles (χ, η) in the axis system of spin A and Euler angles Ω describing the mutual orientation of spin center B with respect to A. Full rotational freedom about the acetylene and ester linkers in combination with a single, harmonic backbone bending mode with a normal distribution of $\pm 15°$ (standard deviation) was approximated. For each of these conformers, the resonance positions of spins A and B were calculated for all orientations of the magnetic field vector B_0 in the molecular axis frame of spin A (typically 20,000 orientations). **A** and **g** axis systems were considered to be collinear to the molecular axis system. The resonance frequencies of spin B can be calculated after describing **A** and **g** of spin B in the coordinate system of spin A. Additionally, an inhomogeneous linewidth has been taken into account by a Gaussian distribution to calculate the final resonance frequencies for spin A and B, respectively. Lorentzian excitation profiles were calculated from the experimental pulse lengths, which empirically describe the excitation profiles of the real pulses with a sinusoidal B_1 distribution over the cavity. This allows computing the excitation functions of spin A, V_0, and of spin B, λ, and thereafter the dipolar distribution function $P(\theta)$ for each conformer. The dipolar coupling constant was computed for each orientation of the magnetic field according to eq. 1.9, determining g_A and g_B for the given field orientation from the copper and nitroxide **g**. The limited field strength (B_1) of the detection and pump pulses

(approximated via their respective pulse lengths t_{PA} and t_{PB}) with respect to the coupling strength was accounted for via a correction of λ (eq. C.1).[46]

$$\lambda\left(\omega_{AB}\right) = \lambda \exp\left(-4\omega_{AB}^2 t_{PA}^2\right) \cdot \exp\left(-4\omega_{AB}^2 t_{PB}^2\right) \qquad\qquad\text{(C.1)}$$

Accounting for delocalization, the dipolar tensor was calculated according to eq. 1.23, which was then multiplied with the dipole moments of the two spins. To take **g**-tensor anisotropy into account the dipole moments were calculated by multiplication of the respective **g**-tensors with the electron spin angular momentum using the high field approximation. The dipolar coupling was then computed from this as the energy difference between the two manifolds of the B spin.

The final PELDOR signal for a given frequency offset $\Delta\nu_{AB}$ between detection and pumping frequency is the sum over all conformers and all magnetic field orientations equally distributed on a sphere (typically 1000×20000).

All simulations were performed with a home-written MATLAB® program. More details regarding the program and structure generation procedure are described elsewhere.[75] Data inversion based on Tikhonov regularization was performed with a program of G. Jeschke[46] and optimized regularization parameters based on the L-curve criterion.

C.5   DFT calculations

The calculations for **9** and **10** were performed using unrestricted Kohn-Sham[204] DFT methods as implemented in GAUSSIAN 03[205] and TURBOMOLE.[206] All structure optimizations were carried out with TURBOMOLE employing Becke's exchange functional B[207] and Perdew's P86[208, 209] correlation functional, together with the TZVP basis set[210] for all atoms and accelerated with the RI approximation using the standard TZVP auxiliary basis set from TURBOMOLE.[211, 212] For the computation of the Mulliken spin-densities with GAUSSIAN 03, a combination was chosen of Becke's three-parameter hybrid exchange functional B3[213] together with the Perdew/Wang correlation functional PW91.[214, 215] An ultra fine integration grid (58410 integration points per atom) and standard SCF=Tight convergence criteria were applied. For these calculations, a decontracted FII-A basis set of Arbuznikov *et al.*[216] (16s,13p,10d)/[11s,10p,10d] was used for Cu and the Huzinaga-

Kutzelnigg-type IGLO-II basis sets[217] were used for all other atoms: (5s,1p)/[3s,1p] for H and (9s,5p,1d)/[5s,4p,1d] for C, N, and O.

Acknowledgements

First of all I would like to thank Dr. Olav Schiemann for the opportunity to work in his group and under his supervision. He introduced me into EPR, pulse EPR, and especially the PELDOR method. He provided excellent scientific support, necessary for my doctoral studies. He has formed the connection between synthesis and modern pulse EPR techniques, which has been essential for my work. I am especially indebted for numberless lively scientific discussions, always challenging my concepts, ideas and interpretations.

I am indebted to Prof. Dr. Thomas F. Prisner for the constant support, working in his well-equipped labs has been a pleasure and his background in spectrometer hardware and spin physics have always helped me in deeper understanding the details of the experiments. He has always encouraged me to work independently and still was always willing to discuss results and ideas. He also wrote the PELDOR simulation program, which I used in slight modification for simulation of the copper-porphyrin data.

This work has been made possible by a tight collaboration with Dr. Jörn Plackmeyer who synthesized the spin-labeled copper-porphyrin and the asymmetric nitroxide triradical. Always willing to discuss what is doable he did a great job, so that I could always rely on his samples.

Dominik Margraf synthesized the polyradical model systems and as office-mates we had a lot of fruitful discussions about PELDOR experiments and simulations, Praktikum and lots of other subjects. He also corrected major parts of this thesis for the English.

Dr. Sevdalina Lyubenova is thanked for lots of small talks and scientific discussions. She explained me the concept of dipolar relaxation, which finally explained spin counting results in mixtures of oligomers. And she corrected major parts of this thesis.

For help with the scientific instruments, especially hardware issues I want to thank Dr. Burkhard Endeward, and Dr. Peter Höfer.

Fascinating discussions about the spin physics and the applicability of all the approximations made for PELDOR data analysis I shared with Dr. Andrij Marko.

Dr. Thorsten Maly and Dr. Jörg Fritscher introduced a stable computer network infrastructure, which I had the pleasure to maintain and expand for quite some time. Jörg also introduced me to quantum chemistry of open-shell systems and all my calculations are based on his optimizations and protocols. Thanks to Thorsten also for the idea of the literature histogram.

I am indebted to my parents for their constant support during my studies always bringing my mind back from science to humanities.

This thesis is dedicated to my longtime companion Katrin Ackermann – for her constant passionate support in every aspect, for motivation, fruitful discussions and for calming me down if necessary. She has always given me the strength to go on…

Bibliography

[1]   B. Loll, J. Kern, W. Saenger, A. Zouni, J. Biesiadka, *Nature* **2005**, *438*, 1040.
[2]   A. M. J. J. Bonvin, R. Boelens, R. Kaptein, *Curr. Opin. Chem. Biol.* **2005**, *9*, 501.
[3]   S. Luca, J. F. White, A. K. Sohal, D. V. Filippov, J. H. van Boom, R. Grisshammer, M. Baldus, *Proc. Natl. Acad. Sci. USA* **2003**, *100*, 10706.
[4]   S. Sharpe, W.-M. Yau, R. Tycko, *Biochemistry* **2006**, *45*, 918.
[5]   J. R. Lakowicz, *Principles of Fluorescence Spectroscopy*, 3rd ed., Springer, New York, **2006**.
[6]   A. J. Hoff, *Advanced EPR. Applications in Biology and Biochemistry*, Elsevier, Amsterdam, **1989**.
[7]   A. Schweiger, G. Jeschke, *Principles of pulse electron paramagnetic resonance*, Oxford University Press, Oxford, New York, **2001**.
[8]   K. Sale, J.-L. Faulon, G. A. Gray, J. S. Schoeniger, M. M. Young, *Protein Sci.* **2004**, *13*, 2613.
[9]   C. Altenbach, T. Marti, H. G. Khorana, W. L. Hubbell, *Science* **1990**, *248*, 1088.
[10]   L. J. Berliner, in *Biological Magnetic Resonance, Vol. 14*, Plenum Press, New York and London, **1998**.
[11]   M. Bennati, T. F. Prisner, *Rep. Prog. Phys.* **2005**, *68*, 411.
[12]   K. Möbius, A. Savitsky, A. Schnegg, M. Plato, M. Fuchs, *Phys. Chem. Chem. Phys.* **2005**, *7*, 19.
[13]   T. Prisner, M. Rohrer, F. MacMillan, *Annu. Rev. Phys. Chem.* **2001**, *52*, 279.
[14]   C. Calle, A. Sreekanth, M. V. Fedin, J. Forrer, I. Garcia-Rubio, I. A. Gromov, D. Hinderberger, B. Kasumaj, P. Léger, B. Mancosu, G. Mitrikas, M. G. Santangelo, S. Stoll, A. Schweiger, R. Tschaggelar, J. Harmer, *Helv. Chim. Acta* **2006**, *89*, 2495.
[15]   O. Schiemann, T. F. Prisner, *Quart. Rev. Biophys.* **2007**, *40*, 1.
[16]   G. Jeschke, *ChemPhysChem* **2002**, *3*, 927.
[17]   G. Jeschke, *Macromol. Rapid Comm.* **2002**, *23*, 227.
[18]   A. D. Milov, K. M. Salikhov, M. D. Shirov, *Fiz. Tverd. Tela* **1981**, *23*, 975.
[19]   A. D. Milov, A. B. Ponomarev, Y. D. Tsvetkov, *J. Struct. Chem.* **1984**, *25*, 710.
[20]   A. D. Milov, A. B. Ponomarev, Y. D. Tsvetkov, *Chem. Phys. Lett.* **1984**, *110*, 67.
[21]   R. G. Larsen, D. J. Singel, *J. Chem. Phys.* **1993**, *98*, 5134.
[22]   A. Godt, M. Schulte, H. Zimmermann, G. Jeschke, *Angew. Chem., Int. Ed.* **2006**, *45*, 7560.
[23]   A. G. Maryasov, Y. D. Tsvetkov, J. Raap, *Appl. Magn. Reson.* **1998**, *14*, 101.
[24]   J. C. P. Poole, *Electron Spin Resonance*, Wiley, New York, **1967**.
[25]   K. Scheffler, H. B. Stegmann, *Elektronenspinresonanz, Grundlagen und Anwendung in der Organischen Chemie*, Springer, Berlin, **1970**.
[26]   J. A. Weil, J. R. Bolton, J. E. Wertz, *Electron Paramagnetic Resonance: Elementary Theory and Practical Applications*, Wiley, New York, **1994**.
[27]   G. Jeschke, Y. Polyhach, *Phys. Chem. Chem. Phys.* **2007**, *9*, 1895.
[28]   L. J. Berliner, S. S. Eaton, G. R. Eaton, in *Biological Magnetic Resonance, Vol. 19* (Ed.: L. J. Berliner), Plenum, New York, **2000**, p. 614.
[29]   M. Mehring, V. A. Weberruß, *Object-Oriented Magnetic Resonance*, Academic Press, San Diego, **2001**.
[30]   R. E. Martin, M. Pannier, F. Diederich, V. Gramlich, M. Hubrich, H. W. Spiess, *Angew. Chem., Int. Ed.* **1998**, *37*, 2833.
[31]   M. Pannier, S. Veit, A. Godt, G. Jeschke, H. W. Spiess, *J. Magn. Reson.* **2000**, *142*, 331.

[32]   G. Jeschke, A. Bender, H. Paulsen, H. Zimmermann, A. Godt, *J. Magn. Reson.* **2004**, *169*, 1.

[33]   A. D. Milov, B. D. Naumov, Y. D. Tsvetkov, *Appl. Magn. Reson.* **2004**, *26*, 587.

[34]   A. G. Maryasov, Y. D. Tsvetkov, *Appl. Magn. Reson.* **2000**, *18*, 583.

[35]   M. K. Bowman, A. G. Maryasov, *J. Magn. Reson.* **2007**, *185*, 270.

[36]   G. E. Pake, *J. Chem. Phys.* **1948**, *16*, 327.

[37]   A. V. Astashkin, J. Seravalli, S. O. Mansoorabadi, G. H. Reed, S. W. Ragsdale, *J. Am. Chem. Soc.* **2006**, *128*, 3888.

[38]   D. D. Thomas, H. Keller, H. M. McConnell, *J. Chem. Phys.* **1963**, *39*, 2321.

[39]   K. Mukai, A. Sogabe, *J. Chem. Phys.* **1980**, *72*, 598.

[40]   S. O. Mansoorabadi, G. H. Reed, in *Paramagnetic Resonance of Metallobiomolecules* (Ed.: J. Telser), American Chemical Society, Washington, D.C., **2003**, pp. 82.

[41]   K. M. Salikhov, S. A. Dzuba, A. M. Raitsimring, *J. Magn. Reson.* **1981**, *42*, 255.

[42]   A. D. Milov, A. G. Maryasov, Y. D. Tsvetkov, J. Raap, *Chem. Phys. Lett.* **1999**, *303*, 135.

[43]   A. D. Milov, A. G. Maryasov, Y. D. Tsvetkov, *Appl. Magn. Reson.* **1998**, *15*, 107.

[44]   A. D. Milov, Y. D. Tsvetkov, F. Formaggio, M. Crisma, C. Toniolo, J. Raap, *J. Am. Chem. Soc.* **2001**, *123*, 3784.

[45]   A. N. Tikhonov, *Numerical Methods for the Solution of Ill-posed Problems*, Kluwer Academic Publishers, Dordrecht, Boston, **1995**.

[46]   G. Jeschke, V. Chechik, P. Ionita, A. Godt, H. Zimmermann, J. Banham, C. R. Timmel, D. Hilger, H. Jung, *Appl. Magn. Reson.* **2006**, *30*, 473.

[47]   Y.-W. Chiang, P. P. Borbat, J. H. Freed, *J. Magn. Reson.* **2005**, *172*, 279.

[48]   G. Jeschke, G. Panek, A. Godt, A. Bender, H. Paulsen, *Appl. Magn. Reson.* **2004**, *26*, 223.

[49]   M. K. Bowman, A. G. Maryasov, N. Kim, V. J. DeRose, *Appl. Magn. Reson.* **2004**, *26*, 23.

[50]   G. Jeschke, A. Koch, U. Jonas, A. Godt, *J. Magn. Reson.* **2002**, *155*, 72.

[51]   Y.-W. Chiang, P. P. Borbat, J. H. Freed, *J. Magn. Reson.* **2005**, *177*, 184.

[52]   V. V. Kurshev, A. M. Raitsimring, Y. D. Tsvetkov, *J. Magn. Reson.* **1989**, *81*, 441.

[53]   A. Raitsimring, J. Peisach, H. C. Lee, X. Chen, *J. Phys. Chem.* **1992**, *96*, 3526.

[54]   A. Raitsimring, R. H. Crepeau, J. H. Freed, *J. Chem. Phys.* **1995**, *102*, 8746.

[55]   G. Jeschke, P. Pannier, A. Godt, H. W. Spiess, *Chem. Phys. Lett.* **2000**, *331*, 243.

[56]   S. Saxena, J. H. Freed, *Chem. Phys. Lett.* **1996**, *251*, 102.

[57]   R. R. Ernst, G. Bodenhausen, A. Wokaun, *Principles of Nuclear Magnetic Resonance in One and Two Dimensions, Vol. 14*, Clarendon Press, Oxford, **1990**.

[58]   P. P. Borbat, R. H. Crepeau, J. H. Freed, *J. Magn. Reson.* **1997**, *127*, 155.

[59]   P. P. Borbat, J. H. Freed, *Chem. Phys. Lett.* **1999**, *313*, 145.

[60]   M. Bonora, J. Becker, S. Saxena, *J. Magn. Reson.* **2004**, *170*, 278.

[61]   N. Bloembergen, E. M. Purcell, R. V. Pound, *Phys. Rev.* **1948**, *73*, 679.

[62]   G. M. Zhidomirov, K. M. Salikhov, *Sov. Phys. JETP-USSR* **1969**, *29*, 1037.

[63]   K. M. Salikhov, A. G. Semenov, Y. D. Tsvetkov, *Electron Spin Echo and its Applications*, Nauka, Novosibirsk, **1976**.

[64]   A. V. Kulikov, G. I. Likhtenstein, *Adv. Mol. Relax. Int. Pr.* **1977**, *10*, 47.

[65]   M. H. Rakowsky, K. M. More, A. V. Kulikov, G. R. Eaton, S. S. Eaton, *J. Am. Chem. Soc.* **1995**, *117*, 2049.

[66]   L. V. Kulik, S. A. Dzuba, I. A. Grigoryev, Y. D. Tsvetkov, *Chem. Phys. Lett.* **2001**, *343*, 315.

[67]   L. V. Kulik, S. V. Paschenko, S. A. Dzuba, *J. Magn. Reson.* **2002**, *159*, 237.

[68]   S. A. Dzuba, Y. Kodera, H. Hara, A. Kawamori, *Appl. Magn. Reson.* **1994**, *6*, 391.

[69]   L. V. Kulik, S. A. Dzyuba, *J. Struct. Chem.* **2004**, *45*, 298.

[70]   V. Pfannebecker, H. Klos, M. Hubrich, T. Volkmer, A. Heuer, U. Wiesner, H. W. Spiess, *J. Phys. Chem.* **1996**, *100*, 13428.

[71]   A. Godt, C. Franzen, S. Veit, V. Enkelmann, M. Pannier, G. Jeschke, *J. Org. Chem.* **2000**, *65*, 7575.

[72]   A. Weber, O. Schiemann, B. Bode, T. F. Prisner, *J. Magn. Reson.* **2002**, *157*, 277.

[73]   G. Jeschke, H. Zimmermann, A. Godt, *J. Magn. Reson.* **2006**, *180*, 137.

[74]   Y. Polyhach, A. Godt, C. Bauer, G. Jeschke, *J. Magn. Reson.* **2007**, *185*, 118.

[75]   D. Margraf, B. E. Bode, A. Marko, O. Schiemann, T. F. Prisner, *Mol. Phys.* **2007**, *105*, 2153.

[76]   A. D. Milov, Y. D. Tsvetkov, *Appl. Magn. Reson.* **1997**, *12*, 495.

[77]   A. D. Milov, Y. D. Tsvetkov, *Appl. Magn. Reson.* **2000**, *18*, 217.

[78]   M. Pannier, V. Schädler, M. Schöps, U. Wiesner, G. Jeschke, H. W. Spiess, *Macromolecules* **2000**, *33*, 7812.

[79]   M. Pannier, M. Schöps, V. Schädler, U. Wiesner, G. Jeschke, H. W. Spiess, *Macromolecules* **2001**, *34*, 5555.

[80]   G. Jeschke, A. Godt, *ChemPhysChem* **2003**, *4*, 1328.

[81]   D. Hinderberger, H. W. Spiess, G. Jeschke, *J. Phys. Chem. B* **2004**, *108*, 3698.

[82]   D. Hinderberger, O. Schmelz, M. Rehahn, G. Jeschke, *Angew. Chem., Int. Ed.* **2004**, *46*, 4616.

[83]   G. W. M. Vandermeulen, D. Hinderberger, H. Xu, S. S. Sheiko, G. Jeschke, H.-A. Klok, *ChemPhysChem* **2004**, *5*, 488.

[84]   G. Jeschke, G. Panek, S. Schleidt, U. Jonas, *Polym. Eng. Sci.* **2004**, *44*, 1112.

[85]   Q. Mao, S. Schleidt, H. Zimmermann, G. Jeschke, *Phys. Chem. Chem. Phys.* **2008**, *10*, 1156.

[86]   S. Ruthstein, A. Potapov, A. M. Raitsimring, D. Goldfarb, *J. Phys. Chem. B* **2005**, *109*, 22843.

[87]   G. Jeschke, S. Schlick, *Phys. Chem. Chem. Phys.* **2006**, *8*, 4095.

[88]   P. Ionita, A. Volkov, G. Jeschke, V. Chechik, *Anal. Chem.* **2008**, *80*, 95.

[89]   A. D. Milov, Y. D. Tsvetkov, F. Formaggio, M. Crisma, C. Toniolo, J. Raap, *J. Am. Chem. Soc.* **2000**, *122*, 3843.

[90]   A. D. Milov, Y. D. Tsvetkov, J. Raap, *Appl. Magn. Reson.* **2000**, *19*, 215.

[91]   A. D. Milov, Y. D. Tsvetkov, F. Formaggio, S. Oancea, C. Toniolo, J. Raap, *Phys. Chem. Chem. Phys.* **2004**, *6*, 3596.

[92]   A. D. Milov, Y. D. Tsvetkov, F. Formaggio, S. Oancea, C. Toniolo, J. Raap, *J. Phys. Chem. B* **2003**, *107*, 13719.

[93]   A. D. Milov, Y. D. Tsvetkov, F. Formaggio, M. Crisma, C. Toniolo, J. Raap, *J. Peptide Sci.* **2003**, *9*, 690.

[94]   E. S. Salnikov, D. A. Erilov, A. D. Milov, Y. D. Tsvetkov, C. Peggion, F. Formaggio, C. Toniolo, J. Raap, S. A. Dzuba, *Biophys. J.* **2006**, *91*, 1532.

[95]   A. D. Milov, S. I. Samoilova, Y. D. Tsvetkov, V. A. Gusev, F. Formaggio, M. Crisma, C. Toniolo, J. Raap, *Appl. Magn. Reson.* **2002**, *23*, 81.

[96]   A. D. Milov, R. I. Samoilova, Y. D. Tsvetkov, F. Formaggio, C. Toniolo, J. Raap, *Appl. Magn. Reson.* **2005**, *29*, 703.

[97]   A. D. Milov, D. A. Erilov, E. S. Salnikov, Y. D. Tsvetkov, F. Formaggio, C. Toniolo, J. Raap, *Phys. Chem. Chem. Phys.* **2005**, *7*, 1794.

[98]   A. D. Milov, Y. D. Tsvetkov, E. Y. Gorbunova, L. G. Mustaeva, T. V. Ovchinnikova, J. Raap, *Biopolymers* **2002**, *64*, 328.

[99]   A. D. Milov, Y. D. Tsvetkov, E. Y. Gorbunova, L. G. Mustaeva, T. V. Ovchinnikova, J.-W. Handgraaf, J. Raap, *Chem. Biodiversity* **2007**, *4*, 1243.

[100] A. D. Milov, R. I. Samoilova, Y. D. Tsvetkov, F. Formaggio, C. Toniolo, J. Raap, *J. Am. Chem. Soc.* **2007**, *129*, 9260.

[101] A. D. Milov, M. I. Samoilova, Y. D. Tsvetkov, M. Jost, C. Peggion, F. Formaggio, M. Crisma, C. Toniolo, J.-W. Handgraaf, J. Raap, *Chem. Biodiversity* **2007**, *4*, 1275.

[102] A. D. Milov, R. I. Samoilova, Y. D. Tsvetkov, C. Peggion, F. Formaggio, C. Toniolo, J. Raap, *Dokl. Phys. Chem.* **2006**, *406*, 21.

[103] S. Pornsuwan, G. Bird, C. E. Schafmeister, S. Saxena, *J. Am. Chem. Soc.* **2006**, *128*, 3876.

[104] S. Pornsuwan, C. E. Schafmeister, S. Saxena, *J. Phys. Chem. C* **2008**, *112*, 1377.

[105] K. Murakami, H. Hara, Y. Masuda, H. Ohigashi, K. Irie, *ChemBioChem* **2007**, *8*, 2308.

[106] A. V. Astashkin, Y. Kodera, A. Kawamori, *Biochim. Biophys. Acta* **1994**, *1187*, 89.

[107] A. V. Astashkin, H. Hara, A. Kawamori, *J. Chem. Phys.* **1998**, *108*, 3805.

[108] T. Yoshii, A. Kawamori, M. Tonaka, K. Akabori, *Biochim. Biophys. Acta* **1999**, *1413*, 43.

[109] K. Shigemori, H. Hara, A. Kawamori, K. Akabori, *Biochim. Biophys. Acta* **1998**, *1363*, 187.

[110] A. Kawamori, N. Katsuta, H. Mino, A. Ishii, J. Minagawa, T.-A. Ono, *J. Biol. Phys.* **2002**, *28*, 413.

[111] A. Kawamori, T.-A. Ono, A. Ishii, S. Nakazawa, H. Hara, T. Tomo, J. Minagawa, R. Bittl, S. A. Dzuba, *Photosynth. Res.* **2005**, *84*, 187.

[112] A. Kawamori, N. Katsuta, H. Hara, *Appl. Magn. Reson.* **2003**, *23*, 557.

[113] H. Mino, A. Kawamori, T.-A. Ono, *Biochemistry* **2000**, *39*, 11034.

[114] M. Bennati, A. Weber, J. Antonic, D. L. Perlstein, J. Robblee, J. Stubbe, *J. Am. Chem. Soc.* **2003**, 14988.

[115] M. Rohrer, O. Brügmann, B. Kinzer, T. F. Prisner, *Appl. Magn. Reson.* **2001**, *21*, 257.

[116] M. M. Hertel, V. P. Denysenkov, M. Bennati, T. F. Prisner, *Magn. Reson. Chem.* **2005**, *43*, 248.

[117] V. P. Denysenkov, T. F. Prisner, J. Stubbe, M. Bennati, *Appl. Magn. Reson.* **2005**, *29*, 375.

[118] V. P. Denysenkov, T. F. Prisner, J. Stubbe, M. Bennati, *Proc. Natl. Acad. Sci. USA* **2006**, *103*, 13386.

[119] D. Biglino, P. P. Schmidt, E. J. Reijerse, W. Lubitz, *Phys. Chem. Chem. Phys.* **2006**, *8*, 58.

[120] V. P. Denysenkov, D. Biglino, W. Lubitz, T. F. Prisner, M. Bennati, *Angew. Chem., Int. Ed.* **2008**, *47*, 1224.

[121] M. Bennati, J. H. Robblee, V. Mugnaini, J. Stubbe, J. H. Freed, P. Borbat, *J. Am. Chem. Soc.* **2005**, *127*, 15014.

[122] M. R. Seyedsayamdost, C. T. Y. Chan, V. Mugnaini, J. Stubbe, M. Bennati, *J. Am. Chem. Soc.* **2007**, *129*, 15748.

[123] C. W. M. Kay, C. Elsässer, R. Bittl, S. R. Farell, C. Thorpe, *J. Am. Chem. Soc.* **2006**, *128*, 76.

[124] A. Savitsky, A. A. Dubinskii, M. Flores, W. Lubitz, K. Möbius, *J. Phys. Chem. B* **2007**, *111*, 6245.

[125] A. Schnegg, A. A. Dubinskii, M. R. Fuchs, Y. A. Grishin, E. P. Kirilina, W. Lubitz, M. Plato, A. Savitsky, K. Möbius, *Appl. Magn. Reson.* **2007**, *31*, 59.

[126] M. Persson, J. R. Harbridge, P. Hammarström, R. Mitri, L.-G. Mårtensson, U. Carlsson, G. R. Eaton, S. S. Eaton, *Biophys. J.* **2001**, *80*, 2886.

[127] L. J. Brown, K. L. Sale, R. Hills, C. Rouviere, L. Song, X. Zhang, P. G. Fajer, *Proc. Natl. Acad. Sci. USA* **2002**, *99*, 12765.

[128] P. G. Fajer, *J. Phys.: Condens. Matter* **2005**, *17*, S1459.

[129] M. Nakamura, S. Ueki, H. Hara, T. Arata, *J. Mol. Biol.* **2005**, *348*, 127.

[130] S. Steigmiller, M. Börsch, P. Gräber, M. Huber, *Biochim. Biophys. Acta* **2005**, *1708*, 143.

[131] Z. Zhou, S. C. DeSensi, R. A. Stein, S. Brandon, M. Dixit, E. J. McArdle, E. M. Warren, H. K. Kroh, L. Song, C. E. Cobb, E. J. Hustedt, A. E. Beth, *Biochemistry* **2005**, *44*, 15115.

[132] Z. Zhou, S. C. DeSensi, R. A. Stein, S. Brandon, L. Song, C. E. Cobb, E. J. Hustedt, A. H. Beth, *Biochemistry* **2007**, *46*, 10248.

[133] K. I. Sen, A. Sienkiewicz, J. F. Love, J. C. vanderSpek, P. G. Fajer, T. M. Logan, *Biochemistry* **2006**, *45*, 4295.

[134] K. I. Sen, T. M. Logan, P. G. Fajer, *Biochemistry* **2007**, *46*, 11639.

[135] S.-Y. Park, P. P. Borbat, G. Gonzalez-Bonet, J. Bhatnagar, A. M. Pollard, J. H. Freed, A. M. Bilwes, B. R. Crane, *Nat. Struct. Mol. Biol.* **2006**, *13*, 400.

[136] P. P. Borbat, J. H. Freed, *Method. Enzymol.* **2007**, *423*, 52.

[137] J. Bhatnagar, J. H. Freed, B. R. Crane, *Method. Enzymol.* **2007**, *423*, 117.

[138] H. Hara, T. Tenno, M. Shirakawa, *J. Magn. Reson.* **2007**, *184*, 78.

[139] K. Sale, L. Song, Y.-S. Liu, E. Perozo, P. Fajer, *J. Am. Chem. Soc.* **2005**, *127*, 9334.

[140] J. E. Banham, C. R. Timmel, R. J. M. Abbott, S. M. Lea, G. Jeschke, *Angew. Chem., Int. Ed.* **2006**, *45*, 1058.

[141] L. Galiano, M. Bonora, G. E. Fanucci, *J. Am. Chem. Soc* **2007**, *129*, 11004.

[142] A. L. Lai, L. K. Tamm, *J. Biol. Chem.* **2007**, *282*, 23946.

[143] S. M. Hanson, N. V. Eps, D. J. Francis, C. Altenbach, S. A. Vishnivetskiy, V. Y. Arshavsky, C. S. Klug, W. L. Hubbell, V. V. Gurevich, *EMBO J.* **2007**, *26*, 1726.

[144] P. G. Fajer, M. Gyimesi, A. Málnási-Csizmadia, C. R. Bagshaw, K. I. Sen, L. Song, *J. Phys.: Condens. Matter* **2007**, *19*, 285208.

[145] J. E. Banham, G. Jeschke, C. R. Timmel, *Mol. Phys.* **2007**, *105*, 2041

[146] G. Jeschke, A. Bender, T. Schweikardt, G. Panek, H. Decker, H. Paulsen, *J. Biol. Chem.* **2005**, *280*, 18623.

[147] G. Jeschke, C. Wegener, M. Nietschke, H. Jung, H.-J. Steinhoff, *Biophys. J.* **2004**, *86*, 2551.

[148] D. Hilger, H. Jung, E. Padan, C. Wegener, K.-P. Vogel, H.-J. Steinhoff, G. Jeschke, *Biophys. J.* **2005**, *89*, 1328.

[149] Q. Xu, J. F. Ellena, M. Kim, D. S. Cafiso, *Biochemistry* **2006**, *45*, 10847.

[150] P. Borbat, T. F. Ramlall, J. H. Freed, D. Eliezer, *J. Am. Chem. Soc* **2006**, *128*, 10004.

[151] D. Hilger, Y. Polyhach, E. Padan, H. Jung, G. Jeschke, *Biophys. J.* **2007**, *93*, 3675.

[152] M. Kim, Q. Xu, D. Murray, D. S. Cafiso, *Biochemistry* **2008**, *47*, 670.

[153] W. M. Oldham, N. V. Eps, A. M. Preininger, W. L. Hubbell, H. E. Hamm, *Nat. Struct. Mol. Biol.* **2006**, *13*, 772.

[154] W. M. Henne, H. M. Kent, M. G. J. Ford, B. G. Hegde, O. Daumke, P. J. G. Butler, R. Mittal, R. Langen, P. R. Evans, H. T. McMahon, *Structure* **2007**, *15*, 839.

[155] P. P. Borbat, K. Surendhran, M. Bortolus, P. Zou, J. H. Freed, H. S. Mchaourab, *PLoS Biol.* **2007**, *5*, e271.

[156] K. Hayashi, Y. Sudo, J. Jee, M. Mishima, H. Hara, N. Kamo, C. Kojima, *Biochemistry* **2007**, *46*, 14380.

[157] M. Vamvouka, J. Cieslak, N. Van Eps, W. Hubbell, A. Gross, *Protein Sci.* **2008**, *17*, 506.

[158] I. Smirnova, V. Kasho, J.-Y. Choe, C. Altenbach, W. L. Hubbell, H. R. Kaback, *Proc. Natl. Acad. Sci. USA* **2007**, *104*, 16504.

[159] N. J. Traaseth, R. Verardi, K. D. Torgersen, C. B. Karim, D. D. Thomas, G. Veglia, *Proc. Natl. Acad. Sci. USA* **2007**, *104*, 14676.

[160] A. K. Upadhyay, P. P. Borbat, J. Wang, J. H. Freed, D. E. Edmondson, *Biochemistry* **2008**, *47*, 1554.

[161] N. Alexander, A. Al-Mestarihi, M. Bortolus, H. Mchaourab, J. Meiler, *Structure* **2008**, *16*, 181.

[162] I. V. Borovykh, S. Ceola, P. Gajula, P. Gast, H.-J. Steinhoff, M. Huber, *J. Magn. Reson.* **2006**, *180*, 178.

[163] O. Schiemann, A. Weber, T. E. Edwards, T. F. Prisner, S. T. Sigurdsson, *J. Am. Chem. Soc.* **2003**, *125*, 3434.

[164] O. Schiemann, N. Piton, Y. Mu, G. Stock, J. W. Engels, T. F. Prisner, *J. Am. Chem. Soc.* **2004**, *126*, 5722.

[165] N. Piton, O. Schiemann, Y. Mu, G. Stock, T. Prisner, J. W. Engels, *Nucleosides, Nucleotides Nucleic Acids* **2005**, *24*, 771.

[166] N. Piton, Y. Mu, G. Stock, T. F. Prisner, O. Schiemann, J. W. Engels, *Nucleic Acids Res.* **2007**, *35*, 3128.

[167] N. Piton, Y. Mu, G. Stock, T. F. Prisner, O. Schiemann, J. W. Engels, *Nucleic Acids Res.* **2007**, *35*, 5985.

[168] O. Schiemann, N. Piton, J. Plackmeyer, B. E. Bode, T. F. Prisner, J. W. Engels, *Nat. Protoc.* **2007**, *2*, 904.

[169] Q. Cai, A. K. Kusnetzow, W. L. Hubbell, I. S. Haworth, G. P. C. Gacho, N. V. Eps, K. Hideg, E. J. Chambers, P. Z. Qin, *Nucleic Acids Res.* **2006**, *34*, 4722.

[170] E. A. Price, B. T. Sutch, Q. Cai, P. Z. Qin, I. S. Haworth, *Biopolymers* **2007**, *87*, 40.

[171] G. P. G. Grant, P. Z. Qin, *Nucleic Acids Res.* **2007**, *35*, e77.

[172] Q. Cai, A. K. Kusnetzow, K. Hideg, E. A. Price, I. S. Haworth, P. Z. Qin, *Biophys. J.* **2007**, *93*, 2110.

[173] P. Z. Qin, I. S. Haworth, Q. Cai, A. K. Kusnetzow, G. P. G. Grant, E. A. Price, G. Z. Sowa, A. Popova, B. Herreros, H. He, *Nat. Protoc.* **2007**, *2*, 2354.

[174] R. Ward, D. J. Keeble, H. El-Mkami, David G. Norman, *ChemBioChem* **2007**, *8*, 1957.

[175] G. Sicoli, G. Mathis, O. Delalande, Y. Boulard, D. Gasparutto, S. Gambarelli, *Angew. Chem., Int. Ed.* **2008**, *47*, 735.

[176] M. K. Bowman, D. Becker, M. D. Sevilla, J. D. Zimbrick, *Rad. Res.* **2005**, *163*, 447.

[177] H. Hara, A. Kawamori, A. V. Astashkin, T.-A. Ono, *Biochim. Biophys. Acta* **1996**, *1276*, 140.

[178] S. Arao, S. Yamada, A. Kawamori, J.-R. Shen, N. Ionnidis, V. Petrouleas, in *EPR in the 21st Century: Basics and applications to material, life and earth science* (Eds.: A. Kawamori, J. Yamaguchi, H. Ohta), Elsevier Science BV, Amsterdam, **2002**, pp. 466.

[179] A. Zouni, H. T. Witt, J. Kern, P. Fromme, N. Krauß, W. Saenger, P. Orth, *Nature* **2001**, *409*, 739.

[180] R. Bittl, A. Kawamori, in *Photosystem II The Light-Driven Water:Plastochinone Oxidoreductase, Vol. 22* (Eds.: T. J. Wydrzynski, K. Satoh), Springer, Dordrecht, **2005**, pp. 389.

[181] S. Kuroiwa, M. Tonaka, A. Kawamori, K. Akabori, *Biochim. Biophys. Acta* **2000**, *1460*, 330.

[182] C. Elsässer, M. Brecht, R. Bittl, *J. Am. Chem. Soc.* **2002**, *124*, 12606.

[183] C. Elsässer, M. Brecht, R. Bittl, *Biochem. Soc. Trans.* **2005**, *33*, 15.

[184] R. Codd, A. V. Astashkin, A. Pacheco, A. M. Raitsimring, J. H. Enemark, *J. Biol. Inorg. Chem.* **2002**, *7*, 338.

[185] I. M. C. v. Amsterdam, M. Ubbink, G. W. Canters, M. Huber, *Angew. Chem., Int. Ed.* **2003**, *42*, 62.

[186] C. W. M. Kay, H. E. Mkami, R. Cammack, R. W. Evans, *J. Am. Chem. Soc.* **2007**, *129*, 4868.

[187] Z. Yang, J. Becker, S. Saxena, *J. Magn. Reson.* **2007**, *188*, 337.

[188] J. S. Becker, S. Saxena, *Chem. Phys. Lett.* **2005**, 248.

[189] A. M. Raitsimring, C. Gunanathan, A. Potapov, I. Efremenko, J. M. L. Martin, D. Milstein, D. Goldfarb, *J. Am. Chem. Soc.* **2007**, *129*, 14138.

[190] E. Narr, A. Godt, G. Jeschke, *Angew. Chem., Int. Ed.* **2002**, *41*, 3907.

[191] S. Stoll, A. Schweiger, *J. Magn. Reson.* **2006**, *178*, 42.

[192] J. Fritscher, M. Beyer, O. Schiemann, *Chem. Phys. Lett.* **2002**, *364*, 393.

[193] R. W. Kreilick, *J. Chem. Phys.* **1967**, *46*, 4260.

[194] G. F. Hatch, R. W. Kreilick, *J. Chem. Phys.* **1972**, *57*, 3696.

[195] J. Shao, E. Steene, B. M. Hoffman, A. Ghosh, *Eur. J. Inorg. Chem.* **2005**, *2005*, 1609.

[196] A. V. Astashkin, A. M. Raitsimring, F. A. Walker, C. Rensing, M. M. McEvoy, *J. Biol. Inorg. Chem.* **2005**, *10*, 221.

[197] M. Iwaizumi, T. Kudo, S. Kita, *Inorg. Chem.* **1986**, *25*, 1546.

[198] C. Elschenbroich, M. Wolf, O. Schiemann, K. Harms, O. Burghaus, J. Pebler, *Organometallics* **2002**, *21*, 5810.

[199] B. E. Bode, D. Margraf, J. Plackmeyer, G. Dürner, T. F. Prisner, O. Schiemann, *J. Am. Chem. Soc* **2007**, *129*, 6736.

[200] B. E. Bode, J. Plackmeyer, T. F. Prisner, O. Schiemann, *J. Phys. Chem. A* **2008**, accepted.

[201] M. Chikira, H. Kon, R. A. Hawley, K. M. Smith, *J. Chem. Soc. Dalton* **1979**, 245.

[202] M. Iwaizumi, Y. Ohba, H. Iida, M. Hirayama, *Inorg. Chim. Acta* **1984**, *82*, 47.

[203] K. L. Cunningham, K. M. McNett, R. A. Pierce, K. A. Davis, H. H. Harris, D. M. Falck, D. R. McMillin, *Inorg. Chem.* **1997**, *36*, 608.

[204] W. Kohn, L. J. Sham, *Phys. Rev.* **1965**, *140*, A1133.

[205] M. J. Frisch, G. W. Trucks, H. B. Schlegel, G. E. Scuseria, M. A. Robb, J. R. Cheeseman, J. J. A. Montgomery, T. Vreven, K. N. Kudin, J. C. Burant, J. M. Millam, S. S. Iyengar, J. Tomasi, V. Barone, B. Mennucci, M. Cossi, G. Scalmani, N. Rega, G. A. Petersson, H. Nakatsuji, M. Hada, M. Ehara, K. Toyota, R. Fukuda, J. Hasegawa, M. Ishida, T. Nakajima, Y. Honda, O. Kitao, H. Nakai, M. Klene, X. Li, J. E. Knox, H. P. Hratchian, J. B. Cross, V. Bakken, C. Adamo, J. Jaramillo, R. Gomperts, R. E. Stratmann, O. Yazyev, A. J. Austin, R. Cammi, C. Pomelli, J. W. Ochterski, P. Y. Ayala, K. Morokuma, G. A. Voth, P. Salvador, J. J. Dannenberg, V. G. Zakrzewski, S. Dapprich, A. D. Daniels, M. C. Strain, O. Farkas, D. K. Malick, A. D. Rabuck, K. Raghavachari, J. B. Foresman, J. V. Ortiz, Q. Cui, A. G. Baboul, S. Clifford, J. Cioslowski, B. B. Stefanov, G. Liu, A. Liashenko, P. Piskorz, I. Komaromi, R. L. Martin, D. J. Fox, T. Keith, M. A. Al-Laham, C. Y. Peng, A. Nanayakkara, M. Challacombe, P. M. W. Gill, B. Johnson, W. Chen, M. W. Wong, C. Gonzalez, J. A. Pople, revision B.03 ed., Gaussian, Inc., Pittsburgh, PA, **2003**.

[206] R. Ahlrichs, M. Bär, H.-P. Baron, R. Bauernschmitt, S. Böcker, N. Crawford, P. Deglmann, M. Ehrig, K. Eichkorn, S. Elliott, F. Furche, F. Haase, M. Häser, C. Hättig, A. Hellweg, H. Horn, C. Huber, U. Huniar, M. Kattannek, A. Köhn, C. Kölmel, M. Kollwitz, K. May, P. Nava, C. Ochsenfeld, H. Öhm, H. Patzelt, D. Rappoport, O. Rubner, A. Schäfer, U. Schneider, M. Sierka, O. Treutler, B. Unterreiner, M. v. Arnim, F. Weigend, P. Weis, H. Weiss, version 5.6 ed., Quantum Chemistry Group, University of Karlsruhe, Karlsruhe, Germany, **2002**.

[207] A. D. Becke, *Phys. Rev. A* **1988**, *38*, 3098.

[208]   J. P. Perdew, *Phys. Rev. B* **1986**, *34*, 7406.

[209]   J. P. Perdew, *Phys. Rev. B* **1986**, *33*, 8822.

[210]   A. Schäfer, C. Huber, R. Ahlrichs, *J. Chem. Phys.* **1994**, *100*, 5829.

[211]   K. Eichkorn, O. Treutler, H. Öhm, M. Häser, R. Ahlrichs, *Chem. Phys. Lett.* **1995**, *242*, 652.

[212]   K. Eichkorn, F. Weigend, O. Treutler, R. Ahlrichs, *Theor. Chem. Acc.* **1997**, *97*, 119.

[213]   A. D. Becke, *J. Chem. Phys.* **1993**, *98*, 5648.

[214]   J. P. Perdew, Y. Wang, *Phys. Rev. B* **1992**, *45*, 13244.

[215]   J. P. Perdew, *Physica B* **1992**, *172*, 1.

[216]   A. V. Arbuznikov, J. Vaara, M. Kaupp, *J. Chem. Phys.* **2004**, *120*, 2127.

[217]   W. Kutzelnigg, U. Fleischer, M. Schindler, in *NMR Basic Principles and Progress, Vol. 23* (Eds.: P. Diehl, E. Fluck, H. Günther, R. Kosferld, J. Seelig), Springer-Verlag, Berlin/Heidelberg, **1990**, pp. 165.

List of Figures

List of Tables

Curriculum Vitae

Personal Data
First Name: Bela
Middle Name: Ernest
Last Name: Bode
Address: Carl-Goerdeler-Straße 5
                   60320 Frankfurt am Main
                   Germany
Date of Birth: December 15th, 1977
Place of Birth: Frankfurt am Main
Marital Status: Single
Citizenship: German

Education (University)
2004-2008   Postgraduate studies supervised by Dr. Olav Schiemann in the group of Prof. Thomas F. Prisner.
2004   Diploma-thesis: „Synthese, EPR-spektroskopische und dichtefunktionaltheoretische Untersuchungen zu DNA/RNA interkalierenden Nitroxid-Spinlabeln" supervised by Dr. Olav Schiemann in the group of Prof. Thomas F. Prisner.
1999-2004   Undergraduate studies in chemistry, Johann Wolfgang Goethe-University, Frankfurt am Main
1998-1999   Undergraduate studies in food chemistry, Johann Wolfgang Goethe-University, Frankfurt am Main

Education (School)
1998   Abitur
1996   High School Diploma
1995-1996   Granting of leave to visit the Burlington High School, Burlington, VT, USA
1994-1998   Max-Beckmann-Schule (Gymnasium), Frankfurt am Main
1988-1994   Musterschule (Gymnasium), Frankfurt am Main
1983-1988   Holzhausenschule (Grundschule), Frankfurt am Main

Honors and Awards
2007   "Ernst Award" of the Magnetic Resonance Division of the German Chemical Society
2007   Magnetic Resonance in Chemistry "Young Investigators Award"
2004   Henkel prize for the best diploma in chemistry 2004 at the Johann Wolfgang Goethe-University, Frankfurt am Main
2001   Dr. Albert-Hloch prize for one of the best three diploma pre-examinations in 2000 at the Johann Wolfgang Goethe-University, Frankfurt am Main

Academic Teachers
N. Auner, W. Aßmus, B. Brutschy, E. Egert, J. Engels, L. Fink, M. Göbel, C. Griesinger, S. Hashmi, K. Hensen, B. Kolbesen, E. Mohler, T. Müller, P. Pickel, T. Prisner, D. Rehm, E.-A. Reinsch, H. Roskos, O. Schiemann, G. Stock, M. Wagner, E.-J. Zehnder.

Publications

1. A. Weber, O. Schiemann, B. Bode, T. F. Prisner, "PELDOR at S- and X-Band Frequencies and the Separation of Exchange Coupling from Dipolar Coupling" *J. Magn. Reson.* **2002**, *157*, 277-285.

2. O. Schiemann, N. Piton, J. Plackmeyer, B. E. Bode, T. F. Prisner, J. W. Engels, "Spin-labeling of oligonucleotides with the nitroxide TPA and use of PELDOR, a pulse EPR method, to measure intramolecular distances" *Nat. Protoc.* **2007**, *2*, 904-922.

3. B. E. Bode, D. Margraf, J. Plackmeyer, G. Dürner, T. F. Prisner, O. Schiemann, "Counting the Monomers in Nanometer-Sized Oligomers by Pulsed Electron–Electron Double Resonance" *J. Am. Chem. Soc.* **2007**, *129*, 6736-6745.

4. D. Margraf, B. E. Bode, A. Marko, O. Schiemann, T. F. Prisner, "Conformational Flexibility of Nitroxide Biradicals Determined from X-Band PELDOR Experiments" *Mol. Phys.* **2007** *105*, 2153-2160.

5. O. Frolow, B. E. Bode, J. W. Engels, "The Synthesis of EPR differentiable Spinlabels and their Coupling to Uridine" *Nucleosides, Nucleotides Nucleic Acids* **2007**, *26*, 655-659.

6. B. E. Bode, J. Plackmeyer, T. F. Prisner, O. Schiemann, "PELDOR measurements on a Nitroxide Labeled Cu(II) Porphyrin: Orientation Selection, Spin-Density Distribution and Conformational Flexibility" *J. Phys. Chem. A* accepted.